Investigation of the effect of large-scale shell asymmetry on Iskra-5 target operation

S. A. Bel'kov, A. V. Bessarab, O. A. Vinokurov, V. A. Gaĭdash, N. V. Zhidkov, V. M. Izgorodin, G. A. Kirillov, G. G. Kochemasov, A. V. Kunin, D. N. Litvin, V. M. Murugov, L. S. Mkhitar'yan, S. I. Petrov, A. V. Pinegin, V. T. Punin, N. A. Suslov, and V. A. Tokarev

All-Russia Scientific-Research Institute of Experimental Physics Russian Federal Center, 607190 Sarov, Nizhegorod Region, Russia

(Submitted 5 January 1998)
Pis'ma Zh. Éksp. Teor. Fiz. **67**, No. 3, 161–165 (10 February 1998)

Experiments designed to investigate the effect of a controlled large-scale asymmetry of a shell containing deuterium-tritium fuel on the shell compression and neutron production under indirect (x-ray) action are performed on the Iskra-5 laser fusion device. The uniformity of the x radiation near the target is not worse than 3%, and the shell asymmetry is varied from 30 to 100%. The observed decrease of the experimental neutron yield as compared with experiments using symmetric targets is in satisfactory agreement with two-dimensional calculations.
 [S0021-3640(98)00103-0]

PACS numbers: 28.52.Cx, 52.58.Ns

Experiments performed on the Iskra-5 laser device to study the compression and heating of deuterium-tritium (DT) fuel by x rays generated inside a spherical converter cavity showed that the target operation is highly stable and that the results obtained are highly reproducible[1–3] (see also Table I below). The multiple re-reflection of laser radiation and x rays that occurs in the cavity symmetrizes the x-ray flux incident on the central capsule holding DT gas. This symmetrization is especially noticeable when the capsule diameter $\oslash_{sh}$ is much smaller than the converter diameter $\oslash_{box}$. Calculations show that for $\oslash_{sh}/\oslash_{box}=0.14$ the characteristic degree of nonuniformity of the irradiation is $\cong 3\%$ (Ref. 2). This is confirmed by the experimentally observed high symmetry of the ''glow'' of the compressed glass capsule in the intrinsic x radiation detected with a pinhole camera. An indirect proof of the comparatively high symmetry is provided by the agreement between the computed and measured neutron yields with the working volume compression (at the moment of neutron production) varying from $\cong 10^2$ to 2×10^3 (Ref. 2).

The results obtained have stimulated experiments with controlled asymmetry of shells containing DT fuel. Asymmetry is obtained by depositing an additional layer of matter on one of the hemispheres of the sphere (see Fig. 1). The main question addressed in the experiment was to determine the degree of asymmetry for which the experimental neutron yield would be markedly different from that obtained in a one-dimensional calculation and from that obtained in experiments with a spherically symmetric shell pos-

TABLE I. Parameters of asymmetric capsules and the main experimental results.

		Capsule parameters				Experimental results				
Experiment No.	D_h, mm	$\varnothing_{sh}$, μ	d_{sh}, μm	dl, μ	P_{DT}, atm	E_L, kJ	N, 10^9	T, keV	$\varnothing_{min}$, μm	$\tau_{\gamma\gamma}$, ns
1	0.6	270	4.9	5	7	8.6	0.77	2.3	–	0.45
2	0.6	273	5.1	9.5	8	9.0	0.77	1.7	–	–
3	0.6	290	5.1	10.5	7.5	7.2	2.8	2.0	70	0.4
4	0.4	272	7.1	10.5	16	8.4	3.8	1.8	60	0.48
5	0.4	301	9.4	10.5	12	8.4	2.7	1.9	78×64	0.55
6	0.4	287	16	18	20	8.5	0.1	–	–	–
7	0.4	301	10	10+ 11.5	14	8.3	0.55	–	55	–

Note: D_h is the diameter of the opening for introducing the laser radiation; $\varnothing_{sh}$ and d_{sh} are the diameter and thickness of the glass microsphere; dl is the thickness of the magnesium coating; P_{DT} is the DT gas pressure; E_L is the energy of the laser radiation introduced into the interaction chamber; N is the neutron yield; T_{DT} is the DT fuel temperature; $\varnothing_{min}$ is the diameter of the compressed region according to the pinhole photograph; $\tau_{\gamma\gamma}$ is the compression time of the shell (time interval between the x-ray pulses generated at the wall of the jacket and in the collapse of the shell). In the experiment marked with an asterisk the target possessed bilateral symmetry.

sessing the same mass as the asymmetric shell. Moreover, it was of interest to determine experimentally the degree of deformation of the heated and compressed capsule according to the image obtained with a pinhole camera. Experimental data obtained in a series of seven experiments are presented below.

The target was similar to the inverted-corona targets[4] and consisted of a thin-walled, spherical copper shell 2 mm in diameter, with six openings, 0.4–0.6 mm in diameter, for introducing the laser beams. The inner surface of the shell was coated with a layer of gold approximately 1 μm thick, and the outer surface was coated with a layer of bismuth 0.1–0.3 μm thick. A glass microsphere filled with a DT gaseous mixture at a pressure P_{DT} was located at the center. To obtain microsphere thicknesses greater than 7 μm, special technologies were used to deposit different substances, such as polyparaxylilene (CH), magnesium, or a glass analog (SiO_2), on its surface.

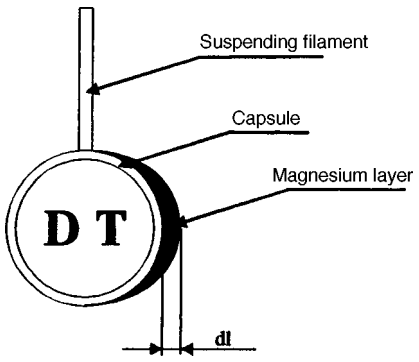

FIG. 1. Diagram of asymmetric capsule.

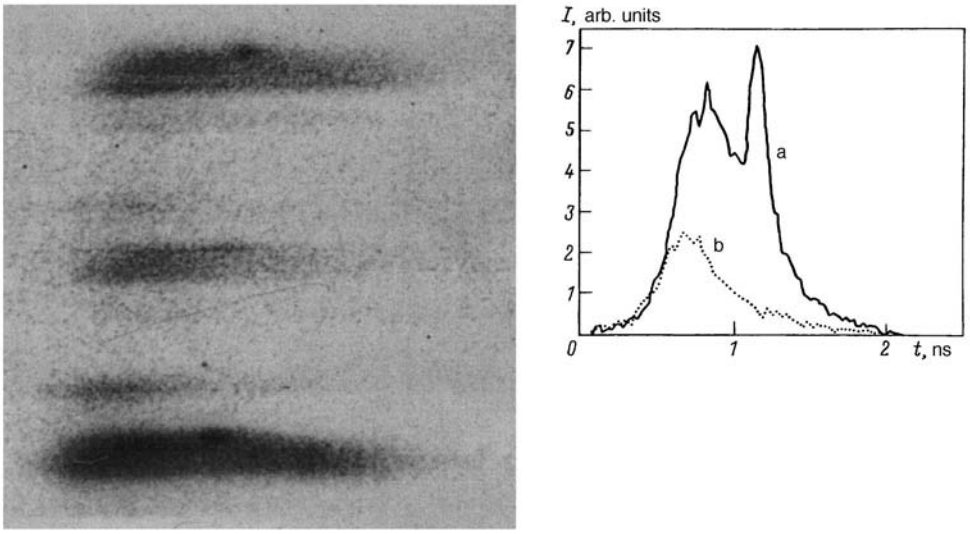

FIG. 2. Image from x-ray image tube (left) and traces of two cross sections (right) from experiment No. 3.

The target was irradiated by 12 laser beams ($\lambda = 1.315$ μm) with a duration of 0.35 ± 0.05 ns. The total energy introduced into the interaction chamber was 5.5–7 kJ (power 15–20 TW). A system of diagnostic apparatus,[3] including x-ray, corpuscular (neutron), and optical diagnostics, was used. The basic experimental results are presented in Table I.

The integrated neutron yield was measured by a complex of techniques based on the activation of copper and indium and by the long-counting method. The neutron spectrum and then the temperatures of the DT ions were determined by the time-of-flight method using two channels with base lines $L_1 = 1249$ cm and $L_2 = 1676$ cm. The time interval $\tau_{\gamma\gamma}$ between the start of the x-ray pulse generated at the surface of the jacket (during the action of the laser radiation) and the start of the x-ray pulse generated during the collapse of the capsule holding the DT gas was determined by detecting the x radiation with an x-ray image tube operating in a mode providing spatial resolution in a definite spectral interval ($h\bar{\nu} \cong 2.5$ keV). The signals corresponding to the two indicated pulses were detected through different input openings (see Fig. 2). The diameter of the compressed core was determined with a pinhole camera. Substructure can be seen in the images of the glow of the compressed core, though appreciable shape asymmetry was observed only in experiment No. 4. The results of the measurements of the spectral fluxes of x rays emanating from the jacket show that under our experimental conditions the effective temperature of the soft ($h\nu \leqslant 1.5$ keV) x rays is $T_{\text{eff}} \sim 160 \pm 15$ eV.[5]

The results obtained on the neutron yield N can be systematized by a generalization of the scaling relation that is well obeyed in the case of spherically symmetric shells holding DT gas (Fig. 3):

$$N \sim m^{4/3} M^{2/3} f(E_\gamma / M_S). \tag{1}$$

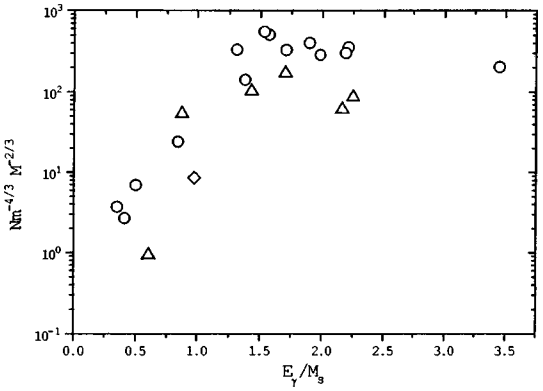

FIG. 3. Normalized neutron yield versus specific energy deposition in experiments with symmetric (○) and asymmetric (△—unilateral asymmetry, ◇—bilateral asymmetry) central capsules.

Here m is the mass of the DT gas, M and M_S are the masses of the shell and its symmetric part (without the magnesium layer), E_γ is the energy of the x rays in the cavity (the values of E_γ in Fig. 3 include an allowance for a model-based estimate of the energy losses to fast ions). The figure supplemented with data from experiments performed with spherical shells. One can see that for $E_\gamma/M_S \geqslant 1.5$ (arbitrary units) the neutron yield is virtually (to within a factor of 2) independent of E_γ/M_S, a circumstance that corresponds to a regime with a completely heated shell. For spherically symmetric shells ~ 280 μm in diameter, the heated thickness equals ~ 7 μm. All shells with $E_\gamma/M_S \geqslant 1.5$ are characterized by the same specific energy deposition, corresponding to heating of the shell to a temperature of ~ 160 eV. For $E_\gamma/M_S < 1.5$ an ablation regime is realized, and the specific energy deposition and the normalized neutron yield decrease.

It is also evident that the behavior of asymmetric targets is qualitatively similar to that of symmetric targets, the neutron yield being lower in absolute magnitude by a factor of ~ 2 for $E_\gamma/M_S \geqslant 1.5$ and ~ 4 for $E_\gamma/M_S \sim 0.5$. Thus the sensitivity to asymmetry is lower in the imploding shell regime. This is natural. The reason for the insensitivity can be explained as follows. The effective solid angle occupied by the layer of Mg coating equals $\sim 1/4$ of the total solid angle. In experiments Nos. 1–3 the glass is ~ 5 μm thick and is heated completely through (from the open side). The energy stored in the x radiation is sufficient under these conditions to heat from within another $\sim$(1.5—2) μm of the glass located beneath the Mg layer. Ultimately, a part of the shell with thickness equal to approximately half the thickness of the shell (~ 2.5 μm) flies into the target from the uncoated side of the target; for the side coated with Mg the corresponding thickness equals ~ 2 μm. The difference is not so large as to decrease the number of neutrons substantially. Two-dimensional calculations performed with the MIMOZA program on the assumption of uniform heating showed that the neutron yield decreases by approximately a factor of 2, in accordance with experiment.

The data on the collapse time $\tau_{\gamma\gamma}$ (Fig. 4) are also in agreement with the ideas developed. One can see (though less clearly, because $\tau_{\gamma\gamma}$ is determined with a lower accuracy ± 0.05 ns) that for $E_\gamma/M_S \geqslant 1.5$ the collapse time $\tau_{\gamma\gamma} \sim 0.3$–$0.4$ ns for symmetric shells and $\tau_{\gamma\gamma} \sim 0.4$–$0.45$ ns for asymmetric shells. The time $\tau_{\gamma\gamma}$ increases for

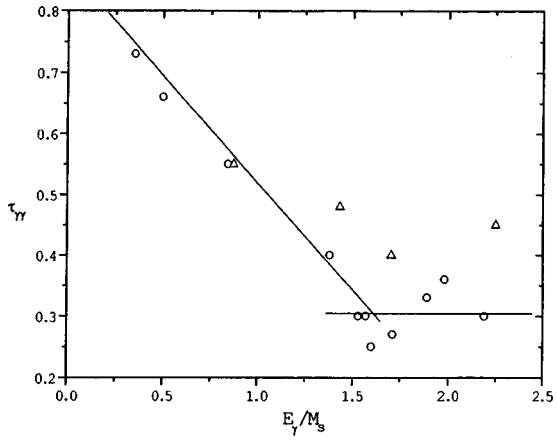

FIG. 4. Collapse time $\tau_{\gamma\gamma}$ versus specific energy deposition in experiments with symmetric (○) and asymmetric (△) central capsules.

$E_\gamma/M_S \leqslant 1.5$. The velocity of convergence of the gas-glass boundary can also be estimated from the value of $\tau_{\gamma\gamma}$ as $V \sim (1.5-3.5)\times 10^7$ cm/s, in agreement with the results of one-dimensional calculations.[2]

In summary, we have performed successful experiments to investigate the operation of the Iskra-5 device using asymmetric shells with an irradiation asymmetry $\leqslant 3\%$. We have found that with $\sim 50\%$ shell asymmetry the neutron yield is lower by a factor of $\sim 2-4$ than in the symmetric case; this yields information about the mechanisms and degree of heating of the shells.

This work was supported by the State Committee of the Russian Federation on Science and Technologies at the Iskra-5 Laser Fusion Device (registration number 01-50).

[1] F. M. Abzaev, V. I. Annenkov, V. G. Bezuglov *et al.*, JETP Lett. **58**, 28 (1993).
[2] G. G. Kochemasov, in *Proceedings of the 23rd European Conference*, St. John's College, Oxford, September 19–23, 1994, Institute of Physics Series Number **140**, 17 (1995).
[3] F. M. Abzaev, A. V. Bessarab, G. A. Kirillov *et al.*, Vopr. At. Nauki Tekh. Ser. Matem. Model., Fiz. Prots., No. 4, 68 (1992).
[4] A. V. Bessarab, V. A. Gaĭdash, G. V. Dolgoleva *et al.*, Zh. Éksp. Teor. Fiz. **102**, 1800 (1992) [Sov. Phys. JETP **75**, 970 (1992)].
[5] A. V. Bessarab, S. G. Garanin, G. A. Kirillov *et al.*, in *Abstracts of the 9th Conference on Diagnostics of High-Temperature Plasmas* [in Russian], St. Petersburg, Russia, June 2–4, 1997.

Translated by M. E. Alferieff

The conformal anomaly associated with an operator product acting in rank 1 symmetric spaces

A. A. Bytsenko[a)]
St. Petersburg State Technical University, 195251 St. Petersburg, Russia

A. E. Goncalves[b)]
Departamento de Fisica, Universidade Estadual de Londrina, Caixa Postal 6001, Londrina-Parana, Brazil

F. L. Williams[c)]
University of Massachusetts, Amherst, Massachusetts 01003, USA

(Submitted 5 January 1998)
Pis'ma Zh. Éksp. Teor. Fiz. **67**, No. 3, 166–171 (10 February 1998)

The conformal anomaly and a contribution to the one-loop effective action associated with the product $\otimes_p \mathcal{L}_p$ of the Laplace operators $\mathcal{L}_p$, $p=1,2$ acting in irreducible rank 1 symmetric spaces are calculated. The explicit form of the zeta functions and the conformal anomaly of the stress-energy momentum tensor is derived. © *1998 American Institute of Physics.* [S0021-3640(98)00203-5]

PACS numbers: 11.25.Hf, 02.30.Tb, 02.30.Jr

1. It is known that the anomaly associated with multiplicative properties of regularized determinants of (pseudo)differential operators can be expressed by means of the noncommutative residue, the Wodzicki residue[1] (see also Refs. 2 and 3). The Wodzicki residue, which is the unique extension of the Dixmier trace to the wider class of (pseudo)differential operators,[4,5] has been considered within the noncommutative geometrical approach to the standard model of the electroweak interactions[6–11] and the Yang–Mills action functional. Some recent papers along these lines can be found in Refs. 12–14. The product of two (or more) differential operators of the Laplace type can arise in higher-derivative field theories (for example, in higher-derivative quantum gravity[15,16]). The partition function corresponding to the product of two elliptic second-order differential operators for the simplest $O(2)$ invariant model of self-interacting charged fields in $\mathbb{R}^4$ (Ref. 17) has been derived recently in Ref. 18.

Note also that the conformal deformations of a metric and the corresponding conformal anomaly can play an important role in quantum theories with higher derivatives. In fact evaluation of the conformal anomaly is actually possible only for even-dimensional spaces, and up to now its computation has been extremely involved. The general structure of such anomaly in curved d-dimensional spaces (d even) has been studied in Ref. 19. Analysis related to this phenomenon for constant-curvature spaces will be briefly mentioned below. The conformal anomaly calculation for a d-dimensional sphere can be found in Refs. 20 and 21. The explicit computation of the anomaly (of the

stress-energy tensor) for scalar and spinor quantum fields in d-dimensional compact hyperbolic spaces has been carried out in Ref. 22 (see also Refs. 23 and 24) using zeta-function regularization and the Selberg trace formula techniques.

2. The purpose of this letter is to analyze a contribution to the effective action (in general form) and the conformal anomaly associated with the product $\otimes_p \mathcal{L}_p$, where $\mathcal{L}_p$, $p=1,2$, are the Laplace operators acting in general rank 1 symmetric spaces. We shall be working with irreducible rank 1 symmetric spaces $M \equiv X = G/K$ of noncompact type. Thus G will be a connected noncompact simple split rank 1 Lie group with finite center and $K \subset G$ a maximal compact subgroup. The following representations of X up to local isomorphism can be chosen

$$X = \begin{bmatrix} SO_1(n,1)/SO(n) & \text{(I)} \\ SU(n,1)/U(n) & \text{(II)} \\ SP(n,1)/(SP(n)\otimes SP(1)) & \text{(III)} \\ F_{4(-20)}/\mathrm{Spin}(9) & \text{(IV)} \end{bmatrix}, \tag{1}$$

where $n \geqslant 2$, and $F_{4(-20)}$ is the unique real form of F_4 (with Dynkin diagram $\bigcirc - \bigcirc = \bigcirc - \bigcirc$) for which the character $(\dim X - \dim K)$ assumes a value of -20 (Ref. 25). We assume that if G_1 or $G_2 = SO(m,1)$ or $SU(q,1)$, then m is even and q is odd.

We shall need further a suitable regularization of the determinant of an elliptic differential operator, and shall make the choice of zeta-function regularization. The spectral zeta function associated with the product $\otimes \mathcal{L}_p$ has the form

$$\zeta(s|\otimes_p \mathcal{L}_p) = \sum_{j \geqslant 0} n_j \prod_p^2 (\lambda_j + b_p)^{-s}, \tag{2}$$

where $\{\lambda_l\}_{l=0}^{\infty}$ is the set of eigenvalues of the Laplace operator L, while $n_l(\chi)$ denote the multiplicity of λ_l; $\mathcal{L}_p \equiv L + b_p$, and b_p are arbitrary constants. We shall always assume that $b_1 \neq b_2$, say $b_1 > b_2$. If $b_1 = b_2$ then $\zeta(s|\otimes \mathcal{L}_p) = \zeta(2s|\mathcal{L})$ is a well-known function.

For $\mathrm{Re}\, s > d/4$ the explicit meromorphic continuation holds:[26]

$$\zeta(s|\otimes_p \mathcal{L}_p) = A \sum_{j=0}^{d/2-1} a_{2j} (\mathcal{F}_j(s) - E_j(s)) + \mathcal{I}(s), \tag{3}$$

where

$$E_j(s) = 4 \int_0^{\infty} \frac{dr r^{2j+1}}{1 + e^{2a(G)r}} \prod_p (r^2 + B_p)^{-s}, \tag{4}$$

which is an entire function of s, and

$$\mathcal{F}_j(s) = (B_1 B_2)^{-s} \times \frac{j!(2B_1B_2/B_1+B_2)^{j+1} F(j+1/2, j+2/2; s+1/2; (B_1 - B_2/B_1+B_2)^2)}{(2s-1)(2s-2)\ldots(2s-(j+1))}, \tag{5}$$

$$\mathcal{I}(s) = (b_1 - b_2)^{1/2-s} \frac{\sqrt{\pi}}{\Gamma(s)} \int_0^{\infty} dt\, \theta(t) I_{s-1/2}\left(\frac{b_1 - b_2}{2} t\right) t^{s-1/2}. \tag{6}$$

In Eqs. (3)–(6) $B_p=\rho_0^2+b_p$, $\rho_0=(n-1)/2$, n, $2n+1$, and 11, respectively, in cases (I)–(IV) in Eq. (1), $F(\alpha,\beta;\gamma;z)$ is the hypergeometric function, $I_\nu(z)$ are the Bessel functions, $\theta(t)$ is an entire function of t, and A is some constant (for more details see Ref. 26). The suitable Harish–Chandra–Plancherel measure is given as follows:

$$|C(r)|^{-2}=C_G\pi r P(r)\tanh(a(G)r)=C_G\pi\sum_{l=0}^{d/2-1}a_{2l}r^{2l+1}\tanh(a(G)r), \tag{7}$$

where

$$a(G)=\left[\begin{array}{ll}\pi & \text{for } G=SO_1(2n,1)\\ \dfrac{\pi}{2} & \text{for } G=SU(q,1), \quad q \text{ odd}\\ & \text{or } G=SP(m,1), \quad F_{4(-20)}\end{array}\right], \tag{8}$$

while C_G is some constant depending on G, and where the $P(r)$ are even polynomials (with suitable coefficients a_{2l}) of degree $d-2$ for $G\neq SO(2n+1,1)$, and of degree $d-1=2n$ for $G=SO_1(2n+1,1)$ (Refs. 24 and 27).

The goal now is to compute the zeta function $\zeta(s|\otimes_p\mathcal{L}_p)$ and its derivative at $s=0$. Thus we have

$$\zeta(0|\otimes_p\mathcal{L}_p)=A\sum_{j=0}^{d/2-1}\frac{(-1)^{j+1}}{2(j+1)}a_{2j}\left\{\sum_l^2 B_l^{j+1}+(2-2^{-2j})\left[\frac{\pi}{a(G)}\right]^{2j+2}\mathcal{B}_{2j+2}\right\}, \tag{9}$$

$$\zeta'(0|\otimes_p\mathcal{L}_p)=A\sum_{j=0}^{d/2-1}a_{2j}\sum_l^4\mathcal{E}_l, \tag{10}$$

where

$$\mathcal{E}_1=j!(B_1^{j+1}+B_2^{j+1})\sum_{k=0}^{j}\frac{(-1)^{k+1}}{k!(j-k)!(j+1-k)!}, \tag{11}$$

$$\mathcal{E}_2=B_2^{j+1}\left(\frac{B_1-B_2}{2B_1}\right)\frac{(-1)^j}{(j+1)!}\sum_{k=1}^{\infty}\frac{(j+k+1)!}{(k+1)!}\sigma_k\left(\frac{B_1-B_2}{B_1}\right)^k, \tag{12}$$

$$\mathcal{E}_3=\log(B_1B_2)\frac{(-1)^j}{2(j+1)}(B_1^{j+1}+B_2^{j+1})-4\int_0^\infty\frac{dr\,r^{2j+1}\log(r^2+B_1/r^2+B_2)}{1+e^{2a(G)r}}, \tag{13}$$

$$\mathcal{E}_4\equiv\mathcal{I}'(s=0), \tag{14}$$

and $\sigma_k=\Sigma_{k=1}^n k^{-1}$.

3. After a standard functional integration in scalar theory the contribution to the Euclidean one-loop effective action can be written as follows

$$W^{(1)}=\frac{1}{2}\log\det(\otimes_p\mathcal{L}_p/\mu^2)=-\frac{1}{2}[\zeta'(0|\otimes_p\mathcal{L}_p)+\log\,\mu^2\zeta(0|\otimes_p\mathcal{L}_p)], \tag{15}$$

where μ^2 is a normalization parameter. As a result we have

$$W^{(1)}=-\frac{1}{2}A\sum_{j=0}^{d/2-1}a_{2j}\left[\sum_{l}^{4}\mathcal{E}_l+\log\,\mu^2(\mathcal{F}_j(0)-E_j(0))\right], \tag{16}$$

where

$$\mathcal{F}_j(0)=\frac{(-1)^{j+1}}{2(j+1)}\sum_{l}^{2}B_l^{j+1}, \tag{17}$$

$$E_j(0)=\frac{(-1)^j}{j+1}(1-2^{-2j-1})\left[\frac{\pi}{a(G)}\right]^{2j+2}\mathcal{B}_{2j+2}, \tag{18}$$

$\mathcal{I}(0)=0$, and $\mathcal{B}_{2n}$ are the Bernoulli numbers.

4. In this section we start with a conformal deformation of a (pseudo-)Riemannian metric and the conformal anomaly of the energy stress tensor. For constant conformal deformations the variation of the connected vacuum functional (effective action) can be expressed in terms of the generalized zeta function related to an elliptic self-adjoint operator $\mathcal{O}$ (Ref. 15):

$$\delta W=-\zeta(0|\mathcal{O})\log\,\mu^2=\int_M dx\langle T_{\mu\nu}(x)\rangle\delta g^{\mu\nu}(x), \tag{19}$$

where $\langle T_{\mu\nu}(x)\rangle$ means that all connected vacuum graphs of the stress-energy tensor $T_{\mu\nu}(x)$ are to be included. Therefore the Eq. (19) leads to

$$\langle T_{\mu}^{\mu}(x)\rangle=(\,\mathrm{Vol}M)^{-1}\zeta(0|\mathcal{O}). \tag{20}$$

In the case of sphere S^d of unit radius we have for example $(\,\mathrm{Vol}S^d)=2\pi^{(d+1)/2}/\Gamma((d+1)/2)$, while the Eq. (3) gives $AC_G=(\mathrm{Vol}M)[(4\pi)^{d/2}\Gamma(d/2)]^{-1}$ (see Ref. 24 for details). As a result we have $(\mathrm{Vol}M)=A(4\pi)^{d/2}\Gamma(d/2)$.

Formulas (3), (17), and (18) give an explicit result for the conformal anomaly, namely

$$\langle T_{\mu}^{\mu}(x)\rangle_{(\mathcal{O}=\otimes\mathcal{L}_p)}=\frac{1}{(4\pi)^{d/2}\Gamma(d/2)}\sum_{j=0}^{d/2-1}\frac{(-1)^{j+1}}{2(j+1)}a_{2j}\times\left\{\sum_{l}^{2}B_l^{j+1}+(2-2^{-2j})\left[\frac{\pi}{a(G)}\right]^{2j+2}\mathcal{B}_{2j+2}\right\}, \tag{21}$$

where d is even.

For $B_1=B_2=B$ the anomaly (21) is associated with Laplace operator $\mathcal{L}=L+b$ and has the form

$$\langle T_{\mu}^{\mu}(x)\rangle=\frac{1}{(4\pi)^{d/2}\Gamma(d/2)}\sum_{j=0}^{\frac{d}{2}-1}\frac{(-1)^{j+1}}{2(j+1)}a_{2j}\left\{B^{j+1}+(2-2^{-2j})\left[\frac{\pi}{a(G)}\right]^{2j+2}\mathcal{B}_{2j+2}\right\}. \tag{22}$$

Note that $B=\rho_0^2+m^2$ for a minimally coupled scalar field of mass m.

The simplest case is, for example, $G=SO_1(2,1)\simeq SL(2,\mathbf{R})$; besides, $X=H^2$ is a two-dimensional real hyperbolic space. Then we have $\rho_0^2=1/4$, $a_{20}=1$, $C_G=1$, $a(G)=\pi$, $|C(r)|^{-2}=\pi r\,\tanh(\pi r)$, and finally $\langle T_\mu^\nu(x\in H^2)\rangle=-(b+1/3)/(4\pi)$.

For a real d-dimensional hyperbolic space $C_G=[2^{d-2}\Gamma(d/2)]^{-2}$, while the scalar curvature is $R(x)=-d(d-1)$. For the conformally invariant scalar field we have $B=\rho_0^2+R(x)(d-2)/[4(d-1)]$. As a consequence, $B_1=B_2$ for all constant-curvature spaces; for hyperbolic spaces, $B=1/4$ and

$$\langle T_\mu^\mu(x\in H^d)\rangle=\frac{1}{(4\pi)^{d/2}\Gamma(d/2)}\sum_{j=0}^{d/2-1}\frac{(-1)^{j+1}}{j+1}a_{2j}\{2^{-2j-2}+(1-2^{-2j-1})\mathcal{B}_{2j+2}\}. \tag{23}$$

Thus in conformally invariant scalar theory the anomaly of the stress tensor coincides with one associated with operator product. This statement holds not only for the hyperbolic spaces considered above but for all constant-curvature manifolds as well.

5. In this paper the one-loop contribution to the effective action (16) and the conformal anomaly of the stress-energy momentum tensor (21) related to the operator product have been evaluated explicitly. In addition we have considered the product $\otimes_p\mathcal{L}_p$ of Laplace operators $\mathcal{L}_p$ acting in irreducible rank 1 symmetric spaces. As an example, the conformal anomaly has been computed for real d-dimensional hyperbolic spaces.

We have shown that for the class of constant-curvature manifolds the conformal anomalies associated with the Laplace-type operator $\mathcal{L}$ and the product $\otimes_p\mathcal{L}_p$ coincide. Our formulas can be generalized to the case of transverse and traceless tensor fields and spinors in real hyperbolic spaces (see, for example, Refs. 28–30). Indeed in the case of the spin-1 field (vector field theory), for instance, we should call attention to the fact that the Hodge–de Rham operator $-(d\delta+\delta d)$ acting on co-exact one-forms corresponds to the mass operator $(L+d-1)g_{\mu\nu}(x)$. The eigenvalues of this operator are $\lambda_l+(\rho_0-1)^2$, and for the Proca field of mass m we have $B=(\rho_0-1)^2+m^2$. Finally, we have also computed the anomaly in a simple situation, namely for conformally invariant scalar fields. Our result (23) coincides with the quantum correction reported in Ref. 22 for compact hyperbolic spaces. The conformal anomaly of dilaton-coupled matter in four dimensions has been calculated recently.[31,32] It would be of great interest to generalize our results to the dilaton-dependent trace anomaly.

An extension of the above evaluation of the effective action and the conformal anomaly for higher spin fields seems to us certainly feasible. Analysis of the multiplicative properties of Laplace type operators and related zeta functions will be interesting in view of future applications to concrete problems in quantum field theory and for mathematical applications as well.

A. A. Bytsenko wishes to thank CNPq and the Department of Physics of Londrina University for financial support and kind hospitality. The research of A. A. Bytsenko was supported in part by Russian Fund for Fundamental Research Grant 98-02-18380-a and by Russian Universities Grant 6-18-1997.

[a)]e-mail: abyts@spin.hop.stu.neva.ru
[b)]e-mail: goncalve@fisica.uel.br
[c)]e-mail: williams@math.umass.edu

[1]M. Wodzicki, ''Non-commutative residue,'' in *Lecture Notes in Mathematics*, Vol. 1289, edited by Yu. I. Manin, Springer-Verlag, Berlin (1987), pp. 320 ff.
[2]M. Kontsevich and S. Vishik, Preprint MPI/94-30 (1994).
[3] M. Kontsevich and S. Vishik, http://xxx.lanl.gov/abs/hep-th/9406140.
[4]A. Connes, Commun. Math. Phys. **117**, 673 (1988).
[5]D. Kastler, Commun. Math. Phys. **166**, 633 (1995).
[6]A. Connes and J. Lott, Nucl. Phys. B **18**, 29 (1990).
[7]A. Connes, *Non-Commutative Geometry*, Academic Press, New York, 1994.
[8] A. Connes, http://xxx.lanl.gov/abs/hep-th/9603053.
[9] A. H. Chamseddine and A. Connes, http://xxx.lanl.gov/abs/hep-th/9606001.
[10]A. H. Chamseddine and A. Connes, http://xxx.lanl.gov/abs/hep-th/9606056.
[11] C. P. Martin, J. M. Garcia-Bondia, and J. C. Varilly, http://xxx.lanl.gov/abs/hep-th/9605001.
[12]W. Kalau and M. Walze, J. Geom. Phys. **16**, 327 (1995).
[13]T. Ackermann, http://xxx.lanl.gov/abs/funct-an/9506006.
[14] T. Ackermann and J. Tolksdorf, http://xxx.lanl.gov/abs/hep-th/9503152.
[15]N. D. Birrell and P. C. W. Davies, *Quantum Fields in Curved Space*, Cambridge University Press, Cambridge, 1982.
[16]I. L. Buchbinder, S. D. Odintsov, and I. L. Shapiro, *Effective Action in Quantum Gravity*, A. Hilger, Bristol, 1992.
[17]K. Benson, J. Bernstein, and S. Dodelson, Phys. Rev. D **44**, 2480 (1991).
[18] E. Elizalde, L. Vanzo, and S. Zerbini, http://xxx.lanl.gov/abs/hep-th/9701060.
[19]S. Deser and A. Schwimmer, Phys. Lett. B **309**, 279 (1993).
[20]E. Copeland and D. Toms, Class. Quantum Grav. **3**, 431 (1986).
[21]V. P. Dergalev and S. D. Odintsov, *Effective Action of Conformally-Invariant Theories in Multidimensional Space*, In Gravity and Fundamental Interactions, Moscow 1988.
[22]A. A. Bytsenko, E. Elizalde, and S. D. Odintsov, J. Math. Phys. **36**, 5084 (1995).
[23]E. Elizalde, S. D. Odintsov, A. Romeo *et al.*, *Zeta Regularization Techniques with Applications*, World Scientific, Singapore, 1994.
[24]A. A. Bytsenko, G. Cognola, L. Vanzo, and S. Zerbini, Phys. Rep. **266**, 1 (1996).
[25]S. Helgason, *Differential Geometry and Symmetric Spaces*, Pure and Applied Math. Ser. **12**, Academic Press, 1962.
[26] A. A. Bytsenko and F. L. Williams, http://xxx.lanl.gov/abs/hep-th/9706120.
[27]F. L. Williams, J. Math. Phys. **38**, 796 (1997).
[28]R. Camporesi, Commun. Math. Phys. **148**, 283 (1992).
[29]R. Camporesi and A. Higuchi, Phys. Rev. D **47**, 3339 (1993).
[30]R. Camporesi and A. Higuchi, J. Math. Phys. **35**, 4217 (1994).
[31] S. Nojiri and S. D. Odintsov, http://xxx.lanl.gov/abs/hep-th/9706009.
[32] S. Nojiri and S. D. Odintsov, http://xxx.lanl.gov/abs/hep-th/9706143.

Published in English in the original Russian journal. Edited by Steve Torstveit.

Spin susceptibility of neutron-irradiation-disordered $YBa_2Cu_3O_{6.9}$ in the normal and superconducting states

A. V. Anan'ev,[a)] Yu. I. Zhdanov, A. P. Gerashchenko, K. N. Mikhalev, S. V. Verkhovskiĭ, E. Yu. Medvedev, K. A. Okulova, N. I. Chebotaev, and V. N. Goshchitskiĭ

Institute of Metal Physics, Urals Branch of the Russian Academy of Sciences, 620219 Ekaterinburg, Russia

(Submitted 8 January 1998)
Pis'ma Zh. Éksp. Teor. Fiz. **67**, No. 3, 172–177 (10 February 1998)

The spin-spin relaxation rate $^{63}T_2^{-1}$ of ^{63}Cu nuclei in CuO_2 layers is measured in the normal and superconducting states of the compound $YBa_2Cu_3O_{6.9}$ ($T_c^{\text{onset}}=94$ K) subjected to radiation-induced disordering by a fast-neutron flux Φ to $T_c^{\text{onset}}=68$ K ($\Phi=7\times10^{18}$ cm^{-2}) and $T_c^{\text{onset}}<4$ K ($\Phi=12\times10^{18}$ cm^{-2}). It is found that as the structural disorder increases, the contribution of the indirect spin-spin interaction $^{63}T_{2G}^{-1}$, which is related to the value of the spin susceptibility at the boundary of the Brillouin zone of the copper planes $\chi_s(\mathbf{q}=\{\pi/\mathbf{a};\pi/\mathbf{a}\})$, decreases slightly at the transition to the superconducting state for the initial sample and remains unchanged for the weakly disordered sample. This behavior of the short-wavelength contribution to the spin susceptibility attests to the stability of the x^2-y^2 symmetry of the energy gap against structural disorder, in accordance with proposed theoretical models of Cooper pairing for high-T_c cuprates.
 [S0021-3640(98)00303-X]

PACS numbers: 61.80.Hg, 76.60.Es, 74.72.Bk, 74.25.Nf

The question of the symmetry of the superconducting order parameter—the energy gap $\Delta(\mathbf{q})$—in high-T_c superconducting cuprates is being widely discussed in connection with a possible important role of antiferromagnetic spin fluctuations in the formation of the ground state of the conduction band. Using the random-phase approximation (RPA) in a two-dimensional Hubbard model, Bulut and Scalapino[1] showed that the nonlocal spin susceptibility $\chi_s(\mathbf{q})$, which is enhanced at the boundary of the Brillouin zone of the CuO_2 layer, behaves differently for the isotropic s-type ($\Delta(\mathbf{q})=\text{const}$) and anisotropic $d_{x^2-y^2}$-type ($\Delta(\mathbf{q})\sim(\cos(\mathbf{q}\cdot\mathbf{x})-\cos(\mathbf{q}\cdot\mathbf{y}))$ superconducting pairings. For the traditional isotropic gap, $\chi_s(\mathbf{Q}=\{\pi/\mathbf{a};\pi/\mathbf{a}\})$ approaches zero at temperatures $T\ll T_c$, while for the case of x^2-y^2 symmetry the spin susceptibility $\chi_s(\mathbf{q}\cong\mathbf{Q})$ near the antiferromagnetic ordering vector decreases only very little in the superconducting state. Discussing the nonphoton channel for superconducting pairing on antiferromagnetic spin fluctuations in the ''nearly antiferromagnetic Fermi liquid'' (NAFL) model, the authors of Refs. 2 and 3 arrived at a similar conclusion. Using the BCS expression for $\Delta(T)$, Ito[4] investigated in the NAFL model the temperature dependence of the spatial dispersion $\chi_s(\mathbf{q})$ and discov-

ered that agreement between the computational and experimental results for $YBa_2Cu_3O_{6.98}$ ($T_c = 94$ K) is observed only in the case of $x^2 - y^2$ symmetry of the superconducting order parameter.[5,6] Since superconductivity in cuprates arises near the metal-insulator transition, the question of the evolution of the symmetry of the superconducting gap in the development of structural disorder, leading to Anderson localization of carriers in CuO_2 layers, remains open.[7] An interesting prediction that the *d* symmetry of the superconducting order parameter is stable against disorder is made in Ref. 8 for systems with a strong ''pairing'' interaction and a short pair correlation length. According to data from resistive measurements,[9] in electron-irradiation-disordered YBaCuO there exists a critical density of defects in the oxygen sublattice (~ 0.04) above which a transition occurs into a nonsuperconducting state of the metal. This degradation of T_c is characteristic for the case of an anisotropic *d* gap. Unfortunately, no data on the magnetic state of the atoms near the radiation-induced point defects, which could rule out possible inelastic magnetic scattering as an alternative cause of the decrease in the critical temperature are not presented in that paper. In our earlier works[10,11] it is shown that structural disorder produced by fast neutrons in $YBa_2Cu_3O_{6.9}$ ($T_c^{\text{onset}} = 94$ K) leads to the formation of wide regions of structural relaxation with a very low concentration of magnetic moments and with metallic conductivity above 80 K. For these regions, the uniform contribution to the spin susceptibility $\chi_s(\mathbf{q}=0)$ was observed to decrease sharply with increasing disorder, accompanied by a decrease in T_c. The spin susceptibility decreases at the transition to the superconducting state, attesting to the fact that the Cooper pairs are in a singlet state.

In the present letter we report the results of measurements of the spin-spin relaxation rate of ^{63}Cu copper atoms in CuO_2 layers for $YBa_2Cu_3O_{6.9}$ ($T_c^{\text{onset}} = 94$ K), subjected to radiation-induced disordering by a fast-neutron flux Φ to $T_c^{\text{onset}} = 68$ K ($\Phi = 7 \times 10^{18}$ cm^{-2}) and $T_c^{\text{onset}} < 4$ K ($\Phi = 12 \times 10^{18}$ cm^{-2}).

Pennington and Slichter[12] showed that the spin-spin relaxation of the nuclear spin is determined by an indirect spin-spin interaction, which leads to a Gaussian decay of the amplitude of the spin echo signal $A(2t) \sim \exp(-0.5 \cdot (2t/T_{2H})^2)$ in experiments on ^{63}Cu NQR lines. Below room temperature the dynamic contribution to $^{63}T_{2G}$ from the neighboring nonresonance ^{65}Cu nuclei, discussed in Refs. 13–15, can be neglected, since it is relatively small. The time constant T_{2G} is determined by a product averaged over reciprocal-lattice vectors

$$\frac{1}{T_{2G}} \propto \sqrt{\sum_q A_{cc}^4(\mathbf{q}) \cdot \mathrm{Re}\{\chi_s(\mathbf{q})\}}, \tag{1}$$

where $A_{cc}(\mathbf{q})$ is the magnetic hyperfine interaction constant of a Cu atom in a layer for the direction along a principal axis of the crystal. In NMR experiments, the real part of the dynamic susceptibility is virtually identical to the value of $\chi_s(\mathbf{q}, \omega = 0)$. In the limit of large correlation lengths $\zeta > \mathbf{a}$, the weight of the terms near the antiferromagnetic ordering vector $\mathbf{Q}$ becomes dominant in Eq. (1) and, as was shown in Ref. 12, the Gaussian contribution becomes proportional to the spin susceptibility near $\mathbf{Q}$, normalized to the correlation length of the antiferromagnetic spin fluctuations,

$$1/T_{2Q} \propto \chi_s(\mathbf{Q})/\zeta. \tag{2}$$

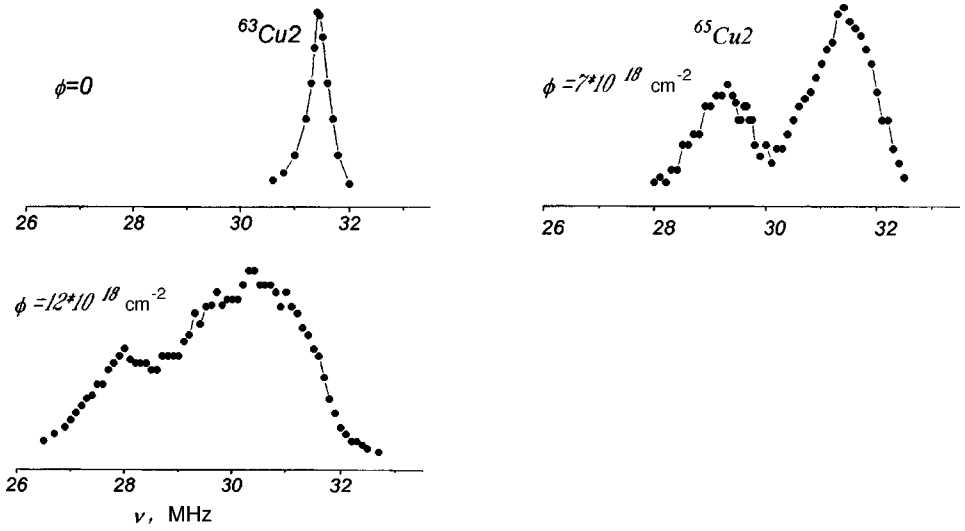

FIG. 1. NQR spectra of a Cu2 line in the initial and disordered $YBa_2Cu_3O_{6.9}$. The spectra were obtained by recording the amplitude of the spin echo of the pulse sequence $\pi/2-\tau-\pi$, where $\tau=15$ ms.

For the initial $YBa_2Cu_3O_{6.9}$ the ratio $\zeta/\mathbf{a}\geqslant 2$ (Ref. 16). As will be shown below, ζ increases in the presence of disorder, reflecting a tendency for short-range magnetic order to form in a strongly disordered ($\Phi\geqslant 20\times 10^{18}$ cm^{-2}) semiconductor state of the cuprate on the insulator side of the Anderson transition.[10] This makes it possible to confine the discussion below to the dominant short-wavelength contributions to the relaxation parameters of ^{63}Cu. Thus, the change in $\chi_s(\mathbf{Q})$ upon transition to the superconducting state in $YBa_2Cu_3O_{6.9}$ can be traced by measuring the spin-spin relaxation rate of ^{63}Cu.

The experiment was performed in zero magnetic field at the frequencies of the ^{63}Cu NQR lines of the Cu2 copper atoms in a CuO_2 layer.[17] The spin echo signal was excited by a sequence of powerful radio pulses $\tau-t-2\tau-t-$echo, with the duration of the second inverting pulse $2\tau\leqslant 2$ μs. The amplitude of the circular component of the rf field H_1 was equal to 220 Oe. Likewise, in all experiments we adhered to a value of Q of the resonance circuit such that the duration of the leading edge of the radio pulse did not exceed 0.1 μm $\ll\tau$. Therefore the excited frequency spectrum was sufficient for inverting the spins $^{63}\mathbf{I}_j$ of the nearest neighbors of the resonant nucleus $^{63}\mathbf{I}_i$, which are located at distances $r_{ij}<(2-3)\zeta$ and make the main contribution to the homogeneous linewidth $(\Delta\nu)_{\text{indir}}$, determined by the indirect interaction of identical spins. The same values of the Gaussian decay $^{63}T_{2G}$ of the echo were obtained in control experiments with half the excitation band, though in this case incomplete excitation of the inhomogeneously broadened NQR line was obtained even for YBaCuO ($\Phi=0$). These experiments lead to a conclusion similar to that drawn in Ref. 17 for $YBa_2Cu_4O_8$. The inhomogeneous linewidth of the Cu2 NQR line is due to a distribution of quadrupole frequencies, and the characteristic change $(\Delta\nu)_{\text{NQR}}$ of the resonance frequency for nuclei lying at a distance of the order of ζ is much smaller than $(\Delta\nu)_{\text{indir}}$. The ^{63}Cu NQR linewidth taken at half maximum (Fig. 1) increases with disorder and at $T<80$ K has the values: $\delta\nu_{0.5}(\Phi=0)=350$ kHz, $\delta\nu_{0.5}(\Phi=7\times 10^{18}\ \text{cm}^{-2})=700$ kHz, and $\delta\nu_{0.5}(\Phi=12\times 10^{18}\ \text{cm}^{-2})=1000$

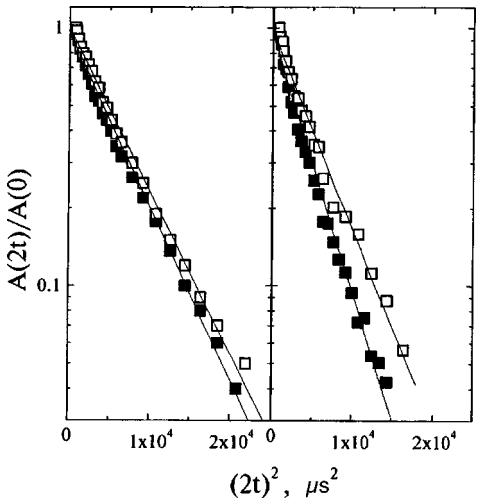

FIG. 2. Decay of the amplitude of the spin echo of ^{63}Cu with allowance for the T_{1R} corrections, for $YBa_2Cu_3O_{6.9}$ ($\Phi = 7\times10^{18}$ cm^{-2}) (left-hand plot) and for $YBa_2Cu_3O_{6.9}$ ($\Phi = 12\times10^{18}$ cm^{-2}) (right-hand plot), measured at the NQR frequency in the Cu2 positions for temperatures of 20 K (■) and 290 K (□).

kHz. In disordered samples the linewidth remained practically constant in the temperature range from 4 to 300 K. Therefore we assume that a 500 kHz band for exciting the spectrum is adequate to avoid problems in the analysis of $^{63}T_{2G}$ over the entire temperature range, in both the normal and superconducting states, for the samples with $\Phi = 0$ and $\Phi = 7\times10^{18}$ cm^{-2}. For the more strongly disordered sample, $\delta\nu_{0.5} > (2\tau)^{-1}$, the data are presented for the purpose of a qualitative discussion of the temperature dependence obtained for $^{63}T_{2G}$ in a nonsuperconducting disordered state of the cuprate on the metallic side of the Anderson transition. Figure 2 displays examples of the decay of the amplitude of the spin echo. These data take into account the additional exponential damping of the echo amplitude due to magnetic spin-lattice relaxation processes, i.e., the damping proportional to $\exp(-2t/T_{1R})$ with $T_{1R} = 3T_{1\mathrm{NQR}}/(2+\mathbf{r})$. The anisotropy coefficient $\mathbf{r} = T_{1\parallel}/T_{1\perp}$ of the spin-lattice relaxation rate of ^{63}Cu was determined from measurements in a magnetic field $B = 9.1$ T in the directions $B \perp c\,(T_{1\perp})$ and $B \parallel c\,(T_{1\parallel} = 3T_{1\mathrm{NQR}})$. As one can see, the sets of data for each of the temperatures are satisfactorily described in semilogarithmic coordinates by straight lines whose slope is proportional to $(^{63}T_{2G})^{-1}$.

Figure 3 shows the results of measurements of $(^{63}T_{2G})^{-1}$ as a function of temperature for disordered $YBa_2Cu_3O_{6.9}$ samples. The data obtained for the initial ($\Phi = 0$) state are close to the published results[18] for the optimally doped $YBa_2Cu_3O_{6.98}$. Near the normal state $(^{63}T_{2G})^{-1}$ increases monotonically with decreasing temperature, following the Curie–Weiss law. A similar behavior of $(^{63}T_{2G})^{-1}$ is predicted for the region of the normal state in the NAFL model, where the spectrum of the spin fluctuations near the wave vector $\mathbf{Q}$ can be described in the effective-field approximation.[12] The value of $(^{63}T_{2G})^{-1}$ decreases very little below T_c. For $T \ll T_c$ this change does not exceed 15% of the value of $(^{63}T_{2G})^{-1}$ near the superconducting transition temperature. As was noted above, the small change in $\chi_s(\mathbf{Q}, T \ll T_c) = (0.9\text{–}1.2)\cdot\chi_s(\mathbf{Q}, T = T_c)$ at the transition to

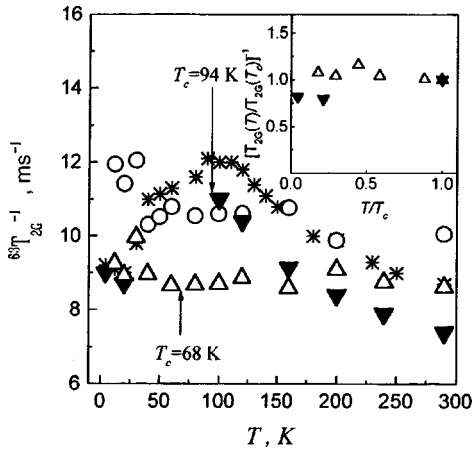

FIG. 3. Temperature dependence of $(^{63}T_{2G})^{-1}$ for $YBa_2Cu_3O_{6.9}$, disordered by fast neutrons: ▽—$T_c^{\text{onset}}=94$ K ($\Phi=0$), △—$T_c^{\text{onset}}=68$ K ($\Phi=7\times10^{18}$ cm^{-2}), ○—$T_c^{\text{onset}}<4$ K ($\Phi=12\times10^{18}$ cm^{-2}). A plot (Ref. 18) of $(^{63}T_{2G})^{-1}$ versus temperature (*) for $YBa_2Cu_3O_{6.98}$ ($T_c=92$ K) is presented for comparison.

the superconducting state is predicted in models of anisotropic pairing with x^2-y^2 symmetry of the superconducting gap.[1–4]

In disordered $YBa_2Cu_3O_{6.9}$ ($\Phi=7\times10^{18}$ cm^{-2}) at temperatures below 200 K the value of $(^{63}T_{2G})^{-1}$ remains unchanged within the error limits of the measurements. This shows that $\chi_s(\mathbf{Q})$ remains constant at the transition to the superconducting state. Therefore it can be concluded that the superconducting order parameter retains its symmetry type in the face of quite substantial disordering of the atomic displacements in the layers adjacent to the CuO_2 layer. This behavior of the short-wavelength part of the spin susceptibility with increasing disorder cannot be explained in models of anisotropic *d* pairing in the weak-coupling approximation, which is characterized by the formation of Cooper pairs with a long coherence length. However, this result apparently can be adequately substantiated in models of superconductivity with strong coupling. Specifically, this refers to the mechanism, which has been proposed for cuprates, of Cooper pairing of carriers on antiferromagnetic spin fluctuations, where T_c is proportional to the characteristic frequency ω_{sf} of spin fluctuations. One can attempt to reveal the trend of the variation of this quantity accompanying disordering by bringing into the discussion previously published data on the nuclear spin-lattice relaxation rate of copper in CuO_2 layers.[19]

When $YBa_2Cu_3O_{6.9}$ becomes disordered, the character of the temperature dependence above T_c changes: The steepness of the growth of the Gaussian contribution to the spin-spin relaxation decreases rapidly with decreasing temperature, and its behavior becomes virtually temperature-independent $(^{63}T_{2G})^{-1}=9.0(5)$ ms^{-1}. In nonsuperconducting $YBa_2Cu_3O_{6.9}$ ($\Phi=12\times10^{18}$ cm^{-2}) $^{63}T_{2G}$ is constant at temperatures where the conductivity is of a metallic character ($T>50$ K). Temperature-independent behavior also appears with disordering for the product $(^{63}T_{1\text{NQR}}T)^{-1}$ (Fig. 4). In the starting compound, $(^{63}T_{1\text{NQR}}T)^{-1}\cong15$ s$^{-1}\cdot$K^{-1} near T_c. As disorder increases, at temperatures ranging from 90 to 200 K the value of this quantity remains unchanged within the error

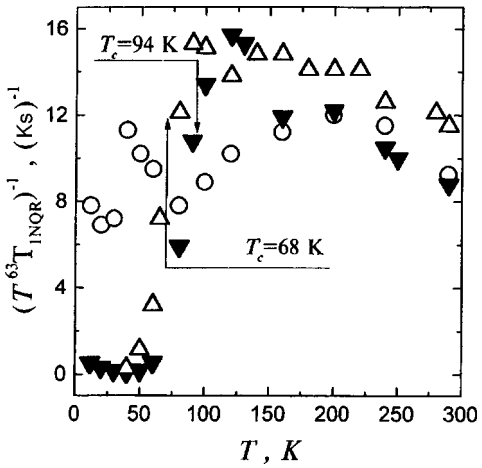

FIG. 4. Temperature dependence of $(^{63}T_{1\mathrm{NOR}}T)^{-1}$ for $YBa_2Cu_3O_{6.9}$ disordered by fast neutrons: ▽—$T_c^{\mathrm{onset}}=94$ K ($\Phi=0$), △—$T_c^{\mathrm{onset}}=68$ K ($\Phi=7\times10^{18}$ cm^{-2}), ○—$T_c^{\mathrm{onset}}<4$ K ($\Phi=12\times10^{18}$ cm^{-2}).

limits of the measurements and equals $(^{63}T_{1\mathrm{NQR}}T)^{-1}\cong14(1)$ s$^{-1}\cdot$K^{-1} for $\Phi=7\times10^{18}$ cm^{-2}. For the nonsuperconducting metal-oxide $\Phi=12\times10^{18}$ cm^{-2}, temperature independence is observed for $(^{63}T_{1\mathrm{NQR}}T)^{-1}\cong10(2)$ s$^{-1}\cdot$K^{-1} at temperatures in the metallic conductivity range ($T>50$ K). For $\xi>\mathbf{a}$ the antiferromagnetic fluctuations make the main contribution to the magnetic relaxation of nuclear spin. This contribution can be represented in the form

$$(^{63}T_{1\mathrm{NQR}}T)^{-1}\propto\frac{\chi_s(\mathbf{Q})}{\Gamma(\mathbf{Q})\xi^2}, \tag{3}$$

where $\Gamma(\mathbf{Q})$ is the characteristic energy of spin fluctuations about the antiferromagnetic ordering vector. In the low-frequency limit this energy is proportional to the quasiparticle density N_Q at the boundary of the Brillouin zone of the CuO_2 layer.[2]

According to Ref. 20, this ''invariant'' behavior of $(^{63}T_{1\mathrm{NQR}}T)^{-1}$ and $^{63}T_{2G}$ is characteristic of a quantum disordered regime with critical exponent $z=2(\omega_{sf}\sim\xi^{-2}N_Q^{-1})$ for a 2D system of interacting spins of the CuO_2 layer in the Heisenberg model. In this regime the magnetic correlation length does not depend on T, in contrast to the quantum critical regime $z=2$ (equivalent to the NAFL approximation) of the initial $YBa_2Cu_3O_{6.9}$, where $\xi^{-2}=\mathbf{a}T+\mathbf{b}$.

It is helpful to consider the changes in the spin-fluctuation parameters implied by the results of the relaxation measurements as interpreted on the basis of the NAFL approximation. In this model, the parameters of the spin-fluctuation spectrum at the center and at the boundary of the Brillouin zone are related through

$$\frac{\xi^4\chi_s(\mathbf{q}=0)}{\Gamma(\mathbf{q}=0)}=\frac{\xi_0^4\chi_s(\mathbf{Q})}{\Gamma(\mathbf{Q})}, \tag{4}$$

where ξ_0 is the characteristic cutoff length of the antiferromagnetic peak in the spectrum of spin fluctuations. A sharp drop in $\chi_s(\mathbf{q}=0)$ (according to data on the shifts of the Cu2 NMR lines[10,11]) with increasing structural disorder, with a much smaller decrease of $\chi_s(\mathbf{Q})/\Gamma(\mathbf{Q})$, signifies an increase in the correlation length of the antiferromagnetic fluctuations $\zeta(\Phi=12\times10^{18}\ \mathrm{cm}^{-2})\cong1.3\xi(\Phi=0)$. Here it is assumed that $\Gamma(\mathbf{q}=0)$, which characterizes the width of the conduction band, does not change with increasing disorder. Thus, the approximate constancy of $^{63}T_{2G}$ in disordered samples attests to a decrease in both the characteristic energy $\Gamma(\mathbf{Q})\sim\xi^{-2}\Gamma(\mathbf{q}=0)$ and characteristic frequency ω_{sf} of the antiferromagnetic fluctuations.

Apparently the temperature independence of $\chi_s(\mathbf{Q})$ is mainly due to the manifestation of localization effects in the character of the carrier scattering and the change which this induces in the degree of screening of spin-spin correlations of neighboring Cu atoms.

This work was performed as part of the Government Programs of the Russian Fund for Fundamental Research in the Field of Condensed Matter Physics, on the topic ''Superconductivity'' (Project 96051) and the Support of Leading Scientific Schools (Project 96-15-96515).

[a)]e-mail: Alexvlan@ifm.ural.ru

[1] N. Bulut and D. J. Scalapino, Phys. Rev. Lett. **67**, 2898 (1991).
[2] P. Monthoux and D. Pines, Phys. Rev. B **49**, 4261 (1994).
[3] P. Monthoux, V. Balatsky, and D. Pines, Phys. Rev. B **45**, 4261 (1992).
[4] Y. Ytoh, J. Phys. Soc. Jpn. **64**, 222 (1995).
[5] T. Imai and C. P. Slichter, Phys. Rev. B **47**, 9158 (1993).
[6] Y. Itoh, H. Yasuoka, Fujiwara *et al.*, J. Phys. Soc. Jpn. **61**, 381 (1991).
[7] B. A. Aleksashin, V. I. Voronin, S. V. Verkhovskiĭ *et al.*, Zh. Éksp. Teor. Fiz. **95**, 678 (1989) [Sov. Phys. JETP **68**, 382 (1989)].
[8] M. V. Sadovskiĭ and A. I. Posazhennikova, JETP Lett. **65**, 270 (1997).
[9] J. Giapintzaks, D. M. Ginsberg, M. A. Kirk, and S. Ockers, Phys. Rev. B **50**, 15967 (1994).
[10] Yu. I. Zhdanov, A. M. Bogdanovich, B. A. Aleksashin *et al.*, Zh. Eksp. Teor. Fiz. **103**, 1762 (1993) [JETP **76**, 868 (1993)].
[11] A. Karkin and B. Goshchitskii, *Electronic States of High-T_c Superconductors Probed by Radiation-Induced Disorder*, Studies of High Temperature Superconductors, edited by A. Narlikar, Nova Science Publishers, New York, Vol. 20**,** 1996.
[12] C. H. Pennington and C. P. Slichter, Phys. Rev. Lett. **66**, 381 (1991).
[13] R. E. Walstedt and A.-W. Cheong, Phys. Rev. B **51**, 3163 (1995).
[14] A. Keren, H. Alloul, Ph. Mendels, and Y. Yoshinari, Phys. Rev. Lett. **78**, 3547 (1997).
[15] N. J. Curo, T. Imai, C. P. Slichter, and B. Dabrovski, Phys. Rev. B **56**, 877 (1997).
[16] D. Thelen and D. Pines, Phys. Rev. B **49**, 3528 (1993).
[17] R. L. Corey, N. J. Curro, C. P. Slichter *et al.*, Phys. Rev. B **53**, 5907 (1996).
[18] Y. Itoh, K. Yoshimura, T. Ohomura *et al.*, J. Phys. Soc. Jpn. **63**, 1455 (1994).
[19] Yu. Zhdanov, B. A. Aleksashin, A. M. Bogdanovich *et al.*, Physica C **165**, 475 (1990).
[20] V. Barzykin and D. Pines, Phys. Rev. B **52**, 13585 (1995).

Translated by M. E. Alferieff

Electron spin resonance and nuclear magnetic resonance of sodium macrostructures in strongly irradiated NaCl–K crystals: Manifestation of quasi-one-dimensional behavior of electrons

F. G. Cherkasov,[a)] R. G. Mustafin, and S. G. L'vov
Kazan Physicotechnical Institute, Russian Academy of Sciences, 420029 Kazan, Russia

G. A. Denisenko
Institute of Crystallography, Russian Academy of Sciences, 11733 Moscow, Russia

H. W. den Hartog and D. I. Vainshtein
University of Groningen, 9747 AG Groningen, The Netherlands

(Submitted 15 December 1997)
Pis'ma Zh. Éksp. Teor. Fiz. **67**, No. 3, 178–183 (10 February 1998)

Data from an investigation of electron spin resonance and nuclear magnetic resonance of NaCl–K (~1 mole%) crystals strongly irradiated with electrons imply the observation of a metal-insulator transition with decreasing temperature and the manifestation of quasi-one-dimensional electron motion in sodium macrostructures. © *1998 American Institute of Physics.* [S0021-3640(98)00403-4]

PACS numbers: 61.80.Fe, 76.30.Lh, 76.60.Es, 72.60.+g, 71.45.Lr

Quasi-one-dimensional inorganic conductors with a complicated crystal structure and unusual properties—Peierls instability, the formation of a charge density wave (CDW) at low temperatures, nonlinear and anisotropic behavior of the conductivity, and so on—are of great interest. The properties of conductors with a CDW have still not been adequately studied, especially at low temperatures.[1] The complexity of the questions and the need to clarify them on more perfect crystals are a constant stimulus for both expanding the range of structures investigated and searching for and obtaining new one-dimensional compounds. Evidently, the suggestion[2] that conducting channels consisting of a quasi-one-dimensional alkali metal can form in simple NaCl-type structures under irradiation with high-energy electrons merits attention. The objective of the present work is to clarify this question experimentally. The methods of investigation consisted of electron spin resonance (ESR) and nuclear magnetic resonance (NMR), which can be used to identify reliably the nature of micro- and macrodefects in irradiated structures.[3]

The ESR and NMR experiments were performed on $3\times3\times1$ mm single-crystal samples of NaCl–KCl (1 mole %). The samples were irradiated in a linear accelerator with electron energy ~3.5 MeV. The total absorbed dose on the sample reached 150 Grad; the irradiation temperature was equal to 100–110 °C. The ESR and NMR signals were measured at 9.4 GHz and 10–105 MHz, respectively, and their behavior was studied in the temperature interval 8–450 K. The magnetic spin susceptibility, which is

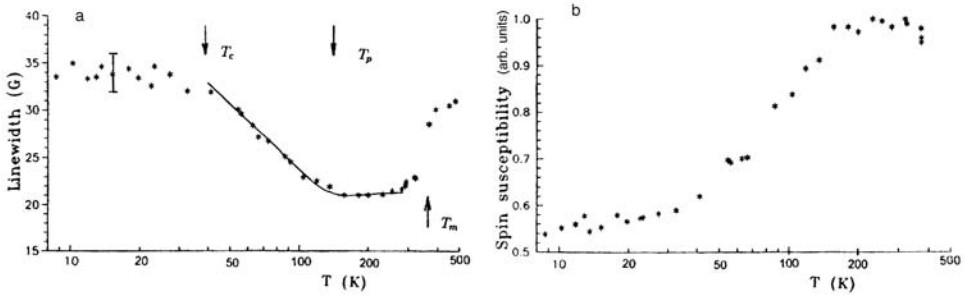

FIG. 1. Temperature dependences of the ESR linewidth (a) and spin susceptibility (b) in an irradiated NaCl–K crystal. The solid line was calculated from Eq. (1).

proportional to the total intensity of the ESR line, was investigated at the same time.

The temperature dependences of the ESR linewidth δH and spin susceptibility χ in irradiated NaCl–K are shown in Fig. 1. The temperature dependence of the intensity I of the NMR signal from metallic ^{23}Na nuclei in the same sample is displayed in Fig. 2 (here, for convenience in describing the data, the characteristic temperature ranges are distinguished from one another by the arrows). At temperatures above $T_p \sim 160$ K the behavior of the entire series of measured parameters was typical for metallic sodium. Here a nearly Lorentzian symmetric shape of the ESR line and a deviation of the g factor of the signal $\Delta g = g - g_0 = (-9 \pm 2) \times 10^{-4}$ from its value for a free electron ($g_0 = 2.0023$) were observed. One can see from Fig. 1 that the temperature dependence $\delta H(T)$ is linear with slope $\sim 2 \times 10^{-2}$ G·K^{-1}, and δH increases by ~ 5.5 G at the point $T_m \approx 370$ K, which is close to the melting point of sodium. The susceptibility χ of the sample behaves similarly to the Pauli susceptibility of the conduction electrons. Two NMR lines from ^{23}Na nuclei were observed: a wide line, corresponding to the nuclei of the ionic lattice of NaCl (and therefore of no interest), and a narrow line, arising at a higher frequency as a result of the presence of mobile electrons and corresponding to the nuclei of metallic sodium. This line is characterized by the standard temperature behavior for nuclei (the intensity is inversely proportional to temperature, Fig. 2), a small width ~ 0.5 kHz, and a Knight shift $K(300\ \text{K}) = 0.108\%$, which was almost temperature-independent. The data obtained (except for the values of δH) are in good agreement with the corresponding published data

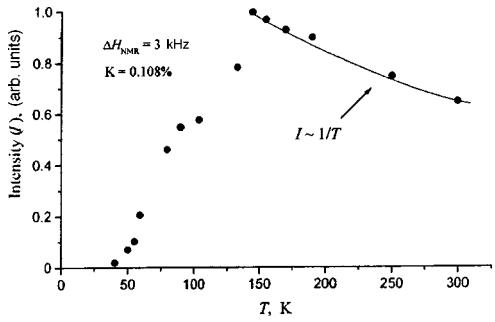

FIG. 2. Temperature dependence of the intensity of the NMR signal from metallic sodium nuclei in NaCl–K.

for sodium (see, for example, Refs. 3 and 4); this confirms the formation of a metallic phase in the sample. The measured value $\delta H(300\ \mathrm{K}) = 22 \pm 2$ G is approximately three times greater than the electron-phonon linewidth in bulk sodium (~ 6 G);[4] this could be a consequence of the additional effective interaction of electrons in the system.

A continuous transition to the properties of the insulator was observed with decreasing temperature. The form of the ESR signal changed, and below the point $T_c \sim 40$ K the signal consisted of a superposition of Lorentzian lines, indicating the appearance of a small variance in the g factors in the system. We were able to measure in the interval 8–30 K the shift of the ESR signal from its position at high temperatures. The shift was equal to $\Delta g = (-12 \pm 3) \times 10^{-4}$. One can see from Fig. 1 that δH increases with decreasing temperature and reaches the value 34 ± 2 G, while χ behaves unusually—it decreases and approaches the value $\chi(300\ \mathrm{K})/2$ (below T_c a ''plateau'' can be seen in both dependences). Near $T_p \sim 160$ K the NMR linewidth increased to ~ 3 kHz and below this temperature it remained constant, while the intensity $I(T)$ decreased continuously to zero. No signal was observed in the interval 8–38 K (Fig. 2).

The observed effects—the vanishing of the NMR signal near T_c and the vanishing of the magnetization $\chi_e(T)$ of the conduction electrons in the system—are a direct consequence of electron localization, which occurs in the region from T_p to T_c. The ''metallic'' ESR and NMR signals are not detected below T_c—a dielectric state of the system arises, and the ESR line observed in the dielectric phase is apparently due to some other (nonconducting) electrons, which contribute a fraction equal to approximately $\chi/2$ to the magnetization. In our view, on the basis of the following considerations, such electrons are F-center electrons. The irradiated alkali-halide crystals comprise systems with paramagnetic defects that can be controlled well. The main defects in strongly irradiated NaCl–K are exchange-coupled F centers (clusters), and when the new phase[b)]—sodium macrostructures (particles or, most likely, chains of the metal)—appears, these centers become the main type of defect in the metal lattice. ESR signals with close values of the g factors are observed from F centers and the metal. It seems to us unlikely that signals from other electronic states appear in the ESR spectrum. In the course of irradiation the electron density and, correspondingly, the intensity of the ESR line from conduction electrons grow and the form of the spectrum changes.[5,6] When the exchange interaction between F-centers becomes strong, which happens when the distance between the centers decreases values of the order of 2–3 lattice constants, the resonance line of the F centers narrows to 30–35 G; the shape of the line looks like a superposition of lines from different clusters of F centers and its integrated intensity (susceptibility) is almost temperature-independent. The interaction with conduction electrons leads to an even greater narrowing of the line from F centers, and the rapid diffusion motion of the conduction electrons averages the g-factor distribution existing in the system. As a result, narrow lines from F-center and conduction electrons become indistinguishable, and at high temperatures a combined resonance of both electronic systems can occur. Since a metal-insulator transition occurs in the system with decreasing temperature, a resonance line characterized by ESR parameters of only F centers will correspond to the dielectric phase, as was conjectured above.

An interesting result was obtained in the ESR measurements: As the temperature decreases, the linewidth δH of the resonance line at $T_p \sim 160$ K starts to increase in inverse proportion to χ (Fig. 1). This fact can shed light on the characteristic features of

the metal-insulator transition in the system and makes it possible to describe the observed behavior of $\delta H(T)$. Let us return to our conjecture that conduction-electron spins (which we denote by the index e) and the localized spins of F-center electrons (s) are both present in NaCl–K on the metallic side of the transition. In the presence of two spin subsystems, a sharp ''bottleneck'' regime (combined e and s electron resonances) is realized in NaCl–K, since the g factors of both systems are equal, $g_e = g_s$, and $1/T_{sL} > 1/T_{eL}$, where T_{sL} and T_{eL} are the spin-lattice relaxation times of the s and e electrons, respectively. A model of ESR of localized spins in a metal has been proposed in Ref. 7. In the case of a bottleneck the linewidth of the resonance line is $\delta H \approx (\chi_s T_{sL}^{-1} + \chi_e T_{eL}^{-1})/(\chi_s + \chi_e)$, i.e., the fraction of the magnetization for each subsystem is multiplied by the spin-lattice relaxation rate in this subsystem. As the temperature decreases, the susceptibility of the system $\chi = \chi_s + \chi_e$ decreases because χ_e decreases (by $\sim 50\%$) and in consequence χ_s—the contribution from localized spins—should be much greater than the Pauli susceptibility χ_e of the conduction electrons. Hence it follows that $\delta H \approx 1/T_{sL}$. Since the spin-lattice relaxation constant is controlled by the interaction with the conduction electrons, we have $1/T_{sL} \approx (1/2)\omega_{hf}^2 T_{se}$, where ω_{hf} is the hyperfine structure constant and T_{se} is the cross-relaxation time of F-center electrons to conduction electrons. From the balance equation $T_{se}/T_{es} = \chi_s/\chi_e$, where T_{es} is the cross-relaxation time of conduction electrons to F-center electrons, we arrive at the desired result[7]

$$\delta H \sim (\chi_s/\chi_e) T_{es}, \tag{1}$$

where χ_e decreases with temperature, χ_s is almost temperature-independent, and $1/T_{es} = 2\pi c \rho J^2$ (c is the localized-spin density, ρ is the density of states at the Fermi surface, and J is the exchange interaction constant of s and e electrons). The behavior of $\delta H(T)$ can be described in the present model of two types of electrons[7] with $\rho = 30\ \mathrm{eV}^{-1}$ (from the free-electron approximation), $J \approx 1.2 \times 10^{-5}$ eV, $\omega_{hf} = 9 \times 10^9\ \mathrm{s}^{-1}$, and density $c \cong 6 \times 10^{18}\ \mathrm{spin/cm}^3$, as found from the ESR measurements. To obtain agreement with experiment, a T-dependent ''intrinsic'' (electron-phonon) linewidth in sodium, which is ~ 6 G at 300 K,[8] must be added to expression (1).

It follows from Fig. 1a that the linewidth increases logarithmically with decreasing temperature, $\delta H \sim \ln(1/T)$. This behavior is confirmed by ESR measurements on samples with a high density of localized impurities (F-centers). Taking into account simultaneously this contribution and the phonon contribution to δH, which decreases with temperature, explains the presence of a minimum in the observed temperature dependence $\delta H(T)$. Figure 3 shows a minimum of the linewidth of the resonance line for three NaCl–K samples with different localized-spin densities. According to Refs. 4 and 8, the temperature-dependent part of the ESR linewidth in alkali metals varies as the temperature-dependent part of the resistivity. As a result, the behavior of the minimum of the linewidth (Fig. 3) is analogous to that of the minimum of the resistivity in dilute alloys with magnetic impurities (Kondo effect[c)]). Within the limits of the measurement accuracy of the electron density c, the temperature of the minimum $T_{\min}$ varies as $\sim c^{1/5}$ (see, for example, Ref. 9). Measurements of the ac conductivity at 400 Hz to 20 kHz in the same types of samples showed a sharp peak near $T_{\min}$ (see Ref. 2). Moreover, the appearance of a maximum in $\delta H(T)$ (instead of a ''plateau'') in some samples at low temperatures was likewise predicted by the theory of Ref. 9. The exchange interaction between conduction electrons and a local moment corresponds to a scattering process in which the spin of the conduction electron can flip and at the same time the orientation of

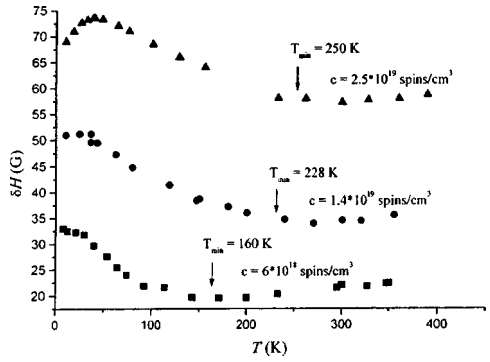

FIG. 3. Minimum of the ESR linewidth in NaCl–K samples with different density of localized impurities (F-centers). The position of the minimum depends on this density.

the impurity spin changes.[9,10] The latter fact could be used to explain the locations of conduction electron localization in the sample, but this requires that the contribution of localized impurities to the linewidth be taken into account in detail on the basis of an accurate model.

It follows from our data that electron localization occurs in NaCl–K and that metallic resonances die out in the transition region (40–160 K). This behavior is typical for quasi-one-dimensional systems and in many cases it is a consequence of a Peierls transition at temperature T_p, which usually lies in the range 100–200 K. Below this temperature lattice distortions arise, giving rise to a gap at the Fermi surface, a decrease of the electron energy, and electron localization. The largest changes in the system occur at temperature $\sim T_p/4$ (transition to a dielectric state, observation of superstructure—a CDW with period $2k_F$, and so on). The hypothesis that the transition in NaCl–K is of a Peierls character can be confirmed or rejected by means of x-ray observations of the superstructure at temperatures below 40 K.

The observation of a frequency dependence of the spin-lattice relaxation rate T_1^{-1} of the metallic nuclei provides a direct check of the quasi-one-dimensionality of the conduction electron motion. Such measurements have been performed on different organic conductors.[11] Figure 4 shows the frequency dependence of the relaxation rate T_1^{-1} of the metallic ^{23}Na nuclei in a NaCl–K crystal at room temperature. One can see that the relaxation rate varies as $T_1^{-1} \sim \nu_n^{-1/2} \sim \nu_e^{-1/2} \sim H_0^{-1/2}$ in magnetic fields 50 G$<H_0<$5 kG, where ν_e is the electronic Larmor frequency and ν_n is the nuclear Larmor frequency. The figure also shows a frequency-independent value of the nuclear relaxation rate in bulk sodium $T_1^{-1}=62.5\ \mathrm{s}^{-1}$ measured in high fields ($H_0 \gg 5$ kG). The diffusive behavior of electrons first appears at frequencies $\omega_e < \omega_c \approx (1/\tau)N$, where ω_e is the electronic frequency, $\tau \cong \lambda/\nu_F$, λ is the electron mean free path (350 Å at 300 K), ν_F is the Fermi velocity, and the parameter $N \cong (d/a)^2$ takes into account the geometry of the conductor (a is the lattice constant and d is the transverse size of a chain). In the case $\omega_e < \omega_c$, there is a high probability that an electron will repeatedly interact with the same nucleus in the time interval $2\pi/\omega_e$. In contrast to the three-dimensional case, this results in a frequency-dependent relaxation rate:[11]

$$(T_1T)^{-1} = C_{1g}(\omega_e) + C_2, \tag{2}$$

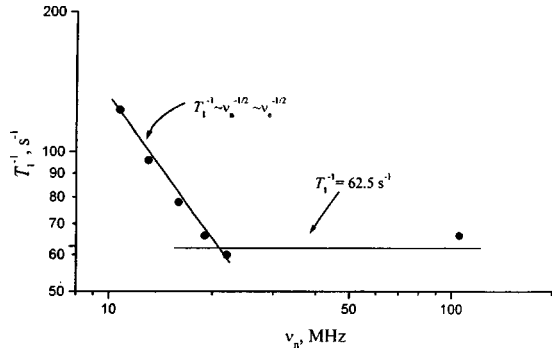

FIG. 4. Frequency dependence of the spin-lattice relaxation rate T_1^{-1} of metallic nuclei in a NaCl–K crystal at room temperature (ν_e(GHz)$=2.486\nu_n$(MHz)).

where

$$g(\omega_e)=\{[1+(1+k)^{1/2}]/2(1+k)\}^{1/2}, \quad k=\omega_e^2\tau_e^2,$$

τ_e is the characteristic electron lifetime on a given chain with a given direction of the spin, and the parameters C_1 and C_2 are independent of ω_e. It follows from Eq. (2) that in the case $k \gg 1$, when relaxation of the electronic spin and hopping between chains can be neglected, a square-root frequency dependence should be observed $g(\omega_e)=(1/\omega_e)^{1/2}$. It is obvious from Fig. 4 that for $\omega_e > \omega_c \approx 2\times 10^{11}$ s^{-1} the nuclear relaxation rate no longer depends on frequency, and the observed value $(T_1T)^{-1}=0.2$ (s·K)$^{-1}$ is close to the value for bulk sodium. Hence the average transverse size of the conducting channels can be estimated as $d \cong a(\nu_F/2\pi\lambda\nu_c)^{1/2} \cong 12a$, i.e., quasi-one-dimensional behavior of the electrons can appear at room temperatures.

We thank K. M. Salikhov, G. B. Teĭtel'baum, Yu. V. Yablokov, B. P. Vodop'yanov, and R. I. Khaĭbullin for helpful discussions. This work was supported by the Russian Fund for Fundamental Research (Grant 96-02-18255).

[a)]e-mail: fred@dionis.kfti.kcn.ru

[b)]Nonequilibrium growth of an electronic structure consisting of F-centers and formation of a metallic lattice on the basis of such a structure occur at high irradiation temperatures and with the participation of impurities, such as K, OH^-, or F. A metallic phase does not arise in pure NaCl crystals.[5,6]

[c)]As is well known,[9,10] the expression for the interaction energy of an electron with impurity atoms contains a term $\mathbf{J}(\mathbf{s}\cdot\mathbf{S})$ (where $\mathbf{s}$ is the electron spin and $\mathbf{S}$ is the impurity spin), which in high orders of perturbation theory leads to a spin-dependent contribution to the electron scattering and therefore to the resistance. Kondo explained the growth in the resistance with decreasing temperature and the appearance of a minimum of the resistance whose position depends on the density of magnetic impurities.

[1] S. N. Artemenko, A. F. Volkov, and S. V. Zaĭtsev-Zotov, Usp. Fiz. Nauk **166**, 434 (1996).
[2] D. I. Vainshtein, H. P. den Hartog, H. W. den Hartog *et al.*, in *Thirteenth International Conference on Defects in Insulating Materials*, Wake Forest University, Winston-Salem, NC, USA, 1996, p. 16; F. G. Cherkasov, R. G. Mustafin, S. G. L'vov *et al.*, in *International Conference on Magnetism*, Austr. Inst. of Physics, Australia, 1997, p. K3-30.
[3] A. E. Hughes and S. C. Jain, Adv. Phys. **28**, 717 (1976).
[4] Y. Yafet, Solid State Phys. **14**, 1 (1963).
[5] D. I. Vainshtein and H. W. den Hartog, Radiat. Eff. Defects Solids **137**, 73 (1995).

[6] S. G. L'vov, F. G. Cherkasov, A. Ya. Vitols *et al.*, Appl. Radiat. Isot. **47**, 1615 (1996).
[7] A. M. Finkel'shteĭn, JETP Lett. **46**, 513 (1987).
[8] B. M. Khabibullin and É. G. Kharakhash'yan, Usp. Fiz. Nauk **111**, 483 (1973) [Sov. Phys. Usp. **16**, 806 (1974)].
[9] A. A. Abrikosov, *Introduction to the Theory of Normal Metals* [in Russian], Nauka, Moscow, 1972.
[10] S. E. Barnes, Adv. Phys. **30**, 801 (1981).
[11] D. Jerome and H. J. Schulz, Adv. Phys. **31**, 299 (1982).

Translated by M. E. Alferieff

Coulomb interaction during coherent transport of electrons in quantum wires

V. A. Sablikov[a)] and B. S. Shchamkhalova
Institute of Radio Engineering and Electronics, Russian Academy of Sciences, 141120 Fryazino, Moscow Region, Russia

(Submitted 16 December 1997)
Pis'ma Zh. Éksp. Teor. Fiz. **67**, No. 3, 184–189 (10 February 1998)

A model is found whereby the Coulomb interaction during electron transport in quantum wires of finite length with current-lead contacts can be taken into account exactly (within the framework of the bosonization method). It is established that the charge density distribution along a wire in the case of the real Coulomb interaction is strongly different from the Luttinger liquid model, where the interaction is assumed to be short-ranged. The charge density near the contacts is found to be much higher than in the model with a short-range interaction, but away from the contacts the two densities are closer to each other. [S0021-3640(98)00503-9]

PACS numbers: 73.20.Dx, 73.23.Hk

1. Electron transport in quantum wires of mesoscopic length arouses great interest among both experimenters[1–3] and theorists,[4–12] since the electron-electron interaction, which is of fundamental importance in mesoscopic systems, should be manifested in the transport characteristics (such as the conductance or admittance). The most widely used approach for analyzing electron-electron interaction effects is based on the Luttinger liquid model, which makes it possible to calculate the conductance in the case when the electron-electron interaction is short-ranged. A parameter g describing the interaction-induced renormalization of the propagation velocity of charge waves arises in the theory. Generally speaking, g is a function of the wave number p of the boson excitations and is estimated as

$$g(p)=(1+V_p/\pi v_F)^{-1/2},$$

where V_p is the Fourier transform of the interaction potential and v_F is the Fermi velocity (here and below $\hbar=1$). The assumption that the interaction is short-ranged means that g is assumed to be constant: $g(p)\approx g(p=0)$.

In reality, however, the Coulomb potential is a long-range potential. It is often considered that the assumption that the potential is short-ranged is justified by the presence of good conductors (field electrodes and current-lead contacts), which screen the electron-electron interaction, in the experimental structures.[13] In reality, however, this is not the case: The screening action of these conductors consists in the fact that image charges are induced on them, as a result of which the electron-electron interaction ac-

quires a dipole character or, generally speaking, a multipole character, but the dependence of V_p on p remains strong. Charge waves under the conditions of a long-range Coulomb interaction have been studied by Shultz[14] for an infinite one-dimensional conductor, for which the interaction potential is a function only of the distance between the electrons $V(x,x')=V(|x-x'|)$. In this case a dispersion relation is obtained for charge waves that is similar to the dispersion relation for one-dimensional plasmons in the random-phase approximation. As was recently determined,[4–7] however, the fact that in real mesoscopic structures the quantum wire is of finite length and the electrons in the wire interact with the current-lead electrodes is of fundamental importance. In such a situation the pair interaction potential $V(x,x')$ depends on the coordinates x and x' of the interacting electrons separately.

Thus, in investigations of phase-coherent electron transport in mesoscopic quantum wires it is necessary to take into account both the nonlocality of the electron-electron interaction and the presence of current-conducting electrodes. The present letter is devoted to solving this problem. We have found a model that is exactly solvable in the framework of the bosonization method and that takes into account the Coulomb interaction of the electrons in a quantum wire with ideally conducting current contacts.

2. Let us consider an interaction potential of the electrons in a quantum wire (channel) of length L, connecting two massive regions serving as current-lead electrodes. Since we are interested in the behavior of the electrons in the wire, we shall assume that the conductivity of the electrodes is ideal and that the characteristic times of the electronic processes in them are short compared with the transit time of electrons in a channel. Then the electrodes can be assumed to be equipotentials. The electrons in a channel interact with one another both directly and via the charges that they induce on the electrode surfaces. We shall represent the electron density $\rho(\mathbf{r})$ in a channel in the form

$$\rho(\mathbf{r})=\chi(\mathbf{r}_\perp)\rho(x), \tag{1}$$

where $\chi(\mathbf{r}_\perp)$ is a function of the radial coordinate and is normalized to unity and $\rho(x)$ is a function of the coordinate along the channel.

The electron-electron interaction energy W is determined by an integral of the product of the charge density $\rho(\mathbf{r})$ by the potential produced at the point $\mathbf{r}$ by a charge located at the point $\mathbf{r}'$:

$$W=\frac{2\pi e^2}{\epsilon}\int d^3r\ \rho(\mathbf{r})\int d^3r'\rho(\mathbf{r}')G(\mathbf{r},\mathbf{r}'), \tag{2}$$

where $G(\mathbf{r},\mathbf{r}')$ is the solution of the equation

$$\nabla^2 G(\mathbf{r},\mathbf{r}')=-\delta(\mathbf{r}-\mathbf{r}') \tag{3}$$

with the boundary conditions $G(\mathbf{r}_s,\mathbf{r}')=0$ on the surface of the electrodes ($\mathbf{r}=\mathbf{r}_s$) and ϵ is the dielectric constant of the material outside the channel.

Fourier transforming with respect to $\mathbf{r}_\perp$ and using Eqs. (1), (2), and (3), we obtain

$$W=\frac{1}{2}\int\int dx\ dx'\rho(x)\rho(x')U(x,x'), \tag{4}$$

where

$$U(x,x')=\frac{e^2}{\pi\epsilon}\int d^2q|\chi_q|^2G_q(x,x'), \tag{5}$$

χ_q is the Fourier transform of the function $\chi(\mathbf{r}_\perp)$, and $G_q(x,x')$ is the solution of the equation

$$(d^2/dx^2-q^2)G_q(x,x')=-\delta(x-x').$$

If it is assumed for definiteness that the surfaces of the electron reservoirs serving as the electrodes are parallel planes perpendicular to the channel, then simple calculations yield

$$G_q(x,x')=\frac{L}{qL\ \sinh(qL)}\begin{cases}\sinh[q(L/2+x)]\sinh[q(L/2-x')], & \text{if} \quad x<x',\\ \sinh[q(L/2-x)]\sinh\,[q(L/2+x')], & \text{if} \quad x>x'.\end{cases} \tag{6}$$

For $|x-x'|\ll a$ the interaction potential U determined by Eqs. (5) and (6) is of the order of L/a; at large distances ($|x-x'|\gg a$) it becomes identical to the Coulomb law $U\approx 1/|x-x'|$, but U vanishes at the electrodes (at x and/or $x'=\pm L/2$). The latter behavior is due to the fact that as an electron approaches the conducting surface of an electrode, the potential of the electron is screened by the induced image charge. The interaction potential given by Eqs. (5) and (6) is the one we will use in the present letter.

3. We shall obtain the equation of motion of electrons in a channel from the bosonized Hamiltonian[15,14]

$$H=\frac{1}{2\pi}\int dx v_F[(1+g_1)\pi^2\Pi^2(x,t)+(1-g_1)(\partial_x\Phi)^2]-e\int dx\rho(x,t)\varphi_{\text{ext}}(x,t)+W, \tag{7}$$

where $\Phi(x,t)$ is the bosonic phase field, $\Pi(x,t)$ is the generalized momentum conjugate to Φ, g_1 is the backscattering parameter,[14]

$$g_1\approx\frac{e^2}{\epsilon h v_F}K_0(2k_Fa),$$

K_0 is a modified Bessel function, and φ_{ext} is the potential of the external field applied to the electrodes.

The electron density ρ (more accurately, its long-wavelength component) can be expressed in terms of Φ as

$$\rho=-\frac{1}{\pi}\partial_x\Phi.$$

The Hamiltonian (7) corresponds to the following equation of motion for the phase Φ:

$$\partial_t\left(\frac{1}{v\widetilde{g}}\partial_t\Phi\right)-\partial_x\left(\frac{v}{\widetilde{g}}\partial_x\Phi\right)=\partial_x\left[e\varphi_{\text{ext}}+\frac{1}{\pi}\int_{-L/2}^{L/2}dx'U(x,x')\partial_{x'}\Phi\right], \tag{8}$$

where

$$v = v_F\sqrt{1-g_1^2}, \quad \tilde{g} = \sqrt{\frac{1+g_1}{1-g_1}}.$$

Following Refs. 5–7, we shall extend Eq. (8) to the contact regions as well, making the assumption that there is no electron-electron interaction in these regions. The boundary conditions should ensure continuity of Φ and the electron flux, whence it follows that the quantity $(v/\tilde{g})\partial_x\Phi$ should be continuous at the boundaries.

4. The phase Φ always changes with time, so that in studying a situation that corresponds even to a constant current it is necessary to start from equations with the time included and then, if necessary, to pass to the constant-current limit. For perturbations that depend on time as $\exp(-i\omega t)$, after a change to dimensionless variables

$$\xi = \frac{x}{L}, \quad u = \frac{v\Phi}{e\tilde{g}LV_a}, \quad f = \frac{\varphi_{\text{ext}}}{V_a},$$

Eq. (8) assumes the form

$$\frac{d}{d\xi}\left[\frac{du}{d\xi} + \beta\hat{V}\frac{du}{d\xi} - f(\xi)\right] + \Omega^2 u = 0, \tag{9}$$

where V_a is the amplitude of the voltage applied to the electrodes, $\beta = e^2\tilde{g}/\pi\epsilon v$, $\Omega = \omega L/v$, and the operator $\hat{V}$ is defined by the equation

$$\hat{V}\psi = \int_{-1/2}^{1/2} d\xi' V(\xi,\xi')\psi(\xi'), \tag{10}$$

where

$$V(\xi,\xi') = 2\int_0^\infty \frac{dy}{\sinh y}|\chi_y|^2 \begin{cases} \sinh[y(1/2+\xi)]\sinh[y(1/2-\xi')], & \text{if} \quad \xi<\xi', \\ \sinh[y(1/2-\xi)]\sinh[y(1/2+\xi')], & \text{if} \quad \xi>\xi' \end{cases}$$

(here $y = qL$). Having solved the equation for the regions outside the channel, we can formulate the boundary conditions for Eq. (9) inside the channel:

$$u_\xi \pm i\Omega\tilde{g}u|_{\xi=\mp 1/2} = 0 \ .$$

In the low-frequency limit Eq. (9) can be solved exactly on account of the fact that it is possible to find for the operator $\hat{V}$ a system of eigenfunctions in terms of which the external potential $f(\xi)$ can be expanded. It is easily verified that the functions

$$\psi_n(\xi) = \sqrt{2}\,\sin\left[\pi n\left(\xi + \frac{1}{2}\right)\right], \quad n = 1,2,3,\ldots,$$

are eigenfunctions for the operator $\hat{V}$ with eigenvalues

$$\lambda_n = 2\int_0^\infty \frac{y\,dy}{y^2+(n\pi)^2}|\chi|^2.$$

In the present electrode geometry $f(\xi)$ is a linear function that can be expanded in terms of $\psi_n(\xi)$ with even n.

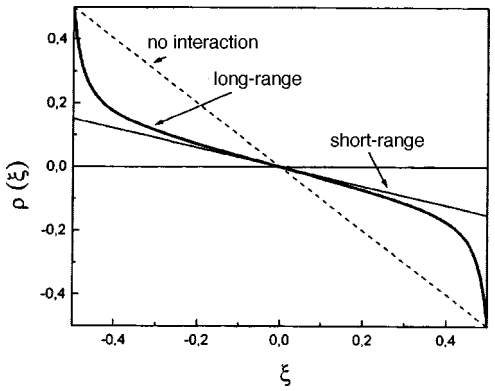

FIG. 1. Electron density distribution (normalized to $2eV_a/h\upsilon_F$) along a quantum wire with a Coulomb interaction between the electrons (solid line), no interaction (dashed line), and a short-range interaction with g_{eff} (fine line); $\varepsilon_F = 5$ meV, $\alpha = 0.02$, $\beta = 0.35$.

Treating Ω as a small parameter and making a direct expansion in terms of it, we find the dimensionless fluctuation of the electron density, $-u_\xi(\xi)$, in the limit $\Omega \to 0$:

$$u_\xi(\xi) = -\sum_{n=1}^{\infty} \frac{(-1)^n}{n(1+\beta\lambda_{2n})} \sin(2\pi n\xi). \tag{11}$$

The dimensional electron density is related with u_ξ by the relation

$$\rho(\xi) = -\frac{2e\tilde{g}V_a}{h\upsilon} u_\xi(\xi). \tag{12}$$

A plot of the function $\rho(\xi)$ is shown in Fig. 1 for a Gaussian electron density distribution (1) over the radial coordinate. Near the electrodes μ_ξ changes rapidly. In this case, using the asymptotic behavior $\lambda_n \sim n^{-2}$, we obtain the following expression for u_ξ near the left-hand electrode ($(1/2+\xi) \ll 1$):

$$u_\xi(\xi) \approx \sinh(2\kappa\xi)/2\sinh\kappa, \tag{13}$$

where $\alpha = a/L$ and $\kappa = \alpha^{-1}\sqrt{\beta/2}$. One can see that the nonequilibrium electron density decreases into the volume of the channel exponentially with a characteristic length

$$\ell = a/\sqrt{2\beta}.$$

At the center of the channel the terms with small values of n make the main contribution to the sum (11). For these terms, for $\alpha \ll 1$ we can set $\lambda_n \sim \ln[1/2\pi^2\alpha^2]$, and thus we find that u_ξ is a linear function:

$$u_\xi(\xi) \approx -\frac{\xi}{\beta \ln(2\pi^2\alpha^2)}. \tag{14}$$

5. It is interesting to compare the above result with the case when there is no Coulomb interaction. The electron density distribution in this case can be found by setting $\beta = 0$ in Eq. (11). Then we have (see the dashed line in Fig. 1)

$$u_\xi(\xi)=\xi. \tag{15}$$

Let us now compare the results of our calculations with the conventional Luttinger liquid model,[4–7] in which only the short-range interaction of the electrons, with an effective interaction parameter $g_{\rm eff}$, is taken into account. In this case, an expression that is identical to Eq. (15) is obtained for the dimensionless density u_ξ, i.e., the density varies linearly along the wire. Switching to the dimensional density according to Eq. (12), where $\tilde{g}$ must be replaced by $g_{\rm eff}$ and v by $v_F/g_{\rm eff}$, we find that in the linear region the dimensional density is close to the result which we have obtained, if we set $g_{\rm eff} \approx [-\beta \ln(2\pi^2\alpha^2)]^{-1/2}$. However, as one can see from the Fig. 1, the real Coulomb interaction leads to a substantial increase in $|\rho(x)|$ near the electrodes.

The physical meaning of the results obtained above is quite clear. In the presence of an external potential difference the electron liquid in the channel is polarized: Electrons are injected from the left-hand reservoir (cathode) and extracted into the right-hand reservoir (anode). Accordingly, an excess of electrons arises on the left, and a deficiency of electrons arises on the right. In the absence of a long-range action, the density of the electron liquid in the low-frequency limit varies linearly, irrespective of the compressibility of the liquid. When the long-range electron-electron interaction is switched on, the charge in the center of the channel is neutralized, but its density near the electrodes, where the electron-electron interaction is weakened, remains unchanged.

The value of the dimensionless electron density $u_\xi(\xi)$ at the boundaries ($\xi = \mp 1/2$) does not depend on the interaction in the channel and equals $\pm 1/2$.

The electric current is defined in terms of the time derivative of the phase $\Phi(x,t)$ and, as calculations show, in the limit $\Omega \to 0$ it is expressed in terms of the boundary value of the perturbation of the electron density:

$$j=\frac{2e^2V_a}{h}u_\xi\big|_{\xi=-1/2}. \tag{16}$$

Therefore the current likewise does not depend on the interaction.[b)] However, such a dependence does arise in the dynamical regime ($\Omega \neq 0$). It will be investigated in a separate study.

It is interesting to note that the universality of the value e^2/h of the steady-state conductance, which follows from Eq. (16), is due to the fact that the current is proportional to the dimensionless boundary value of the density, which in the model studied does not depend on the interaction. Therefore the universality of the steady-state conductance is due to the boundary conditions. However, the boundary conditions employed are not exact. They ignore the possible effect of the proximity of the electron liquid in the channel and in the contact reservoirs, which could be important, since near the contacts the density which we have obtained changes rapidly with distance. The change in the boundary value of the density could be responsible for the breakdown of universality of the conductance.

This work was supported by INTAS (Grant 96-0721), the Russian Fund for Fundamental Research (Grant 96-02-18276), and the Interdisciplinary Science and Technology Program ''Physics of Solid-State Nanostructures'' (Grant 97-1054).

[a)]e-mail: vas199@ire216.msk.su

[b)]The equation relating the current and the density has a different form in the model with a short-range interaction. As one can see from Fig. 1, the density decrease due to the interaction is compensated by renormalization of the velocity.

[1] S. Tarucha, T. Honda, and T. Saku, Solid State Commun. **94**, 413 (1995).
[2] A. Yacoby, H. L. Stormer, N. S. Wingreen *et al.*, Phys. Rev. Lett. **77**, 4612 (1996).
[3] A. Yacoby, H. L. Stormer, K. W. Baldwin *et al.*, Solid State Commun. **101**, 77 (1997).
[4] M. Büttiker and T. Christen, in *Quantum Transport in Semiconductor Submicron Structures*, edited by B. Kramer, NATO ASI Series, 1996, Vol. 326, p. 263.
[5] D. I. Maslov and M. Stone, Phys. Rev. B **52**, R5539 (1995).
[6] V. V. Ponomarenko, Phys. Rev. B **52**, R8666 (1995).
[7] I. Safi and H. J. Schulz, Phys. Rev. B **52**, R17040 (1995).
[8] V. A. Sablikov and B. S. Shchamkhalova, JETP Lett. **66**, 41 (1997).
[9] V. V. Ponomarenko, Phys. Rev. B **54**, 10328 (1996).
[10] I. Safi, Phys. Rev. B **55**, R7331 (1997).
[11] A. Brataas, A. G. Mal'shukov, C. Steineback *et al.*, Phys. Rev. B **55**, 13161 (1997).
[12] Ya. M. Blanter, F. W. J. Hekking, and M. Büttiker, http://xxx.lanl.gov/abs/cond-mat/9710299.
[13] R. Egger and H. Graber, http://xxx.lanl.gov/abs/cond-mat/9709047.
[14] H. J. Schulz, Phys. Rev. Lett. **71**, 1864 (1993).
[15] J. Voit, Rep. Prog. Phys. **58**, 977 (1995).

Translated by M. E. Alferieff

Volume increase and enhanced indications of dielectric behavior during high-temperature annealing of quenched quasicrystal-forming alloys

A. F. Prekul, V. A. Kazanstev, E. V. Shalaeva, and N. I. Shchegolikhina
Institute of Metal Physics, Urals Branch of the Russian Academy of Sciences, 620219 Ekaterinburg, Russia

(Submitted 25 December 1997)
Pis'ma Zh. Éksp. Teor. Fiz. **67**, No. 3, 190–195 (10 February 1998)

A volume increase is observed at the ordering temperatures of icosahedral phases in samples of quenched alloys. The effect is strongest in the systems that are closest to the boundary of the transition to the insulator phase. © *1998 American Institute of Physics.* [S0021-3640(98)00603-3]

PACS numbers: 81.40.Ef, 81.05.Bx, 61.46.Br, 72.60.+g

Intensive experimental and theoretical investigations of the problem of a pseudogap in the electronic structure of high-resistivity states (HRSs) of disordered alloys whose components are all good metals have been conducted since the beginning of the 1970s. In respect to the level of conductivity of HRSs, the entire intermediate region between the conductivity of the maximally dirty metal (Mooij limit $\geqslant 10^4$ S/cm (Ref. 1)) and the minimum metallic conductivity at the limit of the metal-insulator transition (Mott limit $\leqslant 10^2$ S/cm (Ref. 2)) has now been covered. Conventional metallic solutions with an unstable crystal lattice, metallic glasses, and metastable quasicrystalline phases lie near the Mooij limit. Besides materials with a low carrier density, stable quasicrystalline phases of the systems Al–Cu–Fe, Al–Pd–Re, and Al–Pd–Mn are found at the other, ultrahigh-resistivity end of this series. The unifying feature of the electronic properties of HRSs is their mixed character, i.e., the presence of indicators of metallic and insulator behavior simultaneously: finite conductivity at $T=0$ K and finite electronic density of states at the Fermi level, negative temperature coefficient of the resistivity, strong temperature dependence of the Hall effect, absence of the Drude component in the optical conductivity, and a positive dielectric constant in practically the entire IR region of the spectrum.[3]

In the series of HRSs distinguished above, as one passes from the Mooij to the Mott limit the indications of metallic behavior become weaker and the indications of insulator behavior become stronger. For this reason, essentially two questions arise in the pseudogap problem—the question of the parameter controlling the transition from a state with no pseudogap to a state with a pseudogap in the electron spectrum inside a given metallic system and the question of the parameter that controls the depth of the pseudogap or, more precisely, the development of the insulator indications in the HRS series. Thus far these processes have all been studied on the basis of the Hume–Rothery

electronic phase transition mechanism, where the average electron density of the alloy, e/a, appears as the ''intrasystem'' parameter. The electron mean free path,[1,4] the surface area of congruent (nested) sections of the Fermi sphere,[5] and the degree of localization of electronic states in the pseudogap[6] are taken as the ''intersystem'' parameters.

An alternative approach has recently appeared in connection with the development of the ''semiconductor'' hypothesis of the electronic band structure of ultrahigh-resistivity quasicrystalline alloys. It was found that if the finite conductivity at $T=0$ K and finite electron density of states are regarded as nonintrinsic properties of the system, then these alloys can be regarded as gapless or narrow-gap semiconductors.[3,7] Hence the questions of the transition parameters can be investigated on the basis of band-model mechanisms of an electronic metal-insulator transition.

In this connection we call attention to the fact that a single-phase quasicrystalline state can be obtained by means of high-temperature annealing of metastable states obtained by quenching from the melt. For high cooling rates this can be a virtually uniform state of a metallic glass, and for moderate cooling rates it can be a complex mixture of crystalline and noncrystalline phases whose chemical composition can differ appreciably from the nominal composition. The metastable states differ little in their electrical properties, and altogether they are similar to HRSs from the beginning of the series under study. High-temperature annealing destroys this similarity. The conventional HRSs decompose into equilibrium crystalline phases, losing their high-resistivity properties and the indications of dielectric behavior. The stable quasicrystal-forming systems, conversely, become homogenized and acquire ultrahigh-resistivity properties and pronounced indications of dielectric behavior.

The picture of structural variations is quite complicated, but it is noteworthy that it contains two states which can be classified as uniform and single-phase states and which, according to the effect of heat treatment, are related with one another by a ''disorder-order'' transition. There is a metallic glass state on one side and a quasicrystalline state on the other. If this transition is juxtaposed with the proposed metal-insulator transition, this means that fundamental changes in the electrical properties take place with virtually no change in lattice structure, in the sense that chemical disorder remains before and after the transition and there is no lattice periodicity. Under these conditions the metal-insulator transition parameter is most likely the volume of the system.[2]

We performed a series of dilatometric experiments for the purpose of observing the volume increase effect during a homogenizing annealing of quenched samples of quasicrystal-forming alloys. This effect does indeed exist. We observed it in the two stable systems mentioned above, in the alloy with the nominal composition $Al_{62.5}Cu_{25}Fe_{12.5}$ in the Al–Cu–Fe system, in the alloy with nominal composition $Al_{70}Pd_{20}Re_{10}$ in the Al–Pd–Re system, and in the metastable system $Al_{75}Cu_{15}V_{10}$. In addition, this effect is correlated with the change in the electrical properties.

The samples were obtained as follows. The alloy components Al, Cu, Fe, Pd, V, and Re were at least 99.9% pure. In the Al–Cu–V and Al–Cu–Fe systems the melting points of the components do not differ much, so that a composition with three components all at once was prepared in an arc furnace. For homogenization, the ingot was remelted five times and turned over each time. Next, a ~ 2 g quantity of the prepared material was melted in an arc furnace on a flat water-cooled hearth and flattened by a falling copper

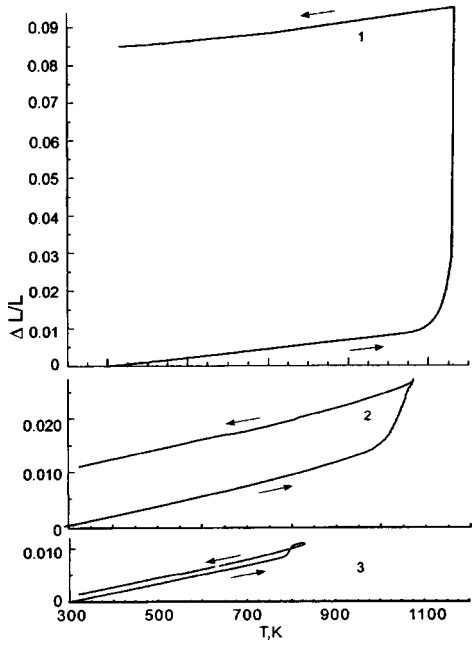

FIG. 1. Relative changes of the linear dimensions of samples of quenched alloys in a regime of continuous slow increase and decrease of temperature: *1*—Al–Pd–Re alloy, *2*—Al–Cu–Fe alloy, *3*—Al–Cu–V alloy.

block. Samples in the form of a parallelepiped 7–10 mm long were cut by an electrospark method from the 3–4 mm-thick plate obtained. The technology for the alloy $Al_{70}Pd_{20}Re_{10}$ differed somewhat from that described. The melting temperatures of Al and Re differ very strongly, so that a Al–Pd alloy was prepared first. Next, a mixture of the ground preliminary alloy and powdered Re, preannealed in vacuum, was heated in an induction furnace at a temperature 200 °C above the melting point of the preliminary alloy for 30 min, with the material remelted twice and ground between the remeltings. A small weighed quantity of the prepared material was melted on the hearth of the arc furnace and flattened into a plate. Just as in the preceding case, samples were cut from the plate. The weight of the ingots was checked at all stages of preparation of the alloys. Chemical analysis of the alloys was performed in the final stage. No appreciable deviations from the nominal composition were observed. Pores were present in the initial materials *in situ*.

Dilatometric experiments were performed with a SINKU–RIKO quartz dilatometer. For a sample 5–10 mm long, the error in measurement of the linear expansion coefficient on the dilatometer does not exceed 1×10^{-7} K^{-1}.

In the first, exploratory experiments we varied the temperature continuously over the interval 20–900 °C at a rate of 3–10 °C/min. Figure 1 shows the results of measurements of the relative elongation $\Delta L/L$ of samples of alloys of the three systems mentioned above. As one can see, the curves are typical for structural phase transitions, except perhaps for the value of the critical temperature and the giant magnitude of the dilatation effect in one of the systems. In the context of the main problem being investigated, we

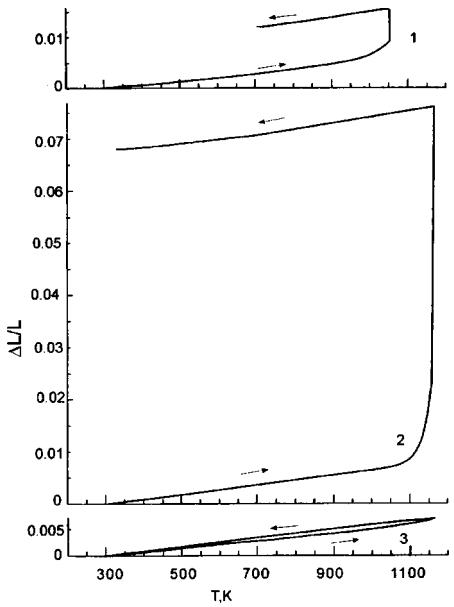

FIG. 2. Relative changes of the linear dimensions of a sample of a quenched Al–Pd–Re alloy in a cyclic annealing regime. The vertical sections of the curves in cycles *1 and 2 correspond to isothermal holds of 30 and 60 min, respectively*.

were interested by the existence of a correlation between the change in volume and the change in the electrical properties. For this reason, the choice of systems for which the results are presented in Fig. 1 is no accident. According to published data, in the series of HRSs which we investigated the system Al–Pd–Re is closest to the ''insulator'' edge (the room-temperature resistivity $\rho_{300} \approx 10\,000\ \mu\Omega \cdot \mathrm{cm}$), the system Al–Cu–Fe occupies an intermediate position ($\rho_{300} \approx 2500\ \mu\Omega \cdot \mathrm{cm}$), and the system Al–Cu–V is closest to the ''metallic'' edge of the series ($\rho_{300} \approx 100\ \mu\Omega \cdot \mathrm{cm}$).[3–8] It is easy to see that the systems fall into the same order in terms of the magnitude of the dilatation effect. Hysteresis of the relative elongation equals about 9% in the Al–Pd–Re alloy, about 1% in the Al–Cu–Fe alloy, and about 0.1% in the Al–Cu–V alloy, corresponding to volume changes of 30%, 5%, and 0.3%, respectively. The scales of the volume and resistivity changes are of the same order of magnitude. It can be conjectured that the volume is the parameter of the transition between systems in the series of HRSs from the ''metallic'' edge to the ''insulator'' edge.

A correlation also exists between the volume change and the change in electrical conductivity within an individual system during annealing. In this respect, the results obtained not with continuous variation of temperature but rather with cyclic annealing, when an isothermal hold of the sample is conducted in each specific cycle at the maximum temperature of the cycle, are more convincing. Not only temperature but also temporal effects can be compared. The behavior of the relative elongation and electrical conductivity in the process of such anneals can be judged from our results, displayed in Figs. 2, 3, and 4, for the alloy $Al_{70}Pd_{20}Re_{10}$. These clearly need no comment. The correlation is complete. We note only that such an experiment cannot be performed on

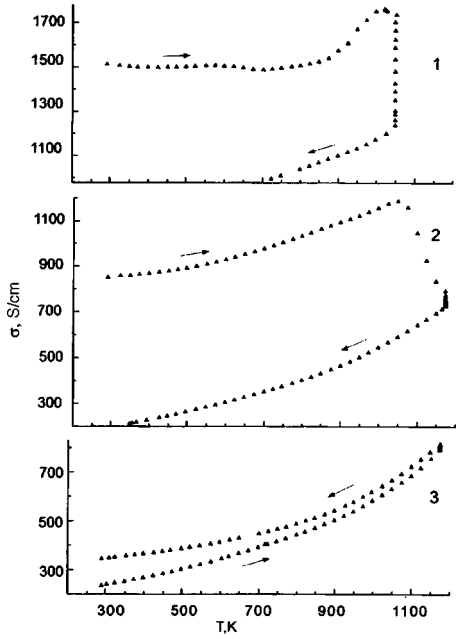

FIG. 3. Variation of the conductivity of a sample of a quenched Al–Pd–Re alloy in a cyclic annealing regime. The vertical sections of the curves in cycles *1* and *2* correspond to isothermal holds of 30 and 60 min, respectively.

just any arbitrary system. The alloy $Al_{70}Pd_{20}Re_{10}$ is distinguished by the fact that it exhibits consistently irreversible changes in its properties during annealing. It can be conjectured on the basis of the results obtained that the volume is the ''intrasystem'' parameter of the transition from the high-resistivity to the ultrahigh-resistivity state.

The values of the critical temperatures are very revealing of the interrelation of the observed changes and the structural state of the samples. In the system Al–Cu–V an abrupt change in volume occurs at 550 °C, in the system Al–Cu–Fe it occurs in the range 730–800 °C, and in the system Al–Pd–Re it occurs in the range 750–900 °C. It is easy to show by comparing with existing published data on structure and structural transformations in the alloys under study[4–9] that these are the ordering temperatures of icosahedral phases, and the irreversible volume changes could be directly related with the formation of these phases and not with pores and other defects, which are always present in real alloys.[10] X-ray diffraction studies of the Al–Pd–Re alloy in the initial state and after annealing showed the following.

The diffraction patterns of the initial state contain lines of an icosahedral phase and many additional lines from crystalline cophases. According to an analysis of the interplanar distances d and intensities I, the additional lines could belong to phases of the type Al_3Pd, Al_3Pd_2, and $Al_{35}Re_{65}$. It is noteworthy that all phases, including the icosahedral phase, are imperfect. The maximum of the line intensities for all phases falls near the reflections $d \approx 2.058$–2.176 Å. Apparently, elements of close packing are present in the lattices of all phases. The interplanar distances of the icosahedral phase are on the average 1% shorter than the tabulated data.[11]

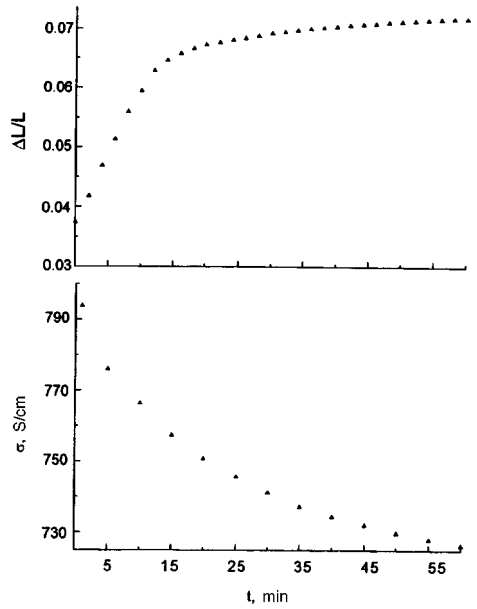

FIG. 4. Time dependences of the relative elongation and conductivity of a sample of a quenched Al–Pd–Re alloy under isothermal annealing in cycle *2* (see Figs. 2 and 3).

After annealing, i.e., after the volume changes are completed, the line intensities of the crystalline phases decrease appreciably, though the lines do not vanish completely. Metastable crystalline phases probably occupy 5–10% of the sample volume. Conversely, the intensity of the lines of the icosahedral phase increases appreciably. The interplanar distances of this phase also increase and approach the tabulated values. As one can see, the results of the direct experiment are consistent with the conclusion drawn above. It looks as if the stable quasicrystals have a looser packing than any other metastable structures in this alloy.

In summary, our results imply that there is a new factor controlling the electronic structure of high-resistivity states of disordered metallic alloys—the volume of the system. Evidently, irrespective of how this factor is taken into account, the mechanism will always reduce to a change in the overlap of the energy bands. At present we favor the following interpretation of the interrelationship of events. The ease with which the lattice structure of metastable phases changes could signify that the system of ions of a given chemical and quantitative composition is in a state of unstable or unbounded equilibrium. For this reason, the natural tendency of a free electron gas to expand stabilizes the state of the ''loosest'' packing with the lowest value of the Fermi energy. This approach is distinguished by the fact that the pseudogap mechanism does not depend directly on the character of the scattering and the electron mean free path. A strong dependence on the symmetry of the wave functions of the collectivized electrons should be expected.

We express our appreciation to Yu. N. Tsiovkin for a discussion of the results and helpful remarks and to N. Yu. Kuz'min and A. B. Rol'shchikov for assisting in the experiments and for arranging the manuscript.

This work was supported by the Russian Fund for Fundamental Research (Project 96-02-19586).

[1] J. H. Mooij, Phys. Status Solidi A **17**, 521 (1973).
[2] N. F. Mott, *Metal-Insulator Transitions*, Taylor and Francis, London, 1974 [Russian translation, Mir, Moscow, 1979].
[3] A. F. Prekul, L. V. Nomerovannaya, A. B. Rol'shikov *et al.*, Fiz. Met. Metalloved. **82**, 75 (1996).
[4] S. J. Poon, Adv. Phys. **41**, 303 (1992).
[5] S. E. Burkov, T. Timusk, and N. W. Ascroft, J. Phys.: Condens. Matter **4**, 9447 (1992).
[6] K. Kimura and S. Takeuchi, in *Quasicrystals: The State of the Art*, edited by D. P. Vincenzo and P. Steihardt, World Sci. Pub. Co., 1991, p. 313.
[7] D. N. Basov, F. S. Pierce, P. Volkov *et al.*, Phys. Rev. Lett. **73**, 1865 (1994).
[8] H. Akiyama, Y. Honda, T. Hashimoto *et al.*, Technical Report of ISSP Ser. A, N2666 (1993).
[9] F. Fandot, A. Quivy, Y. Calvayrac *et al.*, Mater. Sci. Eng., A **133**, 383 (1991).
[10] U. Mizutani, Y. Sakabe, T. Shibuya *et al.*, J. Phys. Condens. Matter **2**, 6169 (1990).
[11] A. Tsai, A. Inoue, Y. Yokoyama *et al.*, Mater. Trans., JIM **31**, 98 (1994).

Translated by M. E. Alferieff

Intersubband collective spin- and charge-density excitations in a system of 2D electrons in the quantum Hall effect regime

V. E. Kirpichev and I. V. Kukushkin
Institute of Solid-State Physics, Russian Academy of Sciences, 142432 Chernogolovka, Moscow Region, Russia

K. von Klitzing and K. Eberl
Max-Planck Institut für Festkörperforschung, 70569 Stuttgart, Germany

(Submitted 30 December 1997)
Pis'ma Zh. Éksp. Teor. Fiz. **67**, No. 3, 196–200 (10 February 1998)

Collective intersubband spin- and charge-density excitations in a system of 2D electrons and the dependence of the excitations on the perpendicular magnetic field are investigated by the inelastic light scattering method. Magnetooscillations of the energies of collective excitations are found, and it is shown that they are observed in the quantum Hall effect regime. The energy of the direct Coulomb interaction of the electrons and its oscillatory variation as a function of the perpendicular magnetic field are measured directly from the energy splitting of the spin and charge excitations. © *1998 American Institute of Physics.* [S0021-3640(98)00703-8]

PACS numbers: 73.40.Hm, 73.20.Mf

1. Free charge carriers in semiconductor structures, such as single GaAs/AlGaAs heterojunctions and quantum wells with modulated doping, are unique objects for investigating effects associated with the electron-electron interaction. This uniqueness is due to the extremely high mobility of the charge carriers and the ease with which the electron density can be varied over wide limits.

Direct measurements of the Coulomb interaction energy in a system of 2D electrons can be made by observing in the spectrum of elementary excitations of the electronic system two collective modes separately—spin-density excitations (SDE) and charge-density excitations (CDE). We note that in contrast to a nonuniform system (which a quasi-two-dimensional electron gas in a quantum well is), it is impossible to observe simultaneously two collective modes in a uniform three-dimensional paramagnetic system in a zero magnetic field.[1]

The energy structure of the size quantization bands of 2D electrons is ordinarily investigated by optical methods—according to resonance absorption of light in the far-IR region[2] or by the inelastic light scattering method.[3] However, it is well known that the intersubband splitting measured in these optical experiments corresponds to the energy of collective charge-density excitations and is found to be exaggerated on account of the

so-called depolarization effect.[4] This phenomenon is caused by the screening of the external electric field by the 2D electrons, so that each electron feels the field differing from the external field by the Hartree field of the other electrons. However, the Hartree approximation overestimates the Coulomb repulsion of the other electrons and the exchange-correlation effects, which decrease the electronic repulsion and the energy shift of the CDE line, must be taken into account accurately.

According to modern theory,[5,6] the energy of the collective spin excitations in an intersubband transition is less than the energy of charge-density excitations by an amount determined by the exchange-correlation interaction. Direct measurements of the Coulomb energy by the inelastic light-scattering method make it possible to compare quantitatively different theoretical models, such as the local density approximation,[7] the random phase approximation,[8] and the Hubbard approximation.[9]

In the present work we study the collective spin and charge excitations according to the spectra of inelastic light scattering by 2D electrons accompanying an intersubband transition in a single quantum well and the magnetic field dependence of these spectra. Oscillations of the Hartree energy as a function of the magnetic field have been found, and it is shown that they are observed in the quantum Hall effect regime.

2. In this work we investigated several single, high-quality (2D electron mobility $(1-2\times10^6$ cm^2/V$\cdot$s at density $(0.6-6.5\times10^{11}$ cm^{-2}) GaAs/AlGaAs wells 250 Å wide, with AlGaAs spacer thicknesses of 400–800 Å. The high quality of the samples is confirmed by the unprecedentedly small linewidths of the luminescence (0.3 meV), inelastic light scattering (0.15 meV), and absorption and scattering resonances (0.05 meV) measured in these structures. A titanium-sapphire laser, tunable in the range 1520–1650 meV, with a characteristic power density 0.1–1 W/cm^2 was used for photoexcitation. The inelastic scattering spectra were detected with a CCD camera and a Ramanor U-1000 double monochromator; these devices gave a spectral resolution of 0.03 meV. All measurements were performed in a nonoptical cryostat with a solenoid ($B=0-11$ T) at a temperature of 1.5 K. An insert consisting of two optical fibers was used. One of these fibers served for photoexcitation and the other for receiving the scattered light. The momentum transferred in light scattering was determined by the configuration of the optical fibers, and in all measurements its characteristic value (the component in the 2D plane) corresponded to the low-momentum limit realized in the backscattering geometry and was equal to $4-5\times10^4$ cm^{-1}. Special polarization measurements were performed separately in an optical cryostat with a solenoid giving a magnetic field of 0–7 T.

3. The characteristic intersubband inelastic light-scattering spectra measured with different values of the perpendicular magnetic field and fixed energy of the pump photon are displayed in Fig. 1. Collective spin- and charge-density excitations as well as a line usually attributed[3] to single-particle excitations (SPE) are observed in these spectra. Identification of the lines is made on the basis of the polarization of the inelastic light scattering spectra, since according to the selection rules charge-density oscillations are observed in a polarization parallel to the photoexcitation and spin-density oscillations are observed in a perpendicular polarization. We specially checked that the inelastic light scattering lines, designated in Fig. 1 as CDE and SDE, were practically completely polarized parallel and transverse to the photoexcitation polarization, respectively, and in addition the polarization directions of these lines were also preserved in a perpendicular magnetic field. These experimental facts confirm the correctness of the identification of

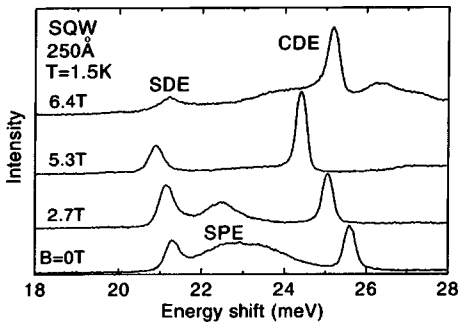

FIG. 1. Intersubband inelastic light-scattering spectra measured in a single quantum well 250 Å wide at $T = 1.5$ K, $E_L = 1573$ meV, and for different values of the perpendicular magnetic field. The 2D electron density in the well is $n_S = 2.7 \times 10^{11}$ cm^{-2}.

the SDE and CDE lines, but the polarization and spectral characteristics of the SPE line that we measured in a magnetic field were at variance with the conventional interpretation of this line in terms of single-particle excitations. We note that the manifestation of single-particle excitations in the inelastic light-scattering spectra is also at variance with the theoretical notions, since the observation of such a process corresponds to the possibility of an intersubband transition of an electron without a collective response of the electronic system. A detailed investigation of the properties of the SPE line will be published separately. In the present letter we shall not employ the conventional[3,10] method of measuring the depolarization and exchange energies on the basis of a comparison of the spectral positions of the three lines—CDE, SDE, and SPE, but rather we shall confine our attention to analyzing the energy splitting of the CDE and SDE lines.

One can see from Fig. 1 that the spectral positions of all observed lines depend on the perpendicular magnetic field, and under resonance conditions the intensities of the lines oscillate in the field. To determine the possible influence of the input and output resonances appearing in the inelastic light-scattering intensity when the energy of the pump or scattered phonon equals the energy of a real state, we measured a series of Raman spectra in magnetic fields from 0 to 11 T (with a step of 0.1 T) for different values of the pump photon energy from 1561 meV to 1595 meV with a step of 1 meV. It was found that despite the magnetooscillations of the intensity of all lines in the light-scattering spectrum (which depend on E_L), the energy shift of all lines relative to E_L is equal for all values of E_L and in all magnetic fields. This enabled us to represent in a single figure (see Fig. 2) all of the measured magnetic field dependences obtained for the energy shift of SDE and CDE lines for different values of E_L. In this figure different symbols correspond to different values of E_L and the magnetic fields corresponding to integer filling factors are indicated at the top (the 2D electron density was also monitored according to the luminescence spectra measured under the same photoexcitation conditions). As one can see from Fig. 2, the energies of both collective modes in the intersubband inelastic light-scattering spectrum depend nonmonotonically on the magnetic field, and the CDE energy has pronounced minima near integer filling factors.

As was noted above, the electron-electron interaction greatly complicates the procedure for determining the intersubband splitting (E_{01}) in optical experiments, since

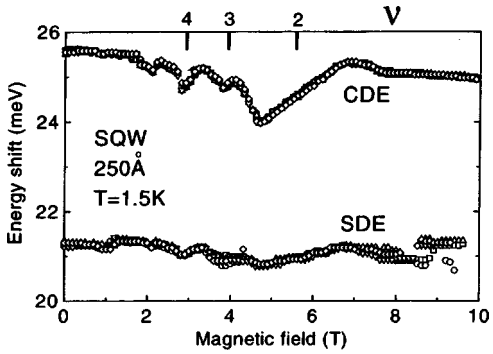

FIG. 2. CDE and SDE mode energies versus the perpendicular magnetic field. The energies were measured in a single quantum well, 250 Å wide, ($n_S = 2.7\times10^{11}$ cm^{-2}) at $T = 1.5$ K for different values of E_L. The different symbols correspond to different values of E_L. The corresponding filling factors are shown on the abscissa at the top.

instead of one single-particle resonance one observes two absorption or scattering features, associated with the excitation of collective spin- and charge-density modes are observed. As shown earlier,[5,10] the energies of these collective modes are determined by the relations

$$E_{\mathrm{CDE}}^2 = E_{01}^2 + E_{\mathrm{dep}}^2 - E_{\mathrm{ex}}^2, \quad E_{\mathrm{SDE}}^2 = E_{01}^2 - E_{\mathrm{ex}}^2,$$

where the term E_{dep} describes the aforementioned depolarization effect and is the analog of the frequency of plasma oscillations in the direction z for a plasma with a three-dimensional density $n_S/\langle z\rangle$ (here $\langle z\rangle$ is the characteristic thickness of the 2D channel),[4] and the term E_{ex} describes the exchange-correlation energy of a pair of particles—an electron in the upper subband and a hole in the ground subband. This effect is ordinarily said to be exciton-like, since it lowers the transition energy.

As one can see from the formulas presented above, the energies E_{CDE}, E_{SDE}, and E_{10} are all required in order to determine E_{dep} and E_{ex}, but to measure only the depolarization term it is sufficient to determine only E_{CDE} and E_{SDE}:

$$E_{\mathrm{dep}}^2 = E_{\mathrm{CDE}}^2 - E_{\mathrm{SDE}}^2.$$

We use this relation to determine the depolarization energy experimentally. Figure 3 displays curves of E_{dep} versus the magnetic field which were obtained in this manner for three different samples with the same quantum well width but different 2D electron densities. It is evident from the figure that this dependence is of an oscillatory character, and in all samples oscillations are observed in the quantum Hall effect regime. We attribute the observed magnetic field dependence of E_{dep} to the oscillatory variation occurring in the screening of the Coulomb interaction as a result of variations of the magnetoconductivity. We note that earlier[11] we observed very similar oscillations of magnetoplasma energy under conditions of the integral and fractional quantum Hall effect for the case of an intraband cyclotron transition. These effects are most likely of the same physical nature and require theoretical explanation.

Comparing the amplitudes of the magnetooscillations of the depolarization energy that we measured on different samples showed that both increasing and decreasing the

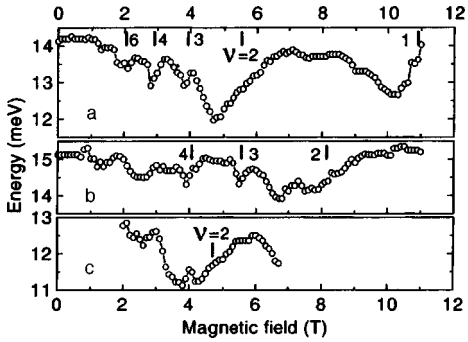

FIG. 3. Depolarization energy $E_{\rm dep}$ versus the magnetic field. The energies were measured for different 250-Å-wide quantum wells: a—$n_S=2.7\times10^{11}$ cm^{-2}, b—$n_S=3.9\times10^{11}$ cm^{-2}, c—$n_S=2.3\times10^{11}$ cm^{-2}. The arrows mark the positions of the integral filling factors.

2D electron density results in a smoothing of the oscillations, and in samples with a well 250 Å wide the maximum amplitude obtains for $n_S=(3-4)\times10^{11}$ cm^{-2}. This fact indicates that in the problem at hand the ratio of the width of the quantum well to the electron-electron distance is an important parameter.

Figure 4 shows the curve of the depolarization energy versus 2D electron density, as measured in a zero magnetic field for different single quantum wells 250 Å wide. The figure also shows (dashed line) the square-root dependence expected in the low-density limit, since, as noted above, $E_{\rm dep}$ corresponds to the energy of oscillations of a plasma with 3D density $n_S/\langle z\rangle$. The characteristic width $\langle z\rangle$ of the 2D-electron wave function giving the best agreement with experiment at low values of n_S was found to be 105 Å, which is in reasonable agreement with the well width. The deviation of $E_{\rm dep}(n_S)$ from a square-root dependence with increasing density is due to the change in $\langle z\rangle$ as well as to the fact that the energy of the charge-density excitations approaches the transverse optical phonon energy (33.6 meV), which results in a higher dielectric constant[4] and a lower energy $E_{\rm CDE}$.

In summary, in the present work the energies of the collective excitations were

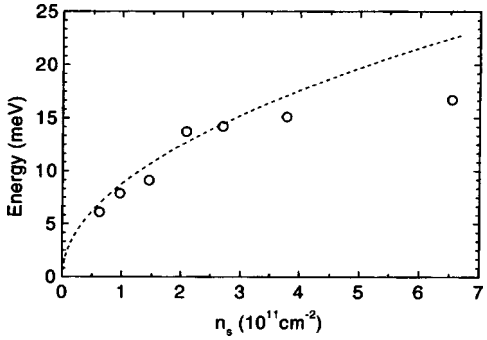

FIG. 4. Depolarization energy $E_{\rm dep}$ versus the 2D electron density n_S. The measurements were performed for $B=0$ T in different 250-Å-wide quantum wells. The dashed line corresponds to the approximation $E\sim B^{1/2}$.

measured as a function of the magnetic field and 2D electron density from the intersubband inelastic light-scattering spectra, and magnetooscillations of the depolarization energy under quantum Hall effect conditions were observed.

This work was supported by grants from the Russian Fund for Fundamental Research and from Volkswagen.

[1] D. Gammon, B. V. Shanabrook, J. C. Ryan *et al.*, Phys. Rev. Lett. **68**, 1884 (1992).
[2] M. Ramsteiner, J. D. Ralston, P. Koidl *et al.*, J. Appl. Phys. **67**, 3900 (1990).
[3] A. Pinczuk, S. Schmitt-Rink, G. Danan *et al.*, Phys. Rev. Lett. **63**, 1633 (1989).
[4] T. Ando, A. B. Fowler, and F. Stern, Rev. Mod. Phys. **54**, 437 (1982).
[5] T. Ando, J. Phys. Soc. Jpn. **51**, 3893 (1982).
[6] A. C. Tselis and J. J. Quin, Phys. Rev. B **29**, 3318 (1984).
[7] W. Kohn and L. Sham, Phys. Rev. **140**, A1133 (1965).
[8] D. A. Dahl and L. Sham, Phys. Rev. B **16**, 651 (1977).
[9] M. Jonson, J. Phys. C **9**, 3055 (1976).
[10] S. Ernst, A. R. Goni, K. Syassen, and K. Eberl, Phys. Rev. Lett. **72**, 4029 (1994).
[11] I. V. Kukushkin, V. I. Falko, R. J. Haug *et al.*, in *High Magnetic Fields in the Physics of Semiconductors*, edited by G. Landwehr and W. Ossau, World Scientific, 1997.

Translated by M. E. Alferieff

Quantum corrections to the conductance of *n*-GaAs films in a strong magnetic field

S. S. Murzin

Institute of Solid-State Physics, Russian Academy of Sciences, 142432 Chernogolovka, Moscow Region, Russia

(Submitted 30 December 1997)
Pis'ma Zh. Éksp. Teor. Fiz. **67**, No. 3, 201–206 (10 February 1998)

The conductance of doped *n*-GaAs films is studied experimentally as a function of magnetic field and temperature in strong magnetic fields right up to the quantum limit ($\hbar\omega_c = E_F$). The Hall conductance G_{xy} is virtually independent of temperature T until the transverse conductance G_{xx} is quite large compared with e^2/h. In strong fields, when G_{xx} becomes comparable to e^2/h, G_{xy} starts to depend on T. The difference between the conductances G_{xx} at the two temperatures 4.2 and 0.35 K depends only weakly on the magnetic field H over a wide range of magnetic fields, while the conductances G_{xx} themselves vary strongly. The results can be explained by quantum corrections to the conductance as a result of the electron-electron interaction in the diffusion channel. The possibility of quantization of the Hall conductance as a result of the electron-electron interaction is discussed. © *1998 American Institute of Physics.* [S0021-3640(98)00803-2]

PACS numbers: 72.80.Ey, 72.20.My

As is well known, quantum interference effects change the temperature dependence of the conductance of disordered metallic systems. According to the theoretical models, in the case of weak spin-spin and spin-orbit scatterings, the change in the conductance of the normal two-dimensional metallic system in a zero magnetic field as the temperature changes from T_0 to T is given by[1,2]

$$\delta G = \frac{e^2}{2\pi^2\hbar}\left\{[p+1-\lambda_0-2\lambda_{\pm 1}-(p-1)\beta(T)]\ln\frac{T}{T_0}-\ln\frac{\ln T_c/T_0}{\ln T_c/T}\right\}. \quad (1)$$

Here p is the exponent of the temperature dependence of the reciprocal of the phase interruption time $1/\tau_\varphi \propto T^p$, T_c is a constant of the order of the Fermi energy E_F divided by the Boltzmann constant k_B, and $\beta(T)$ is a function of $\ln(T_c/T)$, whose values are presented in Ref. 1. The first term p in brackets on the right-hand side of expression (1) is due to single-electron interference (weak localization) and the remaining terms are due to quantum effects in the electron-electron interaction. The second, third, and fourth terms are due to interaction in the diffusion channel. The second term is due to the interaction of an electron and a hole with total spin $j=0$, the third term is due to the

interaction of an electron and hole with total spin $j=1$ and projection of the total spin $m=0$, and the fourth term is due to the interaction of an electron and hole with total spin $j=1$ and spin projection $m=\pm 1$. In addition, the interaction constants are $\lambda_0=\lambda_\pm$. The fifth term is the Maki–Thompson correction. The last term in braces is due to interaction in the Cooper channel. The first and second terms in expression (1) decrease and the remaining terms increase the conductance with decreasing temperature. A magnetic field H suppresses weak localization and the Maki–Thompson corrections in the case $H>H_\varphi=\hbar c/4eD\tau_\varphi$ (D is the electron diffusion coefficient), it suppresses the correction due to interaction in the Cooper channel in the case $H>H_{\rm int}=\pi ck_BT/2eD$, and in the case $H>H_s=\pi k_BT/g\mu_B$ (g is the Landé factor, and μ_B is the Bohr magneton), as a result of the effect on the spin variables, it also suppresses the correction due to the direct interaction in the diffusion channel with the total spin of electron and hole $j=1$ and $m=\pm 1$. With the exception of the Maki–Thompson correction, the electron-electron interaction does not affect the Hall conductance: $\delta G_{xy}=0$. We note that in transitional regions in terms of the magnetic field the corrections to the conductance are not logarithmic.

The results presented above were obtained for the case $\omega_c\tau\ll 1$ (ω_c is the cyclotron frequency and τ is the electron relaxation time). In strong magnetic fields $\omega_c\tau\gg 1$, the only remaining corrections are due to the electron-electron interaction in the diffusion channel and they were studied theoretically in Refs. 3–5. The authors found that near maxima of G_{xx} the results are identical to the results of Ref. 6, initially obtained for the case $\omega_c\tau\ll 1$. Specifically, $\delta G_{xy}=0$. Later, the results of Ref. 6 for δG_{xx} were somewhat altered.[7] Apparently, similar changes must also be introduced for the case of strong magnetic fields, but this was not done. Quantum corrections in a strong field were studied experimentally, as far as I know, only in the GaAs/AlGaAs heterostructures.[8] It was found that at its maxima the conductance G_{xx} varies logarithmically. However, no data on the behavior of G_{xy} are given in this work.

Although quantum corrections to the conductance in 2D films placed in a strong magnetic field have not been studied theoretically, it can be expected that the result in this case will be identical to the results for weak magnetic fields, $\omega_c\tau\ll 1$. The first objective of the present work is to study experimentally the magnetic field and temperature dependences of the conductances G_{xx} and G_{xy} of 2D films of doped n-GaAs in strong magnetic fields right up to the quantum limit ($\hbar\omega_c=E_F$, where E_F is the Fermi energy) and to compare the experimental results with the theory of quantum corrections due to electron-electron interaction.

In Ref. 9, quantization of G_{xx} and, correspondingly, the appearance of minima of G_{xy} at temperatures less than 1 K were found in experimental samples in the quantum limit $\hbar\omega_c>E_F$, while at $T=4.2$ K G_{xy} and G_{xx} are monotonic functions of the magnetic field.[9] Quantization of G_{xy} arises for G_{xx} comparable to e^2/h, when second-order localization corrections can be substantial (the magnetic field suppresses first-order corrections). The second objective of this work is to determine which is the more significant under these conditions: electron-electron interaction or localization effects.

The measurements were performed on samples prepared by molecular-beam epitaxy. A 0.1 μm thick layer of undoped GaAs was deposited on a semi-insulating GaAs (100) substrate at temperature $T=410$ °C. The following were deposited next: an epitaxial layer of undoped GaAs (0.6 μm), a GaAs/AlAs$\times$20 periodic structure with GaAs

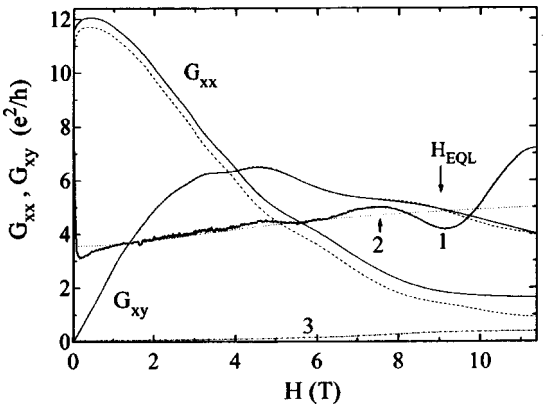

FIG. 1. Hall G_{xy} and transverse G_{xx} (on a square) conductances versus magnetic field at two temperatures. The solid curves are for $T=4.2$ and the dashed curves for $T=0.35$ K. Curve *1*—$\delta G_{xx}(H)$ (difference of the curves $G_{xx}(H)$ at $T=4.2$ K and at $T=0.35$ K), multiplied by 10. Curve *2*—$\delta G_{xx}(H)\cdot 10$, calculated according to Eq. (2) with the constants λ_0 and $\lambda_\pm$ obtained by fitting the temperature dependences of G_{xx} in Fig. 2. Curve *3*—$\delta G_{xx}(H)\cdot 10$ due to second-order localization corrections.

thicknesses equal to 10 monolayers and AlAs thicknesses equal to 5 monolayers, an undoped GaAs layer (1 μm), a layer of silicon-doped n-GaAs (0.1 μm) with a prescribed donor density of 1.5 and 3×10^{17} cm^{-3} for samples 2 and 3, respectively, and once again a layer of undoped GaAs (1 μm). Samples 0.18 mm wide and 3 mm long with legs for measurements of the longitudinal and transverse stresses in and transverse to the planes of the samples were etched from disks. The measurements were performed with a 30 Hz ac current in a magnetic field up to 11.5 T in the temperature range 0.3–4.2 K. The main measurements were performed in a field oriented perpendicular to the plane of the sample.

The volume electron densities n in a strongly doped layer were determined according to the periods of the Shubnikov–de Haas oscillations of the transverse resistance R_{xx}. They equal 1.8 and 2.5×10^{17} cm^{-3} for samples 2 and 3. The electron densities N_s per unit film area and the mobilities $\mu=2400$ and 2500 cm^2/V·s were found from the resistance in a zero magnetic field and the Hall constant. The values obtained for the mobilities are close to the mobilities in single crystals with close densities n.[10] The mean free path lengths, equal to approximately 0.03 μm, as determined from the mobilities, are much less than the film thicknesses d. Dividing n by N_s, we determined the ''effective'' film thicknesses to be 0.07 and 0.083 μm. They are somewhat less than the thicknesses of the doped layers because of the decrease in the electron density near the boundaries. To show in addition that the electron spectrum in the films is three-dimensional, the resistance of sample 2 was measured in a magnetic field parallel to the film plane but once again perpendicular to the current. It was virtually identical to the resistance in a perpendicular field (the positions of the visible maxima and minima of the Shubnikov–de Haas oscillations were also identical).

Figure 1 displays the transverse G_{xx} (on a square) and Hall G_{xy} conductances versus the magnetic field for sample 2 at temperatures $T=0.35$ and 4.2 K. The conductances

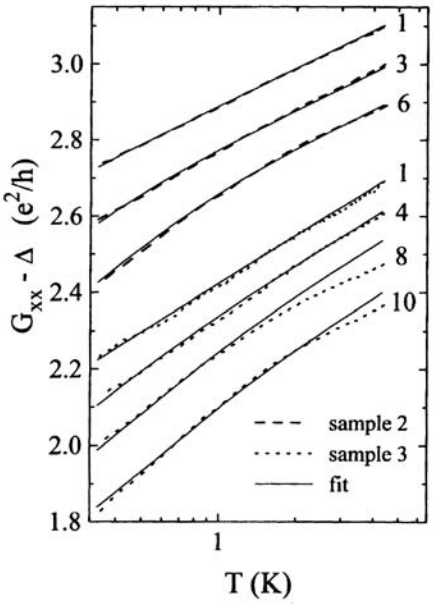

FIG. 2. Temperature dependences of the dissipative conductance G_{xx} in different magnetic fields, indicated by the numbers near the curves. For convenience, all curves except the bottom curve are shifted downwards. The shifts Δ for different curves are (top to bottom) 8.37, 4.89, 1.16, 18.7, 18.13, 2.08, and 0.

were determined by converting from the transverse resistance R_{xx} on a square and the Hall resistance R_{xy}. The transverse conductance G_{xx} at first increases somewhat in weak fields and then decreases by approximately a factor of 10. At $T=4.2$ K G_{xx} is everywhere greater than its value at $T=0.35$ K. The curves $G_{xy}(H)$ are virtually identical, with the exception of the strongest magnetic fields in which G_{xx} is comparable to e^2/h. The difference $\delta G_{xx}=G_{xx}(4.2)-G_{xx}(0.35)$ at first decreases rapidly and then increases slowly. In strong fields δG_{xx} starts to oscillate, while $G_{xy}(H)$ becomes temperature-dependent. The oscillations of $G_{xx}(H)$ and $G_{xy}(H)$ at low temperatures are observed on these samples in the magnetic field range 10–23 T.[9] The temperature dependences $G_{xx}(T)$ for both samples in different magnetic fields are presented in Fig. 2. In weaker fields they are close to logarithmic and in stronger fields they differ appreciably from $\log T$.

The increase of $G_{xx}(H)$ and decrease of δG_{xx} in a weak field are due mainly to the suppression of weak localization. Quantum corrections in this region of magnetic fields were studied in Ref. 11 on samples similar to ours. The small increase in δG_{xx} in fields greater than 1 T and the deviation of the temperature dependences from a logarithmic dependence can be attributed to the effect of a magnetic field on the corrections to the conductance that are due to the electron-electron interaction in the diffusion channel with $j=1$ and $m=\pm 1$. The difference between conductances in a magnetic field at two temperatures T and T_0 in this case should be[2]

$$\delta G_{xx}(H)=\frac{e^2}{2\pi^2\hbar}\left[(1-\lambda_0-2\lambda_{\pm 1})\ln\frac{T}{T_0}+2\lambda_{\pm 1}\int_0^\infty\frac{\partial^2}{\partial\omega^2}\left(\frac{\omega}{\exp\hbar\omega/k_BT-1}\right)\right.$$
$$\left.\times\ln\left|1-\frac{\omega_s^2}{\omega^2}\right|d\omega\right], \qquad (2)$$

where $\omega_s=g\mu_BH$. The experimental results cannot be fit adequately by expression (2), if it is assumed that $\lambda_0=\lambda_{\pm 1}$ and the interaction constant for $j=0$ equals 1. For this reason, we fit the experimental curves choosing as the two independent adjustable parameters the coefficient a_1 of the logarithm and the coefficient a_2 of the integral in expression (2). The results for the temperature dependences are displayed in Fig. 2. The fitted curves describe the experimental results fairly well, with the exception of the curves in 8 and 10 T for sample 3 at temperatures above 2 K. These deviations could be due to the fact that the two-dimensionality condition $d\gg(D\hbar/k_BT)^{1/2}$ is not satisfied. The adjustable parameters are $a_1=0.45$ and $a_2=0.23$ for sample 2 and $a_1=0.57$ and $a_2=0.16$ for sample 3. If it is assumed that the interaction constant for $j=0$ equals 1, then $\lambda_0=0.32$ and $\lambda_{\pm 1}=0.125$ for sample 2 and $\lambda_0=0.2$ and $\lambda_{\pm 1}=0.1$ for sample 3. The dependences $\delta G_{xx}(H)$ calculated using the values obtained for the parameters a_1 and a_2 (curve *2* in Fig. 1) describe the experimental curves well in substantial magnetic field intervals (1–7 T for sample 2).

In fields of about 0.2 T small dips are observed in the curves $\delta G_{xx}(H)$. These dips cannot be due to the behavior of only a weak localization and interaction in the diffusion channel in a magnetic field. Apparently, they are due to the electron-electron interaction in the Cooper channel.

A magnetic field suppresses the first-order localization corrections to the conductance. However, since in strong magnetic fields δG_{xx} become comparable to G_{xx}, there arises the question of what role do localization corrections to the conductance in the next order play. According to the results obtained on the basis of the nonlinear σ model in a magnetic field (see the review in Ref. 12 and references cited therein),

$$\beta=\frac{d\ln G_{xx}}{d\ln L}=-\frac{2}{(2\pi G_{xx})^2}-\frac{6}{(2\pi G_{xx})^4}+O\left(\frac{1}{(2\pi G_{xx})^6}\right). \qquad (3)$$

For our values of G_{xx} (in units of e^2/h) only the first term on the right-hand side of the expression need be retained. Then, solving the equation we obtain

$$G_{xx}=\left(G_{xx,0}^2-\frac{1}{\pi^2}\ln L\right)^{1/2}\approx G_{xx,0}+\frac{p}{4\pi^2}\frac{1}{G_{xx,0}}\ln(T/T_0), \qquad (4)$$

where $L=(D\tau_\varphi)^{1/2}$. The magnetic field dependence of the quantity $\delta G_{xx}=G_{xx}-G_{xx,0}$ for this case is presented in Fig. 1 (curve *3*). The value of G_{xx} at $T=4.2$ K was taken as $G_{xx,0}$ and it is assumed that $p=1$, just as in a zero magnetic field.[1,11] The values of $\delta G_{xx}(H)$ computed in this manner are much smaller than the experimental values (see Fig. 1), i.e., the electron-electron interaction dominates.

Let us discuss the effect of the electron-electron interaction in films with G_{xx} and $G_{xy}>e^2/h$ at low temperatures. As temperature decreases, the dissipative conductance G_{xx} decreases as a result of the electron-electron interaction, while the Hall conductance G_{xy} does not change. It the dissipative conductance vanishes, then according to Laugh-

lin's gauge arguments the Hall conductance should be quantized.[13] Therefore it can be expected that the electron-electron interaction, which decreases G_{xx}, ultimately will result in quantization of $G_{xy}=ie^2/h$. Since there are no distinguished values of i, G_{xy} will apparently approach one of the closest quantized values as temperature decreases, and transitional regions where G_{xy} is not quantized and correspondingly, G_{xx} approaches a constant value should exist. Such behavior of films was conjectured by Khmel'nitskiĭ on the basis of a single-electron analysis.[14] However, for $G_{xx}>e^2/h$ the temperature dependence of G_{xx} due to the interaction is stronger than the temperature dependence of G_{xx} due to single-electron effects. Therefore the quantization of G_{xy} should be due mainly to the electron-electron interaction. In this case, the quantization of G_{xy} and the decrease of G_{xx} should apparently be accompanied by the appearance of Coulomb gaps at the Fermi level.

In summary, the experimental results are described quite well by quantum corrections, due to electron-electron interaction in the diffusion channel, to the conductance, if it is assumed that either $\lambda_0 \neq \lambda_{\pm 1}$ or the second term in brackets in expression (1) is different from 1. The quantization of the Hall conductance observed in Ref. 9 is apparently due to the electron-electron interaction.

I wish to thank N. T. Moshchegov and A. I. Toropov for preparing the samples. This work was supported by the Government Programs ''Physics of Solid-State Nanostructures'' (Grant 1-085/4) and ''Statistical Physics.''

[1] B. L. Al'tshuler and A. G. Aronov, in *Electron-Electron Interaction in Disordered Systems*, edited by A. L. Efros and M. Pollak, North-Holland, Amsterdam, 1987.
[2] P. A. Lee and T. V. Ramakrishnan, Rev. Mod. Phys. **57**, 287 (1985).
[3] A. Houghton, J. R. Senna, and S. C. Ying, Phys. Rev. B **25**, 2196 (1982).
[4] A. Houghton, J. R. Senna, and S. C. Ying, Phys. Rev. B **25**, 6468 (1982).
[5] S. M. Girvin, M. Johnson, and P. A. Lee, Phys. Rev. B **26**, 1651 (1982).
[6] B. L. Altshuler, A. G. Aronov, and P. A. Lee, Phys. Rev. Lett. **44**, 1288 (1980).
[7] A. M. Finkel'shteĭn, Zh. Éksp. Teor. Fiz. **84**, 168 (1983) [Sov. Phys. JETP **57**, 97 (1983)].
[8] M. A. Paallanen, D. C. Tsui, and A. C. Gossard, Phys. Rev. B **25**, 5566 (1982).
[9] S. S. Murzin, A. G. M. Jansen, and P. v. d. Linden, Phys. Rev. Lett. (in press).
[10] Kh. I. Amirkhanov, R. I. Bashirov, and A. Yu. Mollaev, Fiz. Tekh. Poluprovodn. **4**, 1884 (1970) [Sov. Phys. Semicond. **4**, 1616 (1970)].
[11] J. C. Maan, Th. Tnglert, Ch. Uihlein *et al.*, Solid State Commun. **47**, 383 (1995).
[12] Bodo Huckestein, Rev. Mod. Phys. **67**, 357 (1995).
[13] R. B. Laughlin, Phys. Rev. B **23**, 5632 (1981).
[14] D. E. Khmel'nitskiĭ, JETP Lett. **38**, 552 (1983).

Translated by M. E. Alferieff

Transformation of the dimensionality of excitonic states in quantum wells with asymmetric barriers in an electric field

Yu. A. Aleshchenko,[a)] I. P. Kazakov, V. V. Kapaev, and Yu. V. Kopaev
P. N. Lebedev Physical Institute, Russian Academy of Sciences, 117924 Moscow, Russia

(Submitted 5 January 1998)
Pis'ma Zh. Éksp. Teor. Fiz. **67**, No. 3, 207–211 (10 February 1998)

A transformation of the dimensionality of excitonic states from 2D to 3D with increasing external electric field is observed in single GaAs/$Al_xGa_{1-x}As$ quantum-well structures with asymmetric barriers. The binding energy of a 2D exciton remains constant over a wide range of variation of the field, since the decrease in the binding energy is compensated by increasingly larger penetration of the electronic wave function into the barrier layer, where the exciton binding energy is higher because the effective mass is larger and the dielectric constant of AlGaAs is lower than that of GaAs. When the maximum of the electron wave function is displaced into the barrier as the field increases, the exciton binding energy decreases. As the field increases further, a 2D exciton transforms into a quasi-3D exciton, with a heavy hole in the quantum well and an electron in a resonant above-barrier state.
 [S0021-3640(98)00903-7]

PACS numbers: 71.35.Cc, 78.66.Fd, 78.55.Cr

The problem of energy levels in a potential well with asymmetric barriers is well known from quantum mechanics.[1] In contrast to a well with symmetric barriers, where at least one energy level always exists, the presence of a bound state for a particle with mass m in a square well of width d with barriers $U_1 \neq U_2$ and masses m_1 and m_2 is determined by the condition

$$d\frac{\sqrt{2mU_1}}{\hbar} \geqslant \tan^{-1}\sqrt{\frac{m_1}{m_2}\left(\frac{U_1}{U_2}-1\right)}.$$

For smaller values of d, as has been confirmed experimentally for the example of single GaAs/InGaAs/AlGaAs quantum wells with asymmetric barriers,[2] a bound state does not exist, and the corresponding excitonic peak in the photoluminescence spectra vanishes.

In a previous work[3] we investigated the dispersion law $E(k)$ for quantum wells with asymmetric barriers. It was shown that a localized electron state exists in a limited range of wave vectors $(0,k_c)$ in the direction of the layers of the structure. A 2D–3D transformation of the states occurs at $k=k_c$; in addition, an electric field makes it possible to control the value of k_c, i.e., the dimension of the states. In the present work we under-

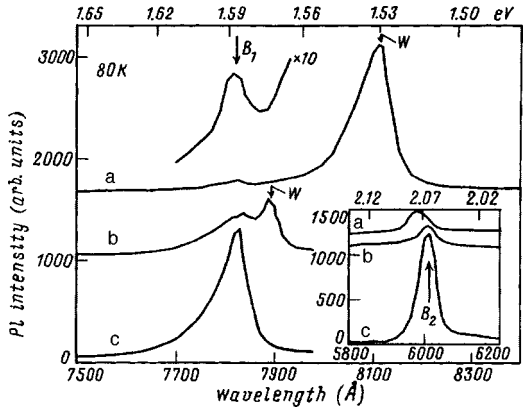

FIG. 1. Photoluminescence spectra of structures with $d=10$ (a), 4 (b), and 3 (c) nm at 80 K. Inset: Short-wavelength sections of the corresponding spectra measured with 10–20-fold amplification.

took detailed photoluminescence investigations of this effect in structures consisting of single GaAs/AlGaAs quantum wells with asymmetric barriers. A characteristic feature of the measurements performed in an electric field was that an electron tends to delocalize (the bound state vanishes) as the field increases, while for a hole, conversely, the quantum well becomes deeper. It was found, specifically, that in contrast to Ref. 2 bound states of an exciton remain in the structure over a wide range of electric fields, when a localized state of an electron in a quantum well no longer exists.

Undoped quantum wells of width $d=10$, 4, and 3 nm, confined between the top and bottom $Al_xGa_{1-x}As$ barrier layers with compositions $x=0.4$ and $x=0.06$ and thicknesses of 10 and 30 nm, respectively, were grown on semi-insulating GaAs substrates with a 250 nm thick GaAs buffer layer by molecular-beam epitaxy. The quantum-well widths were chosen so that in structures with $d=10$ and 4 nm a bound state of an electron would exist in a well without the application of an external electric field, while in a structure with $d=3$ nm there would be no bound state. The electric field could be controlled by introducing a 50 nm thick n^+GaAs:Si (10^{18} cm^{-3}) layer after the buffer layer as the bottom electrode and doping the top protective 10 nm thick GaAs layer with Si up to 10^{18} cm^{-3}. The active layers of the structure were confined between the top and bottom spacers $n^+Al_xGa_{1-x}As$:Si with compositions $x=0.4$ and $x=0.06$ and thicknesses 30 and 25 nm, respectively. The doping levels of the spacers (6.5×10^{17} cm^{-3} for the top layer and $(3-6)\times10^{16}$ cm^{-3} for the bottom layer) were chosen so as to ensure that the flat-band condition is satisfied in the absence of external perturbations. The photoluminescence spectra were measured at a temperature of 80 K with excitation by 488 nm Ar^+ laser radiation and power density on the sample of not more than 40 W/cm^2. The spectra were analyzed with a DFS-24 double monochromator and detected with a photomultiplier in the photon-counting mode.

Figure 1 shows the spectra of structures with $d=10$, 4, and 3 nm (spectra a, b, and c, respectively); the short-wavelength sections of the corresponding spectra are displayed in the inset. The peaks B_1 and B_2, which occur in all spectra, at 1.585 and near 2.07 eV are due to the contributions of the bottom and top AlGaAs barrier layers. The position of these peaks, taking account of the binding energies of $Al_xGa_{1-x}As$ excitons,[4] confirms

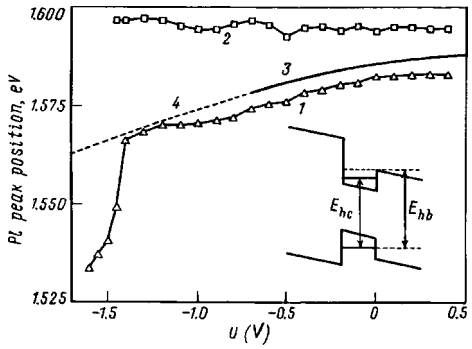

FIG. 2. Curves versus the voltage applied to the top half-transmitting electrode for $C1-H1$ (curve *1*) and low-barrier (curve *2*) excitonic peaks as well as for energies E_{hc} and E_{hb} of structures with $d=4$ nm (curves *3* and *4*). Inset: Schematic illustration of the choice of the parameters E_{hc} and E_{hb} .

that the layer compositions are close to the nominal compositions with $x=0.06$ and 0.4. The intense exciton peak W, due to the first size-quantization sublevels of electrons and heavy holes ($C1-H1$) in the 10-nm-wide quantum well, dominates the spectrum a. For $d=4$ nm the peak W of the quantum well approaches the low-barrier peak B_1, and in addition the intensity of the peak decreases and the peak itself broadens, since the sublevel $C1$ is near the top of the low barrier. In the spectrum of the structure with $d=3$ nm, where there is no bound state of an electron in the well, only the low-barrier luminescence peak B_1 is present.

To follow the evolution of the excitonic state of the quantum well with continuous variation of the height of the low barrier, a top half-transmitting Ni electrode was deposited on structures with $d=4$ and 3 nm and contacts to the electrode and to the n^+ buffer layer were prepared. As the voltage U applied to the half-transmitting electrode varies from $+0.4$ to -1.4 V, the intensity of the $C1-H1$ photoluminescence peak for the structure with $d=4$ nm diminishes and the peak itself broadens and slowly shifts to lower energies (curve *1* in Fig. 2), since the quadratic Stark effect for direct transitions is very weak, while the Franz–Keldysh effect is less than the error in our measurements. For the same reasons, the position of the excitonic peak B_1 of the low barrier remains practically unchanged (curve *2*), though it too weakens and broadens with decreasing U as a result of the weakening of the Coulomb attraction between the electron and hole, forming the exciton, in an electric field. Besides this factor, the increase in the asymmetry of the potential relief for electrons as U decreases also plays an important role in the weakening of the peak $C1-H1$ for the structure with $d=4$ nm.

To interpret the results obtained we performed calculations of the energy of the localized states of electrons and holes as a function of the electric field E, using a method similar to that of Ref. 3. The electric field E was converted into the potential difference U applied to the sample by solving the Poisson equation taking account of all layers comprising the structure. The line 3 in Fig. 2 corresponds to the energy obtained in this manner for the transitions $C1-H1$ (the transition E_{hc} in the inset to Fig. 2). We note that the experimental and theoretical curves are nearly parallel over a substantial voltage range (from $+0.4$ to -0.6 V), since the decrease occurring in the binding energy of the $C1-H1$ exciton as U decreases is compensated by the increasingly larger penetration of

the electron wave function into the low barrier, where, on account of the larger effective mass and the lower dielectric constant in AlGaAs than in GaAs, the binding energy of the exciton is higher. According to the calculations, the electron level leaves the well near $U_c = -0.6$ V.

Despite the fact that the electron level leaves the well at $U_c = -0.6$ V, the excitonic peak W of the quantum well is also observed for $U < U_c$. This last circumstance can be explained on the basis of notions similar to the ''Coulomb well'' model. This model is successful in explaining the substantial oscillator strengths of excitonic transitions in (In, Ga)As/GaAs, CdTe/(Cd, Zn)Te, and CdTe/(Cd, Mn)Te heterostructures with a close to zero valence-band offset (see, for example, Ref. 5). In our case, the electron-confining potential creates a heavy hole, for which the low barrier increases with increasing negative voltage on the top electrode. For this reason, the $C1$–$H1$ transition in the structure with $d = 4$ nm remains direct in real space and the corresponding excitonic peak is observed in the spectra at voltages below $U_c = -0.6$ V also. The additional electron-confining Coulomb potential increases the depth of the well for an electron by an amount δ, equal to several meV. This results in a shift of U_c in the direction of smaller values of U as the ratio of δ to the initial height of the low barrier, but the luminescence peak is also observed for much lower values of U. In the region -1.4 V $< U < U_c$ the luminescence is most likely due to a transition between the localized-hole $H1$ state and electronic states in the continuous spectrum, whose energy falls near the top of the low barrier (the quantity E_{hb} in the inset in Fig. 2). The dotted curve *4* in Fig. 2 reflects the dependence of U_{hb} on U. The maximum of the wave function for such states now lies in the barrier. By its very nature, this is a quasi-3D exciton. For voltages across the structure in the range from -0.7 V to -1.2 V, the experimental curve in Fig. 2 approaches the curve *4* as a result of a decrease in the exciton binding energy with increasing field.

The sharp voltage dependence of the position of the luminescence peak in the region $U < -1.4$ V attests to the fact that in this region the exciton becomes substantially indirect. Such an exciton can exist only in the presence of some structure in the continuous spectrum of electronic states. In our opinion, this structure could be due to resonances in the continuous spectrum as a result of reflections on the jump in the potential formed at the heterointerface between the $Al_{0.06}Ga_{0.94}As$ barrier and the bottom n^+GaAs contact layer. In such a case, the exciton is formed by an electron in a resonance state and a heavy hole localized in the quantum well, while the overlapping of the corresponding wave functions, which is necessary for the oscillator strength to be finite, is produced by electron tunneling from the resonance state into the quantum well through a triangular barrier. As the voltage on the structure varies from -1.4 V to -1.6 V, the width of the triangular barrier at the level of the resonance state changes from 0 to 25 nm.

At voltages from -1.4 V to -1.6 V we noted a strong nonlinearity in the curve of the integrated intensity of the peak W of the quantum well versus the power of the exciting radiation. This nonlinearity can be explained by the screening of the external electric field by photoexcited charge carriers. The effect of the screening is that as the power of the exciting radiation increases, the effective field decreases and corresponds to the flat section of the curve *1* in Fig. 2, where the quasi-3D exciton is direct, and the intensity of the peak W increases sharply. The peak of the quantum-well exciton can be traced in the spectra of the structure with $d = 4$ nm up to a voltage of -1.6 V. At higher voltages, the electric field tears apart the quasi-3D above-barrier exciton. The three-

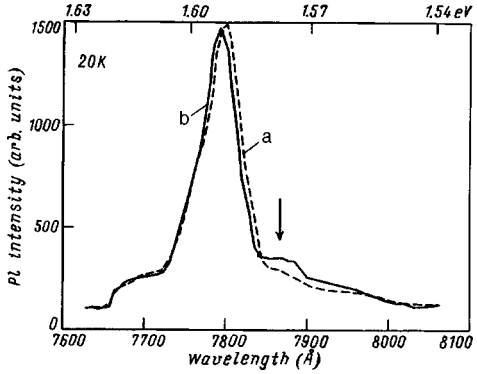

FIG. 3. Photoluminescence spectra of structures with $d=3$ nm, measured at temperature 20 K and voltages -1.0 V (a) and $+0.6$ V (b) on the top electrode. The arrow marks the contribution of the quantum-well exciton.

dimensional exciton of the low $Al_{0.05}Ga_{0.95}As$ barrier is torn apart by an even weaker field, as is indicated by the vanishing of the corresponding peak B_1 even at a voltage of -1.45 V (curve *2* in Fig. 2).

We also attempted to produce an electronic bound state in an electric field. In a structure with $d=3$ nm at temperature 80 K and $U=0$ there is no electronic bound state in the quantum well, so that it is possible to record only the low-barrier peak b_1 in the luminescence spectrum (spectrum c in Fig. 1). As the temperature decreases to 20 K, long-lived states appear in the structures. These states are due to the strong built-in field, opposing the external electric field. The built-in field has the effect that even at a voltage of -1.0 V on a structure with $d=3$ nm a weak shoulder caused by the contribution of the quantum-well exciton (arrow in spectrum a in Fig. 3) is noticeable in the spectrum. The peaks at 1.59 and 1.62 eV are due to contributions of the low-barrier excitons with heavy and light holes, respectively. As the voltage on the structure increases, the asymmetry of the potential relief for electrons decreases, an electron state is present in the well, and the intensity of the quantum-well exciton increases (the peak opposite the arrows in spectrum b in Fig. 3, measured with a voltage of $+0.6$ V on the structure).

We acknowledge V. I. Tsekhosh for growing the structures and S. S. Shmelev for lithography and preparation of the contacts. This work was supported by the Russian Fund for Fundamental Research and the Russian Interdisciplinary Science and Technology Program ''Physics of Solid-State Nanostructures.''

[a)]e-mail: YURIALE@sci.lpi.ac.ru

[1] L. D. Landau and E. M. Lifshitz, *Quantum Mechanics: Non-Relativistic Theory*, Pergamon Press, New York, 1977 [cited Russian original, Nauka, Moscow, 1989].
[2] K. Pieger, J. Straka, A. Forchel *et al.*, in *Proc. MRS Fall*, Boston, 1993, p. 255.
[3] V. V. Kapaev and Yu. V. Kopaev, JETP Lett. **65**, 202 (1997).
[4] L. Pavesi and M. Guzzi, J. Appl. Phys. **75**, 4779 (1994).
[5] A. V. Kavokin, M. A. Kaliteevski, S. V. Goupalov *et al.*, Phys. Rev. B **54**, R11078 (1996).

Translated by M. E. Alferieff

Phase transitions in the ferromagnetic alloys $Ni_{2+x}Mn_{1-x}Ga$

A. D. Bozhko, A. N. Vasil'ev, and V. V. Khovaĭlo
M. V. Lomonosov Moscow State University, 119899 Moscow, Russia

V. D. Buchel'nikov
Chelyabinsk State University, 454021 Chelyabinsk, Russia

I. E. Dikshteĭn, S. M. Seletskiĭ, and V. G. Shavrov[a)]
Institute of Radio Engineering and Electronics, Russian Academy of Sciences, 103907 Moscow, Russia

(Submitted 5 January 1998)
Pis'ma Zh. Éksp. Teor. Fiz. **67**, No. 3, 212–216 (10 February 1998)

The phase diagram of the cubic ferromagnetic shape-memory alloy $Ni_{2+x}Mn_{1-x}Ga$ is constructed theoretically for the case when the Curie temperature is close to the structural transition temperature. This diagram agrees well with the experimental data obtained from resistance and magnetic susceptibility measurements. It is shown that the transition from the paramagnetic cubic phase to the ferromagnetic tetragonal phase can be second-order or first-order. © *1998 American Institute of Physics.* [S0021-3640(98)01003-2]

PACS numbers: 75.50.Cc, 81.30.Bx, 75.30.Kz

The only compound among Mn-containing Heusler alloys that undergoes a martensitic structural transformation to a ferromagnetic phase is the compound Ni_2MnGa (Refs. 1 and 2). For the stoichiometric composition, the ferromagnetic transition temperature ($T_C = 376$ K) differs substantially from the structural transition temperature ($T_M = 202$ K). The temperatures T_C and T_M can be changed by purposefully varying the composition of this compound. To realize such a possibility, some of the Mn atoms must be replaced by Ni atoms in the alloy. Then the distance between the Mn atoms increases, and the exchange integral and together with it the magnetic transition temperature T_C decrease. At the same time, when such a substitution is made, the electron density and the structural transition temperature T_M increase. In this way it is in principle possible to make T_M equal to T_C in the alloy $Ni_{2+x}Mn_{1-x}Ga$ for some value of the concentration x. The problem of the convergence of the structural and magnetic transition temperatures toward one another is important, since for such an alloy this opens up the possibility of using a magnetic field to control effectively the shape memory of the material.

In the present letter the possible magnetic and structural phase transitions in a cubic ferromagnet are analyzed theoretically for the case when the magnetic and structural transition temperatures are close to one another, and the phase diagram obtained is compared with the experimental data. It is shown experimentally that the temperatures

T_C and T_M become equal at $x=0.16-0.19$. Then $T_M \approx T_C \sim 335 \pm 15$ K.

To analyze the phase diagram of the ferromagnet $Ni_{2+x}Mn_{1-x}Ga$ we shall employ the Landau phenomenological model of phase transitions. We shall study a cubic ferromagnet with the point symmetry group O_h with a magnetic phase transition, accompanied by the appearance of a spontaneous magnetization M, and with a characteristic ferroelastic phase transition to a tetragonal phase with D_{4h} symmetry during which spontaneous strains arise.[3–5] In this case, the order parameters describing structural transformations are components of the macroscopic strain tensor e_{ik}. We shall describe the magnetic phase transitions by the components of the macroscopic magnetization M. The expression for the free energy of the ferromagnet, after it is minimized with respect to the components of the strain tensor that are not responsible for the structural phase transition, assumes the form

$$F = F_0 + \frac{1}{2}a(e_2^2+e_3^3) + \frac{1}{3}be_3(e_3^2-3e_2^2) + \frac{1}{4}c(e_2^2+e_3^2)^2 + B\left[\frac{1}{\sqrt{2}}e_2(m_1^2-m_2^2) + \frac{1}{\sqrt{6}}e_3(3m_3^2-m^2)\right] + \frac{1}{2}\alpha(m_1^2+m_2^2+m_3^2) + \frac{1}{4}\delta(m_1^2+m_2^2+m_3^2)^2 + K(m_1^2m_2^2 + m_2^1m_3^2 + m_3^2m_1^2), \quad (1)$$

where $\alpha=\alpha_0(T-T_C)$; δ and K are, respectively, the magnetostriction-renormalized exchange constant and the first cubic anisotropy constant; $e_2=(e_{xx}-e_{yy})/\sqrt{2}$; $e_3=(2e_{zz}-e_{xx}-e_{yy})/\sqrt{6}$; a, b, and c are, respectively, linear combinations of the second-, third-, and fourth-order elastic constants: $a=c_{11}-c_{12}$, $b=(c_{111}-c_{112}-c_{123})/6\sqrt{6}$, $c=(c_{1111}+c_{1112}-3c_{1122}-8c_{1123})/48$, $m=M/M_0$, M_0 is the saturation magnetization far from the Curie point, and B is the relativistic magnetostriction constant. As the point of the structural phase transition from the cubic to the tetragonal phase with the two-component order parameter e_2, e_3 is approached, the elastic modulus $a=c_{11}-c_{12}$ approaches zero, and near the transition point $T=T_M$ it can be written in the form $a=a_0(T-T_M)$. The presence of third-order terms in the free energy gives rise to a first-order structural transition.

To find all possible structural and magnetic phases the energy (1) must be minimized with respect to the variables e_2, e_3, m_1, m_2, and m_3. As a result, we obtain the following states of the ferromagnet and the conditions under which they are stable, assuming for definiteness that $b>0$, $c>0$, $K<0$, and $B>0$ (which corresponds to magnetization orientation in the crystallographic direction [111] in the cubic phase in the stoichiometric alloy Ni_2MnGa):

1) the cubic paramagnetic phase—$m_1=m_2=m_3=0$, $e_2=e_3=0$ is stable for $\alpha \geqslant 0$, $a \geqslant 0$;

2) the tetragonal paramagnetic phase—$m_1=m_2=m_3=0$, $e_2=0$, $e_3=-(b+(b^2+4ac)^{1/2})/2c$ is stable for $\alpha \geqslant 2Bb/\sqrt{6}c$, $a \leqslant b^2/4c$,

$$a \geqslant b^2/4c - \left(\sqrt{6}\frac{\alpha}{4B}\sqrt{c} - \frac{b}{2\sqrt{c}}\right)^2;$$

3) the cubic ferromagnetic phase—$e_2=e_3=0$, $m_1=m_2=m_3=m/(3)^{1/2}$, $m_2=-\alpha/(\delta-4q/3)$, where $q=|K|$, is stable for $\alpha\leqslant 0$, $a\geqslant B^2/q$;

4) the tetragonal canted ferromagnetic phase

$$m_1^2=m_2^2=-\frac{1}{3}\frac{\alpha}{\delta-4q/3}+\frac{Be_3}{\sqrt{6}q},\quad m_3^2=-\frac{1}{3}\frac{\alpha}{\delta-4q/3}-\frac{2Be_3}{\sqrt{6}q},$$

$$e_2=0,\quad e_3=-\frac{b+\sqrt{b^2-4c(a-B^2/q)}}{2c},$$

is stable for

$$a\leqslant b^2/4c+B^2/q,\quad a\geqslant b^2/4c+B^2/q-\left(\sqrt{2/3}\,\frac{q}{B}\cdot\frac{\alpha}{\delta-4q/3}\sqrt{c}+\frac{b}{2\sqrt{c}}\right)^2,$$

$$\alpha\leqslant-\sqrt{6}bB(\delta-4q/3)/4cq;$$

5) the tetragonal collinear ferromagnetic phase

$$m_1=m_2=0,\quad m_3^2=-(\alpha+4Be_3/\sqrt{6})/\delta,$$

$$e_2=0,\quad ae_3+be_3^2+c_3^3+\sqrt{\frac{2}{3}}\,Bm^2=0,$$

is stable in the region bounded by the curves

$$a=b^2/4c+B^2/q-\left(\sqrt{2/3}\,\frac{q\alpha\sqrt{c}}{B(\delta-4q/3)}+\frac{b}{2\sqrt{c}}\right)^2,\quad(\alpha\leqslant 0),$$

$$a=b^2/4c-\left(\sqrt{6}\,\frac{\alpha}{4b}\,\sqrt{c}-\frac{b}{2\sqrt{c}}\right)^2\quad(\alpha\geqslant 0)$$

and the discriminant curve of the cubic equation determining the strain e_3 in the given phase.

In the cubic ferromagnetic phase 3 the magnetization $M\parallel[111]$. In the canted ferromagnetic tetragonal phase 4, M changes direction from [111] to [001] as the temperature increases. Finally, in the tetragonal collinear phase 5 one has $M\parallel[001]$. It follows from symmetry considerations that besides these states, other tetragonal states, whose energy and regions of stability are the same as those indicated above, can also be realized in the ferromagnet. States with $M\parallel[100]$ and $M\parallel[010]$ are equivalent in terms of energy to phase 5. Accordingly, canted states, which are analogous to phase 4 and in which the magnetization changes direction from [111] to [100] and [010], can also be realized. The presence of several phases with the same energies and regions of stability results in the existence of structural and magnetic domains in ferromagnets. We note that from the standpoint of the tetragonal distortion of the lattice, phase 5 has the same symmetry as phase 4, and for this reason transitions between these phases are isostructural.

The lines of phase transitions between possible states are determined from the condition that the energies of the phases are equal. To compare theory with experiment, we

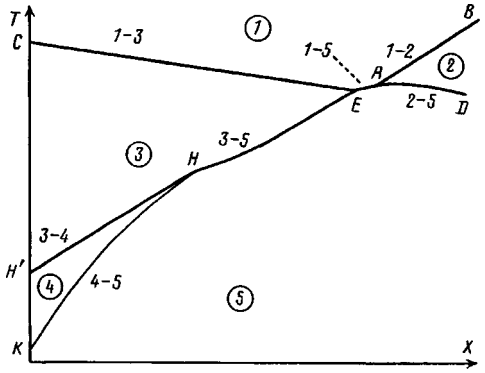

FIG. 1. Phase diagram of a cubic ferromagnet in the (T,x) plane (schematic). The numbers enumerate the phases. The solid lines are lines of phase transitions.

present here the phase diagram in the coordinates temperature T versus concentration x. For this, we propose the following linear dependence of the temperatures T_M and T_C on x:

$$T_M = T_{M0} - 2b^2/(9ca_0) - B^2/(qa_0) + \kappa x, \quad T_C = T_{C0} - \gamma x, \tag{2}$$

where T_{M0} and T_{C0} are the temperatures of the martensitic and magnetic transitions with stoichiometric composition ($x=0$), and κ and γ are proportionality coefficients.

The lines of the phase transitions in the variables T–x have the form

$$(1)\Leftrightarrow(2) \quad T = T_{M0} - B^2/(a_0 q) + \kappa x; \tag{3}$$

$$(1)\Leftrightarrow(3) \quad T = T_{C0} - \gamma x; \tag{4}$$

$$(3)\Leftrightarrow(4) \quad T = T_{M0} + \kappa x. \tag{5}$$

The analytical expressions for the remaining transition lines are too complicated to present here. The T–x phase diagram is displayed in Fig. 1. The coordinates of the characteristic points of this diagram are:

$$A\ \{x_A = [T_{C0} + 8bB/3\sqrt{6}c\alpha_0 - T_{M0} + B^2/qa_0]/(\kappa+\gamma),$$

$$T_A = [\kappa(T_{C0} + 8bB/3\sqrt{6}c\alpha_0) + \gamma(T_{M0} - B^2/qa_0)]/(\kappa+\gamma)\};$$

$$H:\ \{x_H = [T_{C0} - T_{M0} - 2bB(\delta - 4q/3)/\sqrt{6}qc\alpha_0]/(\kappa+\gamma),$$

$$T_H = [\kappa(T_{C0} - 2bB(\delta - 4q/3)/\sqrt{6}qc\alpha_0) + \gamma T_{M0}]/(\kappa+\gamma)\};$$

$$E\ \{x_E = [T_{C0} - T_{M0} - B^2/qa_0 - 4B^2/3\delta a_0]/(\kappa+\gamma),$$

$$T_E = [\kappa T_{C0} + \gamma(T_{M0} - B^2/qa_0 + 4B^2/3\delta a_0)]/(\kappa+\gamma)\}.$$

The following phase transitions from the paramagnetic cubic phase 1 are possible: along the line AB—A first-order structural phase transition to the tetragonal paramagnetic phase 2; along the line EC—an isostructural second-order transition to a cubic

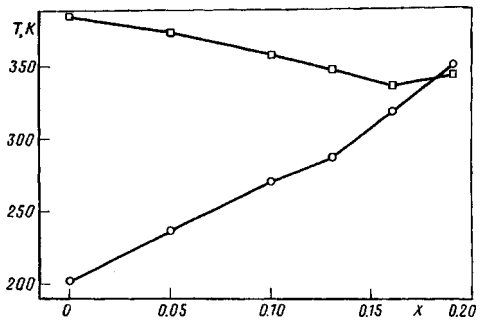

FIG. 2. Experimental $x-T$ phase diagram of the system of alloys $Ni_{2+x}Mn_{1-x}Ga$: □—T_C, ○—T_M.

ferromagnetic phase 3 with $M \parallel [111]$; and, along the line EA—a first-order magnetic and structural phase transition to the tetragonal ferromagnetic phase 5. Besides the transition 1–2 described above, an isostructural second-order magnetic transition from the tetragonal paramagnetic phase 2 to the tetragonal ferromagnetic phase 5 (line AD) is also possible. First-order structural and orientational transitions to the tetragonal phases 4 (line HH') and 5 (line HE) are also possible from the cubic ferromagnetic phase 3. A second-order isostructural orientational phase transition to the phase 5 (line HK) occurs from the phase 4.

The experimental phase diagram constructed for the alloys $Ni_{2+x}Mn_{1-x}Ga$ from measurements of the resistance and magnetic susceptibility is displayed in Fig. 2. One can see that in the concentration interval $0<x<0.19$ the experimental data are in qualitative agreement with the computed $x-T$ diagram. Thus, it follows from Figs. 1 and 2 that the temperature of the magnetic phase transition from the cubic paramagnetic phase 1 to the cubic ferromagnetic phase 3 decreases linearly with concentration. The temperature of the phase transition from the cubic ferromagnetic phase 3 to the tetragonal ferromagnetic phases 4 and 5 (differing by the orientation of the magnetization relative to the crystallographic axes) increases with concentration.

It follows from the phase diagram that the transition between the cubic paramagnetic and ferromagnetic phases (the line EC) and the tetragonal paramagnetic and ferromagnetic phases (the line AD) are second-order phase transitions. This is a typical situation for phase transitions in magnets at the Curie point. The transition from the cubic paramagnetic phase to a martensitic tetragonal ferromagnetic phase is, however, a first-order phase transition (the line EA). This effect is entirely due to the interaction of the structural and magnetic order parameters. For close values of T_M and T_C, the first-order phase transition is accompanied by the existence of a latent heat of transition and hysteresis in the temperature dependences of the resistance and magnetic susceptibility.

The work was supported by Russian Fund for Fundamental Research Grant 96-02-19755 and ISSEP Grant 615p.

[a)]e-mail:shavrov@mail.cplire.ru

---

[1] P. J. Webster, K. R. A. Ziebeck, S. L. Town, and M. S. Peak, Philos. Mag. **49**, 295 (1984).
[2] A. N. Vasil'ev, A. R. Keiper, V. V. Kokorin *et al.*, Int. J. Appl. Electromagn. Mater. **5**, 163 (1994).
[3] M. A. Fradkin, Phys. Rev. B **50**, 16326 (1994).
[4] Yu. M. Gufman, *Structural Phase Transitions* [in Russian], Nauka, Moscow, 1982.
[5] Yu. A. Izyumov and V. N. Syromyatnikov, *Phase Transitions and Symmetry of Crystals* [in Russian], Nauka, Moscow, 1984.

Translated by M. E. Alferieff

Radio-frequency modulation of the reflection of light in semiconductor heterostructures

O. A. Ryabushkin[a)] and V. A. Sablikov

Institute of Radio Engineering and Electronics, Russian Academy of Sciences, 141120 Fryazino, Moscow Region, Russia

(Submitted 5 January 1998)
Pis'ma Zh. Éksp. Teor. Fiz. **67**, No. 3, 217–221 (10 February 1998)

A contact-free method of modulation spectroscopy of semiconductor heterostructures is developed. The method employs the effect of an intensity-modulated rf or microwave field on the reflection of the probe light and makes it possible to investigate electron-hole interaction effects in different layers of a heterostructure. A model is proposed which explains the characteristic features of the rf-modulated optical reflection spectra observed on selectively doped GaAs/AlGaAs heterostructures is proposed. © *1998 American Institute of Physics.* [S0021-3640(98)01103-7]

PACS numbers: 78.66.Fd, 78.40.Fy, 78.70.Gq

1. Optical methods, such as photoluminescence (PL) spectroscopy and modulation spectroscopy, have been used to investigate semiconductors and semiconductor structures for more than 40 years now. In modulation spectroscopy, the electroreflectance (ER) method, which is used in a wide temperature range, and its contact-free modification—the photoreflectance (PR) method are most widely used. Despite their obvious advantages these methods do have drawbacks that limit their applicability. In the ER method the drawback is the need to produce electrical contacts, while in the case of PR at low temperatures there arises the problem of separating the PR and PL spectra. This happens because of the strong increase (by several orders of magnitude) in the PL amplitude which makes it difficult to measure reflection. This problem is especially acute for modern heterostructures, in the investigation of which PR is used to determine the built-in and photoinduced electric fields.[1] In the present letter we propose a contact-free method of modulation spectroscopy that preserves the advantages of the PR and ER methods and can be used right down to ultralow temperatures. The method is based on modulation of the reflection of the probe light by a rf or microwave electric field. Two measurement regimes are possible:

1) If the amplitude of the field is constant in time, then a change in the optical reflection is detected at the frequency of this field, which can be quite high (all the way up to $\sim 10^{12}$ Hz). This is essentially the case of electroreflection in the rf or microwave ranges;

2) if, however, an amplitude-modulated microwave field is used, then the optical

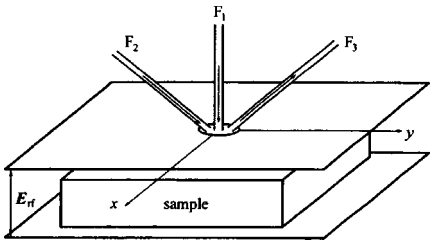

FIG. 1. Spatial arrangement of the heterostructure, the optical fibers (F_1, F_2, F_3), and the rf field E_{rf}.

response is detected at the modulation frequency; in this case, the rf or microwave modulation reflectance—RMR or MMR—method is realized.[2–4]

2. The experiments were performed on GaAs/$Al_xGa_{1-x}As$ semiconductor heterostructures with a two-dimensional electron gas (2DEG). The heterostructure was sandwiched between flat capacitor plates, to which an amplitude-modulated voltage $U_{rf}(1+\sin(\Omega t))\sin(2\pi ft)$ was applied. The frequency f of the field varied from 10^5 to 3×10^7 Hz. The amplitude E_{rf} of the rf field was equal to $\sim10^3$ V/cm, and the modulation frequency was equal to 10^2–10^4 Hz. The probe light beam was brought up to the sample and extracted by means of the optical fibers F_2 and F_3 through a small opening in the capacitor plate (Fig. 1). The spectrum-integrated intensity of the probe light beam varied in the range 10^{-5}–1 W/cm^2. The RMR signal was measured by synchronous detection at the modulation frequency. Besides RMR, measurements of PR and PL were also performed. Optical excitation was performed with a He–Ne laser ($\lambda=633$ nm), whose radiation was delivered through the optical fiber F_1. The excitation intensity was modulated at a low frequency 10^2–10^3 Hz. It is important that in the RMR method studied there is no optical pumping and for this reason there are no PL or PR signals.

Figure 2 shows the PR and RMR spectra taken at a temperature of 290 K in a field $E_{rf}\sim10^3$ V/cm for a GaAs/$Al_xGa_{1-x}As$ ($x\sim0.2$) heterostructure with a GaAs buffer layer ~0.7 μm thick. The method used in the present work to obtain the RMR spectra with low-frequency modulation of the rf field is simplest to implement, and it is most informative in the case when internal fields which vary slowly in time are under study. In

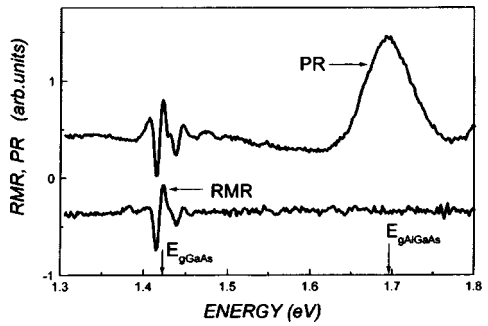

FIG. 2. Photoreflectance (PR) and rf modulation reflectance (RMR) spectra at room temperature. The vertical arrows indicate the band gaps in GaAs and AlGaAs. For clarity, the RMR spectrum is shifted by -0.5 units relative to the zero level.

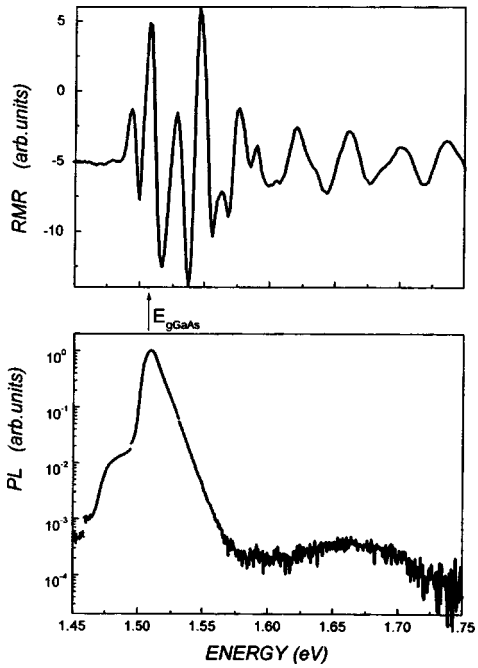

FIG. 3. RMR ($E_{rf}=3\times10^3$ V/cm) and PL spectra at 77 K.

the case when fast processes in heterostructures are of interest, it is best to measure the spectra at a high frequency, which are synchronous with the rf or microwave field.

Figure 3 displays RMR and PL spectra at 77 K. A characteristic feature of the RMR spectrum is the high amplitude of the oscillations for $h\nu<E_{g\mathrm{GaAs}}$. These oscillations are due to excitonic states in the GaAs buffer layer. Oscillations in a wide range of energies $h\nu$ from 1.505 to 1.85 eV, which are due to the Franz–Keldysh effect, are also interesting. It would be interesting to compare these spectra with the PR spectra. However, the characteristic amplitudes of the PR signal at 77 K are extremely low—at the level of the PL signal. In contrast to the PR spectra, however, the characteristic amplitudes of the RMR signals increase by several orders of magnitude as the temperature decreases to 77 K. In our view, the main advantages of the RMR method appear at low temperatures; when RMR spectra are recorded, there are no photoinduced charge carriers and hence no recombination of photoinduced charge carriers.

3. Let us now analyze the RMR signal for the example of a selectively doped GaAs/AlGaAs heterostructure. The spectrum of the RMR signal near the absorption edge is shown in Fig. 4a. The quite complicated form of the spectrum indicates that several processes, occurring at the optical reflection depth, are involved. This depth is of the order of the reciprocal of the light absorption coefficient at $h\nu\sim E_g$, which for GaAs equals $\sim1-2$ μm. Therefore the detected signal is determined by the buffer layer and the substrate region adjoining it.

The RMR signal is due to the change induced by the rf field in the electric field in these parts of the heterostructure. Since the measurements are performed in the regime of

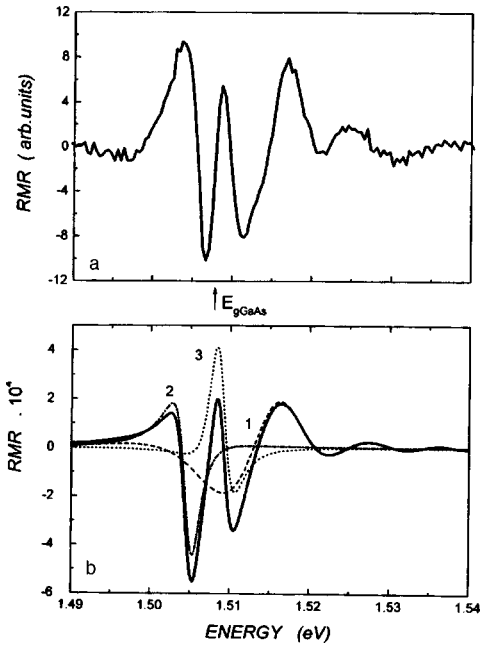

FIG. 4. a—RMR spectrum at 77 K with $E_{rf} \sim 5 \times 10^2$ V/cm, spectral resolution 0.5 meV; b—computed RMR spectrum of a heterostructure (solid line) and components due to the layers 1, 2, and 3 (curves *1*, *2*, and *3*).

low-frequency modulation, the RMR is due to the low-frequency component of the field; this component arises as a result of the detection of the external high-frequency field. The oscillations in the RMR spectrum with photon energy above 1.51 eV are evidently due to the Franz–Keldysh effect in the region of strong fields in the buffer layer. The sharp lines for $h\nu < E_g$ are due to the electron-hole Coulomb interaction. As is well known,[1,4–11] such an interaction changes the permittivity and produces the sharp features observed in the modulation spectra for sufficiently weak electric fields (compared with $E_x \sim e/a_x^2$, where a_x is the exciton radius). The field $E_x \sim 10^3$ V/cm, and therefore such an excitonic effect could be due only to the part of the GaAs buffer layer where the field is weak, i.e., near a superlattice layer (Fig. 5). However, neither the excitonic ''line'' nor the Franz–Keldysh oscillations permit describing completely the structure of the observed spectrum at $h\nu \sim 1.51$ eV. The RMR peak observed here is due to interband transitions in a weak field in the absence of an excitonic effect. Such a situation is realized in the layer of the substrate adjoining the superlattice layer.

In summary, the following three-layer model of the part of the heterostructure that determines optical reflection (Fig. 5) can be used to describe the observed spectrum:

1) layer 1, where the strong field E_1 is concentrated and which adjoins the two-dimensional electrons;

2) layer 2, bordering the superlattice and possessing a weak electric field E_x that does not destroy the excitonic states; and,

3) layer 3, which borders the substrate and where a built-in electric field E_3 is

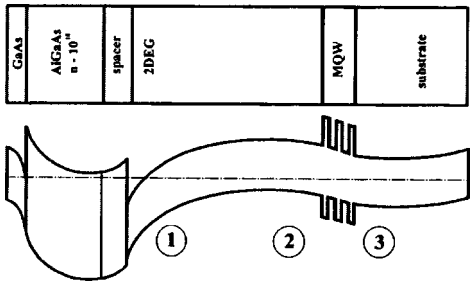

FIG. 5. Schematic arrangement of the layers and the energy diagram of the experimental structure. The GaAs buffer layer is conventionally divided into three regions: *1*) strong-field region (2DEG localization region), *2*) excitonic region, *3*) weak-field region, GaAs region, containing the boundary of the buffer layer and the substrate.

likewise present and, as one can see from Fig. 5, is directed opposite to the field E_1.

The reflection spectrum calculated for this model is presented in Fig. 4b. The contribution of layer 1 is obtained according to the Aspnes theory[9] taking account of the broadening and optical transitions from the heavy-hole subband. The contribution of layer 2 with a strong excitonic effect was found by subtracting the excitonic spectrum in the absence and presence of an external field taking account of the change in the width and position of the excitonic level.[1,5,6,10] The contribution of interband transitions in layer 3 was calculated as the third energy derivative[9] of the dielectric function for the critical point M_0. It is significant that a spectrum shape agreeing with experiment is obtained if the phase of the low-frequency component of the field in layers 2 and 3 is opposite to the phase of the field in layer 1. This means that the built-in electric field in regions 2 and 3 is most likely directed opposite to the field in layer 1. The total optical reflection coefficient was calculated taking account of the arrangement of the layers in the sample and the absorption and interference of light. To obtain quantitative agreement between the computed and observed spectra, it was necessary to take account of the temperature modulation of the permittivity. The broadening of the low-energy edge ($h\nu \sim 1.4-1.5$ eV) of the spectrum is due to the heat effect. The best agreement between the computed and experimentally observed RMR spectrum in the energy range 1.48–1.54 eV is achieved with the following parameters: broadening in the regions 1, 2, and 3 equal to, respectively, $\Gamma_1 = 5$ meV, $\Gamma_2 = 2.0$ meV, and $\Gamma_3 = 2.2$ meV; the built-in electric field in the region 1 $E_1 = 2 \times 10^3$ V/cm; the amplitude of the low-frequency component of the rf field $E_1 = 2 \times 10^3$ V/cm (in region 1), $E_2 = 10^3$ V/cm (in region 2), and $E_3 = 10^3$ V/cm (in region 3); the rf field induced heating $\Delta T = 3 \times 10^{-3}$ K. The remaining parameters required for the calculations are taken from the literature.[6–8,11]

In summary, the observed spectra have a clear physical nature and a quantitative description of the spectrum can be obtained on the basis of a quite simple physical model. The qualitative difference between the RMR and PR spectra can be explained by the fact that the PR spectrum is determined by the regions of the sample where built-in electric fields are present and give rise to spatial redistribution of the nonequilibrium charge carriers and thereby produce the photoinduced electric field that is responsible for the modulation of the reflection coefficient. For this reason, for example, the excitonic effects in the PR spectrum are quite weak, since they are significant in regions with a weak field.

In the case of RMR, however, the low-frequency ac electric field arises in the entire sample, including in locations where the internal electric fields are weak. In our experiments this led to the appearance of optical responses, which are absent in the PR spectrum, from layers 2 and 3.

The proposed method makes it possible to investigate the electron-hole interaction in layers of semiconductor structures with strongly different built-in electric fields. On account of the low intensity of the probe light and the absence of a pump light, nonequilibrium charge carriers do not arise and there is no PL. This is the reason why the proposed method holds promise for developing methods of nondestructive diagnostics and for investigating semiconductor heterostructures in a wide temperature range.

This work was supported in part by the Russian Fund for Fundamental Research (Grant 96-02-18476-a) and the Russian Ministry of Science in the program ''Physics of solid-state nanostructures'' (Grant 97-1054).

[a)]e-mail: roa228@ire216.msk.su

---

[1] O. J. Glembocki and B. V. Shanabrook, in *Semiconductors and Semimetals*, Vol. 36, *The Spectroscopy of Semiconductors*, edited by D. G. Seiler and C. L. Littler, Academic Press, New York, 1992, pp. 222–292.
[2] O. A. Ryabushkin, V. A. Sablikov, M. P. Meleshkevich, and A. N. Pershinov, in *European Quantum Electronics Conference, Technical Digest*, Hamburg, 1996, p. 73.
[3] O. A. Ryabushkin, V. A. Sablikov, M. P. Meleshkevich, and A. N. Pershinov, in *Proceedings of the 23rd International Symposium on Compound Semiconductors*, St. Petersburg, Russia, September 23–27, 1996, Institute of Physics Conference Series, No. 155, 1997, p. 93.
[4] O. A. Ryabushkin, in *Abstracts of Invited Lectures and Contributed Papers of the International Symposium Nanostructures: Physics and Technology*, St. Petersburg, 1997, p. 270.
[5] Ch. Tanguy, Phys. Rev. Lett. **75**, 4090 (1995).
[6] Ch. Tanguy, Appl. Phys. **80**, 4626 (1996).
[7] S. Pond and P. Handler, Phys. Rev. B **8**, 2869 (1973).
[8] S. Adachi, Phys. Rev. B **41**, 1003 (1991).
[9] D. E. Aspnes, in *Handbook on Semiconductors*, Vol. 2, *Optical Properties of Solids*, North-Holland, Amsterdam, 1980.
[10] D. F. Blossey and P. Handler, in *Semiconductors and Semimetals*, Vol. 9, Academic Press, New York, 1972.
[11] N. H. Lu and T. M. Hsu, Phys. Rev. B **52**, 8191 (1995).

Translated by M. E. Alferieff

On the unified nature of the longitudinal and transverse acoustoelectric effects in type-II superconductors

E. D. Gutlyanskiĭ[a)]

Scientific-Research Institute of Physics at Rostov State University, 344090 Rostov-on-Don, Russia

(Submitted 12 March 1997; resubmitted 19 January 1998)
Pis'ma Zh. Éksp. Teor. Fiz. **67**, No. 3, 222–227 (10 February 1998)

A longitudinal ultrasonic wave should drag the vortex structure of superconductors at an acute angle with respect to the direction of wave propagation. This motion engenders longitudinal and transverse electric fields in the superconductor and, moreover, effects of the ''optical rectification'' type contribute to the observed longitudinal and transverse electric fields. The effect should be observed in all type-II superconductors above the irreversibility line. Both fields have extrema with respect to temperature and magnetic field. In contrast to the acoustoelectric effect in the normal state, the sign of the induced electric field depends on the external magnetic field. © *1998 American Institute of Physics.* [S0021-3640(98)01203-1]

PACS numbers: 74.60.−w, 72.50.+b

It is well known that in any solid with normal electrons (for example, in metals, semiconductors, and so on) a longitudinal ultrasonic wave will drag electrons.[1] In Refs. 2–4 it was shown theoretically that a longitudinal ultrasonic wave can give rise to motion of a vortex structure in the direction of wave propagation, that this motion results in the appearance of a transverse electric field, and that effects of the ''optical rectification'' type make a comparable contribution to this field.[4] Such an electric field has been observed experimentally by Zavaritskiĭ[5] and is related with the drag effect. In Refs. 6 and 7 it was found that the conventional acoustoelectric effect (longitudinal electric field) changes sign below the superconducting transition point. In Ref. 8 the existence of this electric field was explained theoretically by the presence of normal charge carriers in the superconductor below the transition point and by the fact that above and below the transition point the normal charge carriers are holes and electrons, respectively.

The objective of the present letter is to show that the longitudinal and transverse acoustoelectric effects are of a unified nature and are consequences of both the existence of a mobile vortex structure and the characteristic features of the acoustovortex interaction. Let us consider a uniform and isotropic superconductor in an external magnetic field B_0 directed along the negative z axis. For definiteness, let us assume that an ultrasonic plane wave propagates in the positive direction along the y axis and has the form $\mathbf{U}=\mathbf{U}_0\exp(iky-i\omega t)$, where $\mathbf{U}$ is the deformation vector of the ion lattice of the superconductor, $\mathbf{k}$ is the wave vector, and ω is the frequency of the oscillations. We shall write all

equations in the laboratory coordinate system. In this case the first London equation has the form[9]

$$\Lambda \frac{\partial \mathbf{j}_s}{\partial t} = \mathbf{E} - \mathbf{B}_\nu \times \dot{\mathbf{W}}, \tag{1}$$

where $\Lambda = m/n_s q^2 = \lambda_L^2 \mu_0$; m, q, and n_s are the mass, charge, and density of the superconducting charge carriers, respectively; λ_L is the London penetration depth; E is the intensity of the electric field in the laboratory coordinate system; $\dot{\mathbf{W}}$ is the local velocity of the vortex structure; and, $\mathbf{B}_\nu$ is the magnetic induction produced by the vortex structure of the superconductor.

The superconducting current can be expressed in terms of the total electric current in the system and the ionic current (we neglect the normal component of the current)

$$\mathbf{j}_s = \mathbf{j} + q n_s \dot{\mathbf{U}}. \tag{2}$$

Substituting expression (2) into Eq. (1), applying the operator $\nabla\times$ to both sides of Eq. (1), and using Maxwell's equations

$$\nabla \times \mathbf{E} = -\partial \mathbf{B}/\partial t, \tag{3}$$

$$\nabla \times \mathbf{H} = \mathbf{j}, \tag{4}$$

after simple manipulations we obtain the expression

$$\frac{\partial}{\partial t}\left(-\lambda_L^2 \nabla^2 \mathbf{B} + \mathbf{B} + \frac{m}{q} \nabla \times \dot{\mathbf{U}} \right) = \nabla \times (\dot{\mathbf{W}} \times \mathbf{B}_\nu), \tag{5}$$

which in the harmonic approximation has the form

$$\mathbf{B} - \lambda_L^2 \nabla^2 \mathbf{B} = -\frac{m}{q} \nabla \times \mathbf{U} + \nabla \times (\mathbf{W} \times \mathbf{B}_\nu). \tag{6}$$

Let us now write the local equation of motion of the vortex structure (neglecting the inertial mass of the vortex), which follows from the condition of balance of the forces: $\mathbf{F}_{fr} = \mathbf{F}_L$, where $\mathbf{F}_L = \mathbf{J}_s' \times \mathbf{B}_\nu$ is the Lorentz force and $\mathbf{F}_{fr} = \eta(\dot{\mathbf{W}} - \dot{\mathbf{U}}) - \tilde{\eta}(\dot{\mathbf{W}} - \dot{\mathbf{U}}) \times \mathbf{B}_\nu$ is the frictional force of the vortex structure against the crystal lattice of the superconductor, and $\mathbf{J}_s'$ is the current density in the local coordinate system tied to the vortex structure. Since $\mathbf{j}_s' = \mathbf{j}_s - q n_s \dot{\mathbf{W}}$, we obtain the equation of motion of the vortex structure

$$\eta(\dot{\mathbf{W}} - \dot{\mathbf{U}}) - \tilde{\eta}(\dot{\mathbf{W}} - \dot{\mathbf{U}}) \times \mathbf{B}_\nu = (\mathbf{j}_s - q n_s \dot{\mathbf{W}}) \times \mathbf{B}_\nu, \tag{7}$$

where η and $\tilde{\eta}$ are the longitudinal and transverse coefficients of viscosity of the vortex structure, respectively. In addition, $\tilde{\eta} = (q/h)\eta'$, η' is the transverse coefficient of viscosity (introduced in Refs. 10–12) for a single vortex, and h is Planck's constant. (A discussion of the microscopic nature of this coefficient is contained in Ref. 13.)

For a complete description of the motion of the vortex structure under the action of an ultrasonic wave it is necessary to take account of the fact that the density of the vortices (the distribution of $\mathbf{B}_\nu$ in the superconductor) and their local velocity are not independent quantities but rather they are related by the continuity equation.

The continuity equation for the vortex structure is

$$\partial \mathbf{B}_\nu / \partial t = \nabla \times (\mathbf{B}_\nu \times \dot{\mathbf{W}}). \tag{8}$$

The equations (6) and (8) completely describe the motion of the vortex structure under the action of a longitudinal ultrasonic wave.

To take account of the back effect of the motion of the vortex structure on the crystal lattice of the superconductor, it is necessary to write down the equation from the theory of elasticity that describes the propagation of an ultrasonic wave in the superconductor. This equation is

$$\rho \ddot{\mathbf{U}} = \rho \cdot c_t \Delta \mathbf{U} + \rho (c_l^2 - c_t^2) \nabla (\nabla \cdot \mathbf{U}) - q n_s \dot{\mathbf{U}} \times \mathbf{B} - q n_s \mathbf{E} + \mathbf{F}_{fr}. \tag{9}$$

Here ρ is the density of the superconductor, and c_l and c_t are the velocity of longitudinal and transverse ultrasonic waves in the absence of a vortex structure. The third and fourth terms in this equation describe the effect of the electric and magnetic fields on the ionic lattice of the superconductor, and the fifth term describes the effect of friction. If the first two additional terms are neglected, then Eq. (9) is identical to the equation from the theory of elasticity that is used in, specifically, Refs. 14–16, and in the case when the propagation of only a transverse wave is considered, Eq. (9) is identical to Eq. (2) of Ref. 17.

To solve the problem of the combined motion of the elastic continuum and the vortex lattice it is necessary to solve the system of equations (6)–(9). These equations form a nonlinear system, which we shall solve by the method of successive approximations. First, we find the superconducting current generated by the motion of the ionic lattice and the vortex structure. Let us set $\mathbf{B}_\nu = \mathbf{B}_0 + \mathbf{\Delta B}_\nu$ and $\dot{\mathbf{W}} = \dot{\mathbf{W}}_1 + \dot{\mathbf{W}}_2$, where $\mathbf{B}_0$ is the uniform component of the magnetization of the superconductor that coincides with the external field and $\mathbf{\Delta B}_\nu$ are the magnetization oscillations due to the oscillations of the density of the vortex structure. Equations (6) and (8) in linearized form are

$$\mathbf{B} - \lambda_L^2 \nabla \mathbf{B} = -\frac{m}{q} \nabla \times \mathbf{U} + \nabla \times (\mathbf{W}_1 \times \mathbf{B}_0), \tag{10}$$

$$\frac{\partial \Delta \mathbf{B}_\nu}{\partial t} = -\nabla \times (\mathbf{B}_0 \times \mathbf{W}_1). \tag{11}$$

Solving Eq. (10) for **B** and using the Maxwell's equation (4) we find the total current in the superconductor as

$$\mathbf{j} = \frac{1}{\mu_0 (1 + \lambda_L^2 k^2)} \left[-\frac{m}{e} (\mathbf{k} \cdot \dot{\mathbf{U}}) \mathbf{k} + \frac{m}{e} \mathbf{k}^2 \dot{\mathbf{U}} - (\mathbf{k} \cdot (\mathbf{W} \times \mathbf{B}_0)) \mathbf{k} + \mathbf{k}^2 (\mathbf{W} \times \mathbf{B}_0) \right]. \tag{12}$$

It is convenient to write the linearized equation of motion (8) of the vortex structure in the form

$$\eta_0 (\dot{\mathbf{W}}_1 - \mathbf{U}) + \alpha \dot{\mathbf{W}} \times \mathbf{B}_0 = \mathbf{J} \times \mathbf{B}_0 + \alpha \dot{\mathbf{U}} \times \mathbf{B}_0, \tag{13}$$

where $\alpha = q n_s - \tilde{\eta}$, and η_0 is the zeroth order in the expansion of the coefficient of viscosity in terms of the oscillations of the density of the vortex structure ($\eta = \eta_0 + \eta_{,B} \cdot \Delta B_\nu$, $\eta_{,B} = (d\eta / dB)(B_0)$). Solving simultaneously Eqs. (12) and (13) and the linear-

ized equation from the theory of elasticity leads to damping, variation of the velocity, and transformation of elastic waves into one another. These effects are discussed in part in Refs. 14–19.

In the present work, we are interested in drag and acoustoelectric effects. For this reason, we shall now examine the terms in Eq. (8) that are of second-order in the deformation vector of the ion lattice of the superconductor, and we shall neglect the back effect of the vortex lattice on the motion of the ion lattice of the superconductor. In second-order perturbation theory, after averaging over time, the equation for the constant component of the velocity of the vortex structure has the form

$$\eta_0\langle\dot{\mathbf{W}}_2\rangle+\alpha\langle\dot{\mathbf{W}}_2\rangle\times\mathbf{B}_0=\langle\mathbf{J}\times\Delta\mathbf{B}_\nu\rangle-\eta_{,B}\langle\Delta B_\nu(\dot{\mathbf{W}}_1-\dot{\mathbf{U}})\rangle$$
$$-\alpha\langle\dot{\mathbf{W}}_1\times\Delta\mathbf{B}_\nu\rangle+\alpha\langle\dot{\mathbf{U}}_1\times\Delta\mathbf{B}_\nu\rangle. \tag{14}$$

Here and below the brackets $\langle\ldots\rangle$ represent time-averaging. It is easy to see from Eq. (14) that, besides the Lorentz force, the viscosity contributes to the drag of the vortex structure.

The equations (11), (12), and (14) completely determine $\langle\dot{\mathbf{W}}_2\rangle$. Calculations show that a longitudinal ultrasonic wave[b)] gives rise not only to longitudinal but also transverse motion of the vortex structure. The projections of the velocity vector of the vortex structure on the y and x axes are

$$\langle\dot{\mathbf{W}}_2\rangle_y=\frac{1}{2}\omega k\left(\frac{\eta_{,B}B_0}{\eta_0}-1\right)^2\frac{Y^2-1}{Y^2+1}\frac{X^2}{1+X^2}U_0^2, \tag{15}$$

$$\langle\dot{\mathbf{W}}_2\rangle_x=\frac{1}{2}\omega k\left(\frac{\eta_{,B}B_0}{\eta_0}-1\right)^2\frac{Y}{Y^2+1}\frac{X^2}{1+X^2}U_0^2, \tag{16}$$

where

$$X=\frac{D}{\omega\eta_0(1+Y^2)},\quad D=\frac{B_0^2}{\mu_0(1+\lambda_L^2k^2)},\quad Y=\frac{\alpha B_0}{\eta_0}.$$

It is evident from expressions (15) and (16) that viscosity makes a large contribution to the drag of the vortex structure by the ultrasonic wave. Specifically, there will be no drag in the region of the phase diagram of the superconductor where the FF regime operates. In this regime the coefficient of viscosity has the form $\eta=BB_c/r_n$, and this form of the coefficient of viscosity makes expressions (15) and (16) vanish.

In the experimental investigation of the effect described above, the main observable quantity is the intensity of the electric field induced by the motion of the vortex structure, specifically, the constant component of this field.[5–7] We shall now calculate this component. The electric field induced by the motion of the vortex structure is given by

$$\mathbf{E}=\mathbf{B}\times\dot{\mathbf{W}}. \tag{17}$$

Since we are interested in the constant component of the electric field, let us substitute the expansions $\mathbf{B}=\mathbf{B}_0+\Delta\mathbf{B}$ and $\dot{\mathbf{W}}=\dot{\mathbf{W}}_1+\dot{\mathbf{W}}_2$ into Eq. (17) and average over the time. The result is

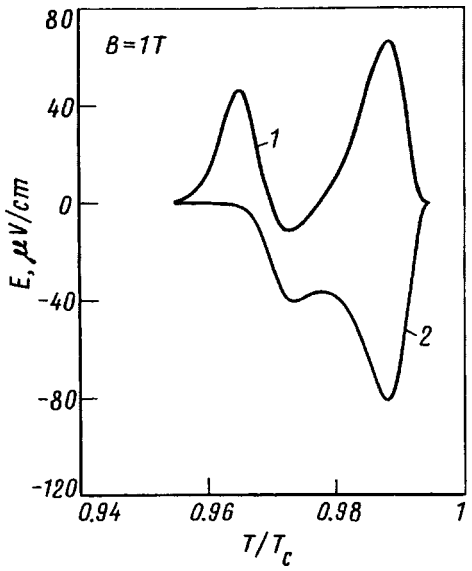

FIG. 1. Transverse E_t (curve *1*) and longitudinal E_l (curve *2*) electric fields induced in $YBa_2Cu_3O_7$ in an 1 T external magnetic field by a longitudinal acoustic wave with amplitude 10^{-8} m and frequency 100 MHz versus temperature.

$$\langle \mathbf{E} \rangle = \langle (\mathbf{B}_0 + \Delta\mathbf{B})(\dot{\mathbf{W}}_1 + \dot{\mathbf{W}}_2) \rangle = \mathbf{B}_0 \times \langle \dot{\mathbf{W}}_2 \rangle + \langle \Delta\mathbf{B} \times \dot{\mathbf{W}}_1 \rangle. \tag{18}$$

The term $\langle \mathbf{B}_0 \times \dot{\mathbf{W}}_1 \rangle = 0$, and the term $\langle \mathbf{\Delta B}_0 \times \dot{\mathbf{W}}_2 \rangle$ was dropped, since it is a third-order infinitesimal in the amplitude of the ultrasonic wave.

Figures 1 and 2 display the numerical results. It is evident from Eq. (18) that, besides drag, an optical rectification type effect contributes to the electric field intensity.[4] In addition, the contributions of the first and second terms in Eq. (18) are comparable. The projections of the electric field on the x and y axes are

$$\langle \mathbf{E}_y \rangle = \frac{1}{2}\omega_k B_0 Y \left[\left(\frac{\eta_{,B} B_0}{\eta_0} - 1 \right)^2 \left(\frac{1}{Y^2+1} \right) - 1 \right] \frac{X^2}{1+X^2} U_0^2, \tag{19}$$

$$\langle \mathbf{E}_x \rangle = \frac{1}{2}\omega_k B_0 \left[\left(\frac{\eta_{,B} B_0}{\eta_0} - 1 \right)^2 \left(\frac{Y^2-1}{Y^2+1} \right) + 1 \right] \frac{X^2}{1+X^2} U_0^2. \tag{20}$$

It follows from expressions (19) and (20) that an acoustoelectric effect should be observed in the region FF, even though there is no drag of the vortex structure in this region, and the projections $\langle E_x \rangle$ and $\langle E_y \rangle$ are proportional to each other: $\langle E \rangle_y = -Y \langle E \rangle_x$. It would be interesting to check this scaling relation experimentally.

$YBa_2Cu_3O_7$. The magnitude of the effect depends on the parameter α. The sign of the parameter is known, since it is proportional to the charge of the current carriers. It can vary in modulus from zero (in very dirty superconductors) to the maximum value qn_s (in very clean superconductors).[13] We do not know the coefficient α for $YBa_2Cu_3O_7$, but the charge carriers are holes and therefore α is positive; we shall set α equal to the

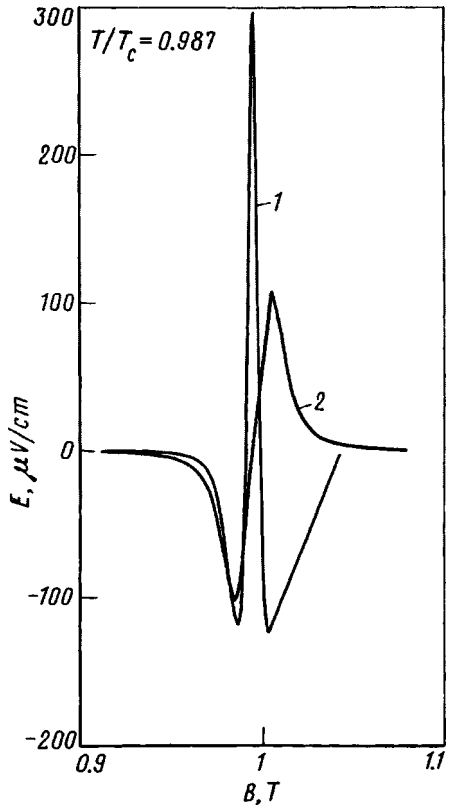

FIG. 2. Transverse E_t (curve *1*) and longitudinal E_l (curve *2*) electric fields induced in $YBa_2Cu_3O_7$ by a longitudinal acoustic wave with amplitude 10^{-8} m and frequency 100 MHz at a fixed temperature equal to 0.952 in units of T/T_c, where T_c is the superconducting transition temperature, versus the external magnetic field.

maximum value. Therefore we shall estimate the upper limit for the longitudinal acoustoelectric effect.[c)] All other material parameters are assumed to be the same as in Ref. 4. As one can see from Fig. 1, the longitudinal acoustoelectric effect does indeed change sign below the transition point (in the normal state the acousto-emf is positive, since the current carriers are holes; see, for example, Ref. 20), and the temperature dependence of the intensity of the longitudinal electric field is very close to the experimental dependence.[6,7] Moreover, the sign of the effect can be changed by increasing the magnetic field (Fig. 2). It would be interesting to check this fact experimentally.

In summary, it has been shown in this letter that the longitudinal and transverse acoustoelectric effects are of the same nature and should be observed in all type-II superconductors above the irreversibility line. Earlier, these effects were considered to be independent of one another.[2–8] Both effects have extrema as functions of the temperature and magnetic field. The proposed theory explains the maximum observed in Ref. 5 for the transverse acoustoelectric effect as a function of the magnetic field and predicts the existence of another maximum at a lower temperature. The theory explains, without using artificial assumptions, the existence of the longitudinal acoustoelectric effect observed in

Refs. 6 and 7 in the superconducting state and the fact that the sign of this effect is different from its sign in the normal state.

I am grateful to the Russian Fund for Fundamental Research for supporting this work (Grant 96-02-188505).

[a)]e-mail: gutlian@iphys.rnd.runnet.ru

[b)]Calculations for the case of a transverse wave can be easily performed on the basis of the formalism proposed in this letter. It is not presented here for lack of space.

[c)]The longitudinal acoustoelectric effect does not occur if $\alpha = 0$, while the transverse effect exists for all values of α.

---

[1] R. H. Parments, Phys. Rev. **89**, 990 (1953).
[2] E. D. Gutlyanskiĭ, JETP Lett. **59**, 480 (1994).
[3] E. D. Gutliansky, Physica C **235–240**, 2080 (1994).
[4] E. D. Gutlyanskiĭ, Fiz. Tverd. Tela (St. Petersburg) **38**, 1341 (1996) [Phys. Solid State **38**, 743 (1996)].
[5] N. V. Zavaritskiĭ, JETP Lett. **57**, 707 (1993).
[6] Yu. V. Ilisavskiĭ, É. Z. Yakkhind *et al.*, JETP Lett. **52**, 542 (1991).
[7] Yu. V. Ilisavskiĭ, É. Z. Yakkhind *et al.*, Fiz. Tverd. Tela (Leningrad) **33**, 824 (1991) [Sov. Phys. Solid State **33**, 469 (1991)].
[8] A. V. Goltsev, Z. Phys. B **93**, 425 (1994).
[9] P. Nozieres and W. F. Vinen, Philos. Mag. **14**, 667 (1966).
[10] H. E. Hall and W. F. Vinen, Proc. R. Soc. London **238**, 215 (1956).
[11] V. Ambegaokar, B. I. Halperin, D. R. Nelson, and E. D. Siggia, Phys. Rev. B **21**, 1806 (1980).
[12] S. J. Hagen, C. J. Lobb, R. L. Green *et al.*, Phys. Rev. B **41**, 11630 (1990).
[13] E. B. Sonin, Phys. Rev. B **55**, 485 (1997).
[14] J. Pankert, Physica C **168**, 335 (1990).
[15] E. D. Gutlyanskiĭ, Fiz. Nizk. Temp. **18**, 428 (1992) [Sov. J. Low Temp. Phys. **18**, 290 (1992)].
[16] E. D. Gutliansky and T. V. Kolesnikova, Physica C **235–240**, 2078 (1994).
[17] E. B. Sonin, Phys. Rev. Lett. **76**, 2794 (1996).
[18] D. Dominguez, B. Bulaevskii, B. Ivlev *et al.*, Phys. Rev. Lett. **74**, 2579 (1995).
[19] D. Dominguez, B. Bulaevskii, B. Ivlev *et al.*, Phys. Rev. **51**, 15649 (1995).
[20] V. L. Bonch-Bruevich and S. G. Kalashnikov, *Semiconductor Physics* [in Russian], Nauka, Moscow, 1975.

Translated by M. E. Alferieff